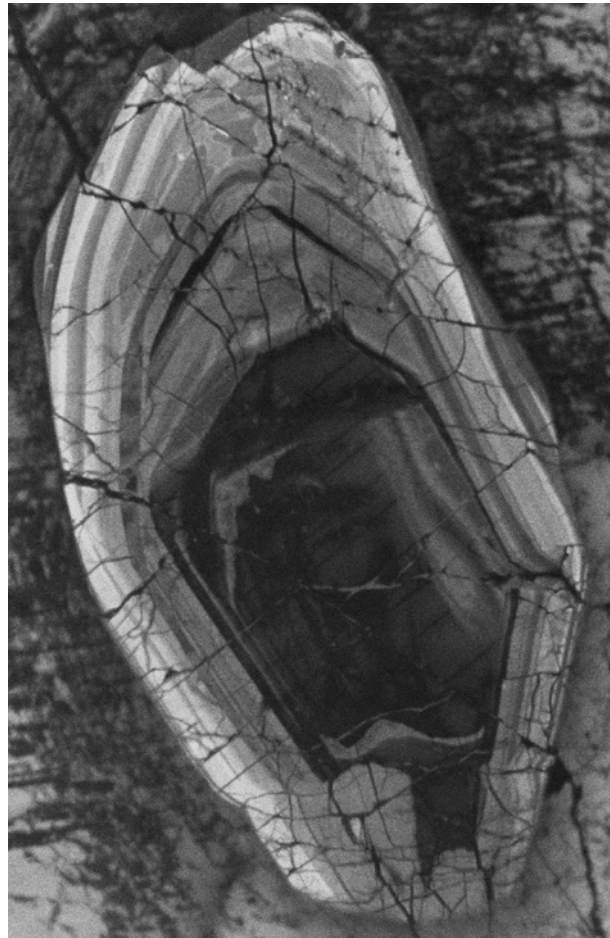


# The Guarda Structure, NE-Portugal: A meteorite impact crater or not?

*Marit E. van Zalinge*<sup>1</sup>

<sup>1</sup>Department of Earth Sciences, Faculty of Geosciences, Utrecht University, The Netherlands



31-03-2012

Prof. dr. M. R. Drury

Drs. M. F. Hamers

## Abstract

---

The Guarda Structure is a circular structure located in the Iberian Massif, just northeast of the city Guarda, Portugal. The structure has a diameter of  $\pm 35$  km and is formed in Variscan granitoids. Monteiro (1991) suggested that the Guarda Structure is a deeply eroded complex multi-ring impact crater. He mentioned that the circular topography and the hydrographic pattern in combination with decorated planar features in quartz crystals are evidence for an impact crater centered at  $40^{\circ} 37'N$  and  $7^{\circ} 6'W$ . However, convincing evidence is missing and it remains unclear whether the Guarda Structure is an impact crater. During this study, field data and rock samples were collected in the Guarda Structure and detailed light microscopy and SEM-analyses were done on potential shock microstructures in quartz, zircon and monazite, to prove whether the Guarda Structure is an impact crater or not. Typical impact rocks and impact geology were not found in the Guarda Structure. Compared to minerals from confirmed craters, quartz, zircon and monazite from the Guarda Structure lack all forms of shock microstructures. The circular topography of the structure and the associated circular drainage pattern could be formed due to lithology differences within the Guarda Structure or due to a dome-like structure. Light microscope analyses are good methods to study planar shock microstructures (PMs) in zircon and monazite. PMs in zircon probably develop over a wide shock pressure range  $>10$ - $35$  GPa, but show also some restrictions, since PMs mainly form in zircons that are  $>100$   $\mu$ m. Shocked monazites contain three types of PMs and granular texture that probably start to develop at shock pressures between  $>10$ - $15$  GPa and  $>30$  GPa respectively.

---

# Contents

General Introduction	<b>6</b>
<u>Chapter 1: Field observations</u>	
1.1 Introduction	<b>7</b>
1.1.1 Complex impact structures	7
1.1.2 The Guarda Structure	8
1.2 Geological Setting	<b>8</b>
1.2.1 Variscan orogeny	8
1.2.2 Granitoids in the CIZ	9
1.3 Methods and samples	<b>10</b>
1.3.1 Satellite images	10
1.3.2 Fieldwork	10
1.4 Results	<b>11</b>
1.4.1 Topography and shape of the Guarda Structure	11
1.4.2 Field observations	12
1.5 Discussion	<b>16</b>
1.5.1 Maximum age of alleged crater	16
1.5.1.1 Stephanian-Permian extensional uplift	16
1.5.1.2 Structural uplift during meteorite impact	17
1.5.1.3 Tertiary erosion and denudation	17
1.5.2 Field observations	18
1.5.3 Topography and shape	19
1.5.4 Drainage network in the Guarda Structure	20
1.5.4.1 Anomalous Drainage pattern	20
1.5.4.2 Dome-like structure	20
1.5.4.3 Lithology	22
1.5.5 The Guarda Structure and related mass extinctions	22
1.6 Conclusion and further research	<b>22</b>
References	<b>23</b>
<u>Chapter 2: Planar Microstructures in Quartz</u>	
2.1 Introduction	<b>25</b>
2.1.1 Shock Lamellae (PDFs)	25
2.1.2 PDFs versus Tectonic Deformation lamellae	26
2.1.2.1 Optical Microscopy	26
2.1.2.2 SEM analyses	26
2.1.3 Planar Microstructures in quartz from the Guarda Structure	27
2.2 Samples and Methods	<b>28</b>
2.2.1 SEM-background	29
2.3 Results	<b>29</b>
2.4 Discussion	<b>33</b>
2.4.1 Sample 2.5a	33

2.4.2 Sample 3.3b	34
2.4.3 Sample 1.6g	34
2.4.3.1 Hydrothermal veins and zoning	34
2.4.3.2 Deformation lamellae	35
2.4.3.3 Age of deformation lamellae and possible involved tectonics	35
2.4.4 Guarda Structure versus Ries Crater	35
2.4.5 Post shock annealing of PDFs in quartz	36
2.5 Conclusion and further research	<b>37</b>
References	37

### Chapter 3: Shock Microstructures in Zircon

3.1 Introduction	<b>40</b>
3.1.1 Planar and non-planar microstructures	40
3.1.1.1 Terminology of planar microstructures	41
3.1.2 High Pressure Polymorph Reidite	42
3.1.3 Granular texture	42
3.1.4 Decomposition of Zircon	43
3.1.5 Overview shock microstructures in zircon	43
3.2 Background of the Vredefort Dome	<b>44</b>
3.3 Methods and Samples	<b>44</b>
3.4 Results	<b>44</b>
3.4.1 Summary of the results	50
3.5 Discussion	<b>50</b>
3.5.1 Nature of planar microstructures in zircon	51
3.5.2 Relation crystal size and PM development	51
3.5.3 Guarda Structure versus Vredefort Dome	51
3.5.4 Shock pressures forming PMs	52
3.5.4.1 Previous work	52
3.5.4.2 Shock pressure distribution in the Vredefort Dome	52
3.6 Conclusion and further research	<b>54</b>
References	55

### Chapter 4: Shock Microstructures in Monazite

4.1 Introduction	<b>57</b>
4.1.1 Shock Microstructures in monazite	57
4.1.2 Monazite as impact dating tool	57
4.2 Methods and samples	<b>58</b>
4.3 Results	<b>58</b>
4.3.1 Summary of the results	59
4.4 Discussion	<b>63</b>
4.4.1 Nature of planar microstructures in monazite	63
4.4.2 Guarda Structure versus Vredefort Dome	65
4.4.3 Pressure range for shock microstructures in monazite	65
4.5 Conclusion and further research	<b>66</b>

References	66
Final Conclusions	<b>68</b>
Acknowledgements	68
Appendix 1: Table and map with all collected samples in the Guarda Structure	69
Appendix 2: Elevation map and 3D-image of the Guarda Structure	74
Appendix 3: Thin sections scans with the analyzed zircon and monazite grains	75

## **General introduction**

### **The Guarda Structure**

The Central Iberian Zone (CIZ) is part of the Iberian Massif and is located in central Portugal. The CIZ is characterized by large volumes of Variscan granitoids (e.g. Azevedo and Valle Aguado, 2006; Dias et al., 1999; Sant'Ovaia et al., 2010). In one area of the CIZ, the Beira Alta province, NE of the city Guarda, a circular structure is visible in the topography, the Guarda Structure. The lithology of the Guarda Structure is dominated by different types of granitoids, small amounts of pre-Ordovician meta-sedimentary slates and graywackes. Quartz veins, basalt-dolerite dykes and small Permo-Triassic gabbroic intrusions are common as well (Neves Ferro et al., 1962; Monteiro, 1991).

In 1991 Monteiro suggested that the Guarda Structure is a deeply eroded complex multi-ring impact crater. He claimed that the circular topography in combination with the hydrographic pattern are evidence for a crater with a diameter of 35km, centered at 40° 37'N and 7° 6'W. In the center of the crater Monteiro (1991) found a breccia dyke. This breccia dyke has a very fine matrix and contains several fragments of the common lithology: granitoids, pre-Ordovician slates and fragments of the gabbroic and dolerite rocks. Monteiro (1991) claimed he found decorated planar features in quartz crystals from the breccia dyke, as well as other shock metamorphic features in granitoids from the Guarda Structure.

### **Missing evidence**

Although the findings of Monteiro (1991) could indicate that the Guarda Structure is a complex multi-ring impact crater, his evidence is still very questionable. There's a lack of detailed field observations and a lack of clear images of the planar elements and decorated planar features. I suggest that, based on satellite images and the abstract Monteiro published in 1991, it's not possible to conclude that the Guarda Structure is a multi-ring impact crater. The aim of this research is to present convincing evidence that will point out whether the Guarda Structure is a crater or not. In order to achieve this goal, field data and rock samples were collected in the Guarda Structure and detailed light microscopy and SEM-analyses were done on potential shock microstructures in quartz, zircon and monazite. The microstructures in the samples from the Guarda Structure are compared to shocked quartz, zircon and monazite from two confirmed impact structures; the Ries Crater, Germany and the Vredefort Dome, South Africa. The usability of optically visible shock microstructures in zircon and monazite will be studied as well.

To clearly present all data, this report is divided in four chapters. The first chapter will present and discuss the field observations. The second chapter gives an overview of potential shock microstructures in quartz from the Guarda Structure and the comparison material. In the last two chapters potential shock microstructures in zircon and monazite, and the comparison with zircon and monazite from the Vredefort Dome will be presented.

# Chapter 1: Field Observations

## 1.1 Introduction

### 1.1.1 Complex impact structures

Meteorite impacts transform a landscape very radically, leaving behind different types of impact rocks and a very distinct morphology. The first indication of a possible meteorite impact structure is a distinct circular (or nearly circular) feature in the topography or bedrock geology. This circular region commonly shows distinctive and often anomalous bedrock geology in comparison to the surroundings (French, 1998). Even after millions of years an impact crater can still be recognized in a landscape (e.g. French, 1998; Grieve, 1991).

There are different types of impact craters, depending on the size of the impacting body (French, 1998). Only craters with a diameter >4 km (for crystalline rocks) have a complex structure. Complex impact craters are characterized by a central uplift, a generally flat floor and a faulted outer rim (Grieve, 1991). At larger crater diameters the impact structure becomes more complicated. As the crater size increases, the character of the central uplift changes; the single central peak is progressively replaced by a more complex series of concentric rings (French, 1998).

Figure 1 shows a simplified cross section of a complex impact crater, from the crater rim to the central uplift. The locations of the different types of impact rocks are schematically shown. Parautochthonous rocks, exposed in the central uplift, are extremely brecciated and fractured. These rocks could contain shock features, such as shatter cones, pseudotachylite breccias, impact melts and dyke-like intrusive bodies of allogenic breccias. The latter show a sharp contact and clear cross-cutting relation against the subcrater rocks. The dykes are polymict and could be up to tens of meters width and a kilometer long. They contain rounded and angular fragments of target rock that range

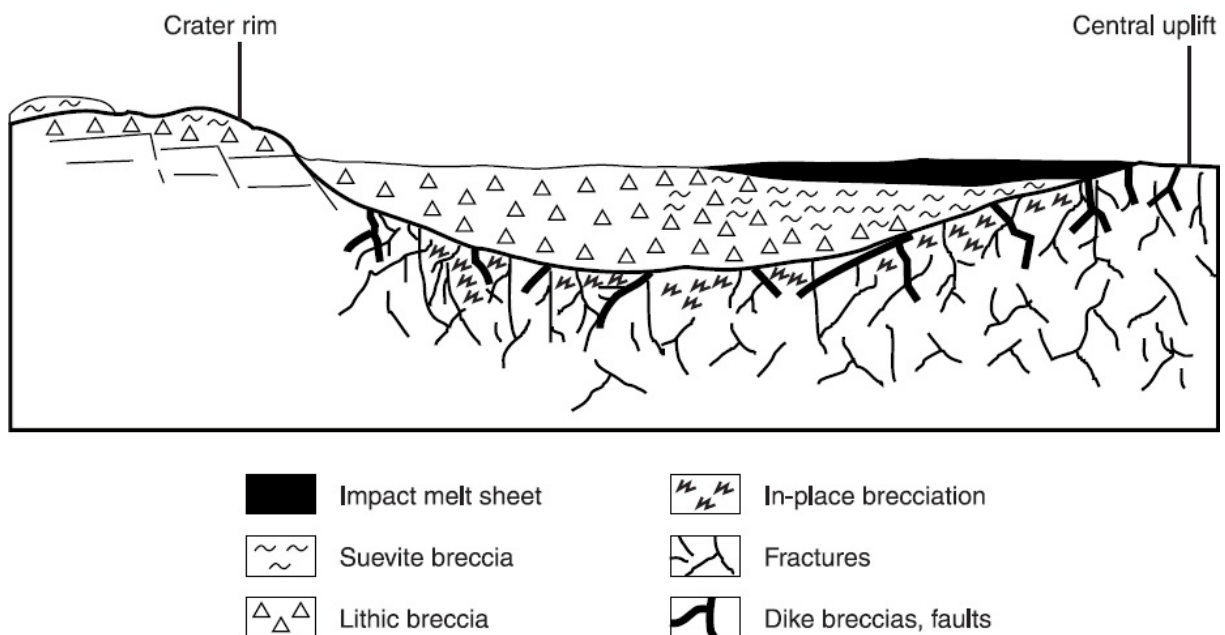


Figure 1. Cross-section of a complex impact crater (from rim to central uplift) with the different types of impact rock. The parautochthonous rocks may contain fractures such as shatter cones, pseudotachylite breccias, in-place brecciation and dike-like intrusive bodies. The crater is filled with mainly lithic and suevite breccias and on top a sheet of impact melt may occur (modified from French, 1998).

from millimeters to meters in size. In addition, they frequently contain allochthonous material, derived from rocks above the present location of the dyke. Most of the fragments in the parautochthonous rocks are highly shocked (French, 1998). Lithic breccias and melt-bearing suevite breccias cover the parautochthonous rocks and fill the crater. An impact melt sheet may occur at or toward the top of the crater fill. The ejecta layer is deposited on the target rocks around the crater (not visible in figure 1). Almost all ejecta are deposited within a distance of 5 times the radius of the crater. For a detailed description of all rock types, I refer to French (1998).

Impact structures formed on Earth's surface are influenced by all kinds of denudation processes, resulting in erosion of the crater. The so distinctive rim uplift and ejecta deposits are only observed at relatively young structures such as the 15 Ma Ries Crater, Germany and the 50 ka Barringer Meteor Crater, U.S.A.. In older crater structures only the parautochthonous rocks and some of the breccias that fill the crater might be preserved (French, 1993).

### **1.1.2 The Guarda Structure**

Monteiro (1991) suggested the Guarda Structure is a complex multi-ring impact crater with a diameter of 35 km. He claimed that the circular topography, the hydrographic pattern in combination with decorated planar features, found in a breccia dyke from the center of the structure, are evidence for an impact crater. According to Monteiro (1991), the breccia dyke is probably associated with dolerite dykes in the Guarda Structure, because the breccia dyke forms a dyke with various thicknesses and has an irregular attitude crosscutting the Variscan granitoids as well.

The aim of the first part of this research is to make field observation and search for typical impact evidence, such as shatter cones and pseudotachylites, in the Guarda Structure. Field observations are supported by analysis of geological maps and satellite images.

## **1.2 Geological Setting**

### **1.2.1 Variscan orogeny**

The Guarda Structure is located in the European Variscan fold belt. The European Variscan fold belt was formed by the collision of Laurasia and Gondwana to form the supercontinent Pangaea and extends over more than 3000 km from the Iberian Peninsula to Eastern Germany. This collision started during late Devonian and ended in the Permian (390-280Ma) (Sant'Ovaia et al., 2010). Its magmatic and tectonometamorphic features have been explained by an obduction-collision orogenic model with left-lateral transpression. From Early Devonian to Mid-Carboniferous (390-330 Ma) active continent-continent collision took place. This was followed by post-thickening extension from the Mid-Carboniferous to the Permian (330-280 Ma) (Dias et al., 1998).

The Iberian Massif is a great domain of the European Variscan fold belt. Julivert et al. (1972) subdivided The Iberian Massif in five segments: the South Portuguese Zone, the Ossa Morena Zone, The Central Iberian Zone (CIZ), the West Asturian Leonese Zone and the Cantabrian zone. In 1987 Farias et al. (as cited in Sant'Ovaia et al., 2010) added The Galicia Trás-os-Montes Zone to the other five segments. Figure 2 shows the different zones of the Iberian Massif. The Guarda Structure is located in the Central Iberian Zone (CIZ).

The northwestern part of the Iberian Massif, including the West Asturian Leonese Zone, The Galicia Trás-os-Montes zone and the Central Iberian Zone, experienced three phases of ductile deformation

(D1, D2 and D3) (Sant’Ovaia et al., 2010) and one brittle deformation phase (D4) (Dias et al., 1998). Table 1 is an overview of the different deformation phases and their main characteristics and timing. Deformation phases D1 and D2 are related to the continent-continent collision and D3 and D4 are correlated to the following post-thickening extension tectonics. During this post-thickening extension huge amounts of granites were emplaced in the northern part of Portugal (Dias et al., 1998).

Table 1. The different deformation phases of the Variscan orogeny present in the northwestern part of the Iberian Massif and their main characteristics and age (Dias et al., 1998 and Sant’Ovaia et al., 2010).		
Deformation phase	Main characteristics	Timing
D1	Subvertical folds with a slaty cleavage	380-360 Ma, Mid-Upper Devonian
D2	Recumbent folds with schistosity or axial plane crenulation associated to large thrust zones or sub-horizontal extensional shear zones	360-330 Ma, Mid-Carboniferous
D3	Subvertical strike-slip shear zones and vertical folds with sub horizontal axes	330-300Ma, Namurian-Westphalian
Post D3 / D4	A set of conjugate strike-slip faults (NNW-SSE dextral and NNE-SSW sinistral faults)	300-280Ma, Permian

### 1.2.2 Granitoids in the CIZ

The Variscan Granites represent around 60-70% of the outcropping rocks in the CIZ (Sant’Ovaia et al., 2010). These granites were emplaced in the CIZ during deformation phases D3 and D4 (Dias et al., 1998). Syn-D3, late-D3 as well as post D3 granites were defined. Ferreira et al. (1987, as referred in Dias et al., 1998), made a classification for the CIZ granitoids, based on dominant mineral content and emplacement age. Ferreira et al. (1987, as referred in Sant’Ovaia et al 2010) suggested that the CIZ granites were divided into two main groups: dominant biotite granites (biotite >> muscovite) and two-mica granites (muscovite > biotite). Azevedo and Valle Aguado (2006) modified the classification of Ferreira et al. (1987) and the classification is shown in table 2.

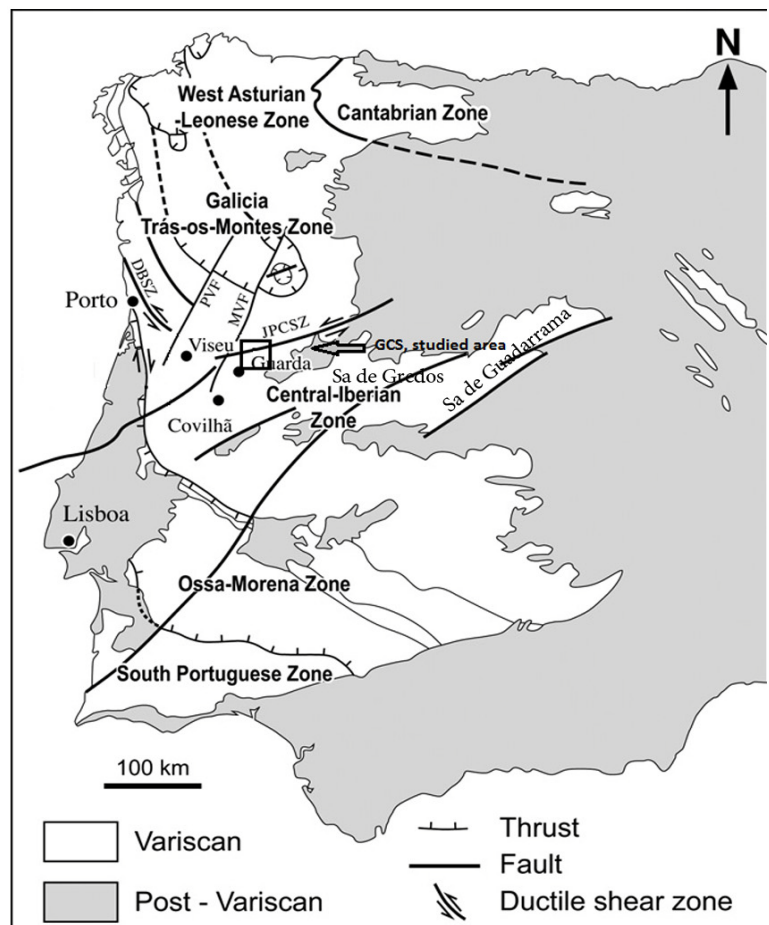


Figure 2. The Iberian Massif and its six different zones. The Guarda Structure is located within the small square, close to the city Guarda, west of the Sierra de Gredos and below the JPCSZ: Juzbado-Penalva do Castelo Shear Zone (Modified from Saint’Ovaia et al., 2010).

Table 2: Classification of the different granitoids in the CIZ and their ages. (Modified from Azevedo and Valle Aguado, 2006)		
Classification	Rocks present	Ages
Syn –D3 granites	- Two-mica peraluminious, granodiorites and biotite granites. - All types show various deformation structures	320-310 Ma
Late-post-D3 granites	- biotite and two-mica granites, sometimes phenocrytic - granodiorites, diorites, gabbros and quartz-monzodiorites.	310-290 Ma

Based on radiometric age dating, two cycles of magmatic activity can be distinguished in the CIZ. The syn-D3 granites were emplaced between 320-310 Ma and the late and post-D3 granites between 310-290 Ma (Azevedo and Valle Aguado, 2006). All granites are crosscut by many NE-trending quartz veins and more randomly trending aplite-pegmatite veins. (Sant O’vaia et al., 2010).

>80% of the outcropping rocks in the Guarda Structure are late-post-D3 granitoids. Detailed geological mapping (Neiva and Ramos, 2010; Neiva et al., 2011; Neves Ferro et al., 1962) pointed out that there are two main types of late-post D3 granites present in the Guarda Structure (Figure 3). In the outer rings we find coarse-grained phenocrytic granite (++ granite); granite with feldspatic phenocrysts with an age of  $304.1 \pm 3.9$  Ma. In the center of the structure there is fine to coarse grained non-phenocrytic granite (T-granite) (Neiva et al. 2011 claimed that this granite is also phenocrytic, but during this fieldwork non-phenocrytic granite was observed). T-granite is slightly younger in age,  $299.1 \pm 1.3$  Ma (Neiva et al., 2011). Other rocks that are present in the structure are pre-Ordovician meta-sedimentary slates and graywackes and small Permo-Triassic gabbroic intrusions (e.g. Monteiro, 1991; Neiva et al., 2011; Neves Ferro et al., 1962)

### 1.3 Methods and Samples

#### 1.3.1 Satellite images

To study the topography and morphology of the Guarda Structure, Google Earth © 2011 and ArcGis (ArcMap 10) were used. The source for the satellite images used in ArcGis is Bingmaps Aerial.

#### 1.3.2 Fieldwork

The locations of the collected rocks were registered with a Garmin GPS 72 and uploaded in Google Earth © 2011. To get a better overview of the lithology and geology, geological map 18-A Vila Franca das Naves (Neves Ferro et al. 1962), was placed in Google Earth © 2011. Appendix 1 is a detailed overview (table and map) of the collected rocks in and around the Guarda Structure. In total 99 rock samples were collected. Afterwards, 24 thin sections were made of selected rocks. Some rocks were selected to determine the unknown composition of the rock (1.5, 1.5-2, 3.6a and 4.10a). The other thin sections were used to look at the microstructures in quartz, zircon and monazite (Chapters 2, 3 and 4).

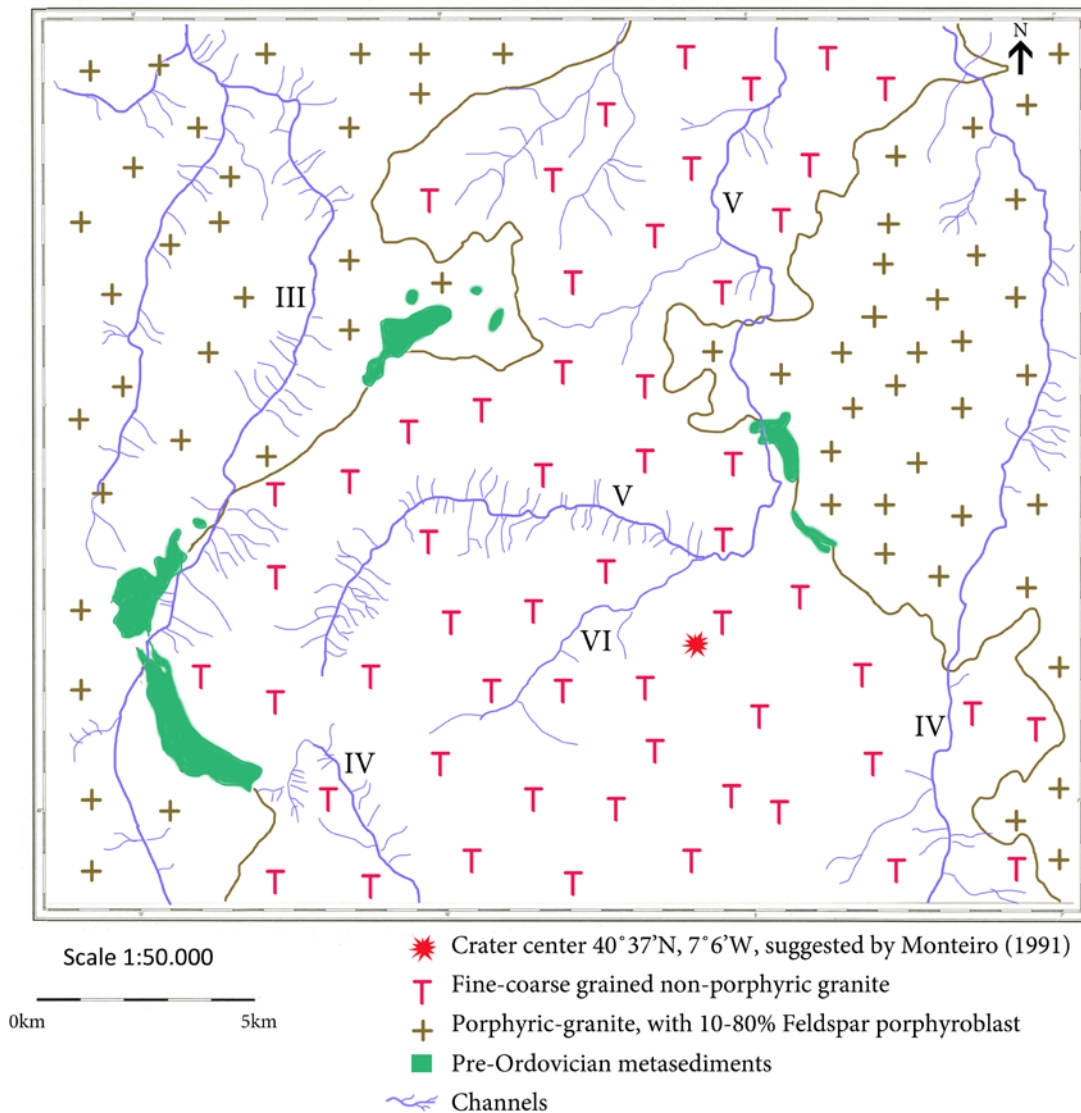


Figure 3. Simplified map of the lithology and dominant channels in the center of the Guarda Structure. There are two main types of granites; the phenocytic-and (+ granite) and the younger non-phenocytic granite (T-granite). The channels are Ribeira de Massueime (III), Ribeira das Cabras (IV), Ribeira da Pega (V) and Ribeira dos Montes (VI). Channels have another flow direction in the non-phenocytic granite compared to the phenocytic granite (Modified from Neves Ferro et al., 1962).

## 1.4 Results

### 1.4.1 Topography and shape of the Guarda Structure

Appendix 2 is an elevation map of the Guarda Structure and its surroundings. Monteiro (1991) suggested that the crater center is located at 40° 37'N and 7° 6'W. The elevation of the area varies between the 200-2000m above sea level. The topography differences of the Guarda Structure lie between 500-1000m. The structure exists of an inner part more than 10 km in diameter, one ring of higher elevation (700-1000m) with a width of 5-10km and two smaller rings, <0.1 km in width, of lower elevation (700-500m). These lower rings are characterized by incised channels. The circular form is clearly visible in the east, south and west side of the structure. At the north side the circular structure is missing.

#### 1.4.2 Field observations

The hilly landscape of the Guarda Structure is characterized by moorland like vegetation, agriculture and isolated groups of well-rounded granite boulders (figure 4). Between these well-rounded granite boulders there are large joints and the granite is very weathered. These groups of granite boulders are randomly distributed in the landscape.



*Figure 4. The landscape of the Guarda Structure is characterized by moorland-like vegetation and isolated groups of well-rounded granite boulders.*

As mentioned in paragraph 1.2.1, two main types of granites are present in the Guarda Structure. The outer ring of the structure is dominated by phenocrystic granite (++) granite); fine to coarse grained granite with mafic xenoliths and feldspatic phenocrysts. The amount of the feldspatic phenocrysts varies between 10 - 80%. Besides the feldspatic phenocrysts, quartz, biotite and muscovite are the most common minerals. In the center of the structure fine to coarse grained non-phenocrystic granite without mafic xenoliths (T-granite) is present. Quartz, feldspar, biotite and muscovite are the dominant minerals in this granite (figure 3 and 5). Along a road, east of Pinhel, the transition between ++ granite and T-granite is observed. The outcrop is characterized by chaotic magmatic flow patterns.

Both types of granite are often strongly fractured and weathered. Such outcrops are typified by granite that falls apart when you strike it with a hammer or even when touching it with your hand. There are harder round granite boulders in this softer material. These outcrops are characterized by some small faults, many joints, veins and vegetation on top. Granite in those outcrops often has an orange- brownish color (figure 6). Granite from isolated boulders (figure 4 and 6) has the same orange-brownish color and it also falls apart easily. In quarries and mines, granite is very often fresh (figure 7). Besides some joints and small faults these rocks looked fairly unaffected by fractures, faults and weathering

All granites are crosscut by different types of veins and dykes. Most common are quartz veins, varying from centimeters to meters in width. A few dark- grey/green very fine grained mafic dykes (dolerite) and pegmatite veins are found as well. These veins are up to 50 centimeters wide (figure 8). There are some other veins and dykes in the Guarda Structure that differ from ones mentioned previously and it is worthwhile mentioning these separately. In the center of the crater there is a fine grained grey dyke with white and brown fragments (figure 9). The dyke is located in T-granite and is found next to a mafic/dolerite dyke. Near the village of Cadafaz, in the outer part of the structure at ~20 km from the center, a 4 meter wide dyke crops out at the side of the road. The dyke is intruded in ++ granite (figure 10). There is a sharp transition between dyke and granite. The dyke is full of circular structures and these circular structures are full of little black spheroids.

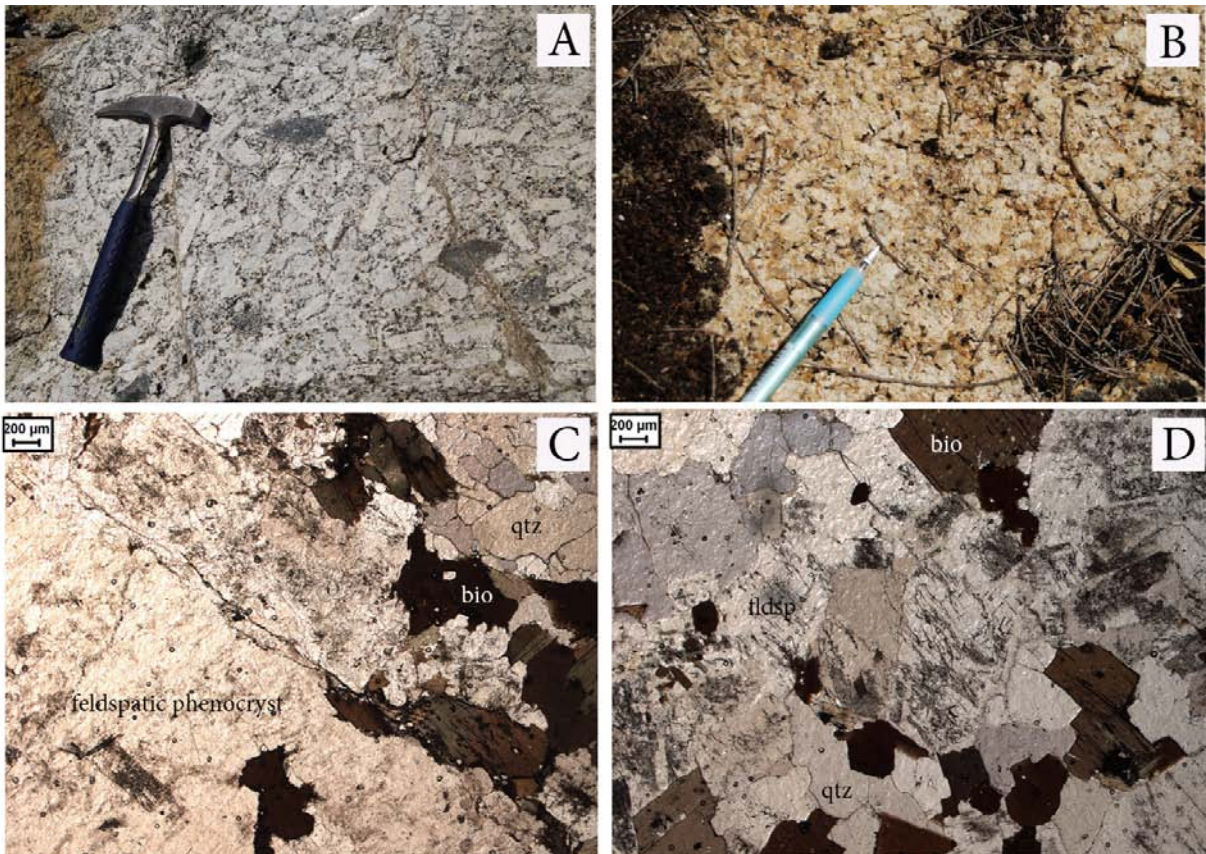


Figure 5. (a) ++ Granite with ~80% feldspatic phenocrysts. Between the feldspatic phenocrysts there are mainly quartz and mica crystals. Within the ++ granite there are often mafic fine grained xenoliths. (b) T-granite has often a yellowish color. In this granite there are neither phenocrysts nor mafic xenoliths. (c) Higher magnification of the ++ granite and (d) T-granite. Mineralogy of both granites is dominated by feldspar (fldsp), quartz (qtz) and biotite (bio).

Figure 6. (a) Granite outcrop along the road near Pera de Moco. The granite falls apart easily when striking it with a hammer. (b) Granite boulder protrudes from the outcrop. (c) Most granites, especially the well-rounded boulders have orange/brownish color.

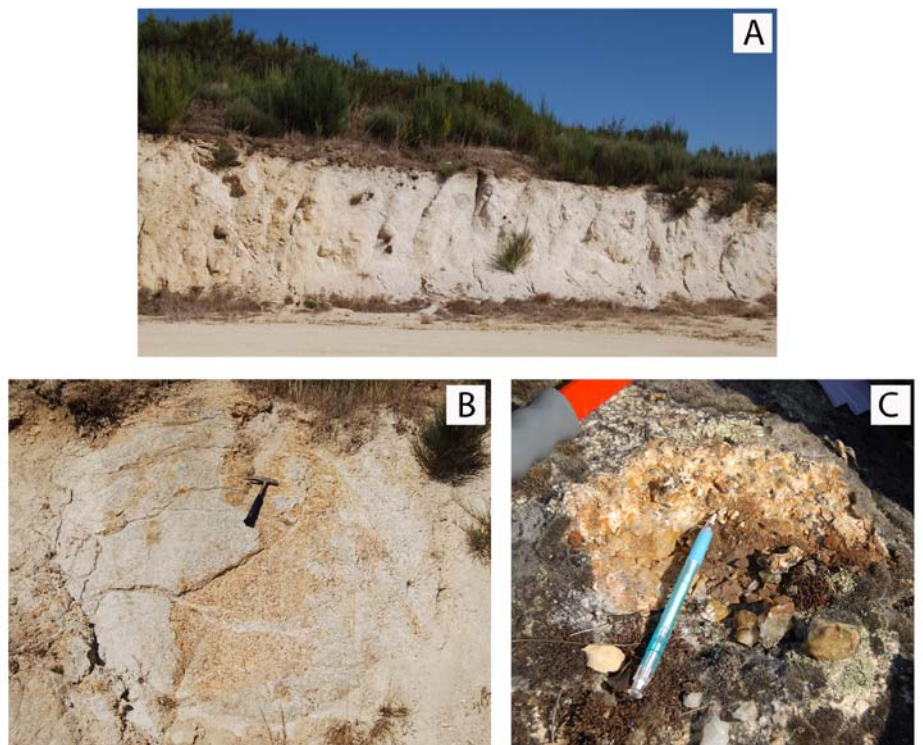




Figure 7. Quarry between Aldeia Rico and Acores with typical fresh granite with only some small faults and joints. The horizontal color differences are caused by a varying water level.



Figure 8. (a) Pegmatite vein crosscutting xenoliths and phenocrysts in ++ granite and (b) pegmatite veins crosscutting very fine T-granite. (c) Greenish mafic/dolerite dyke that crosscuts ++ granite in the quarry from Figure 7.

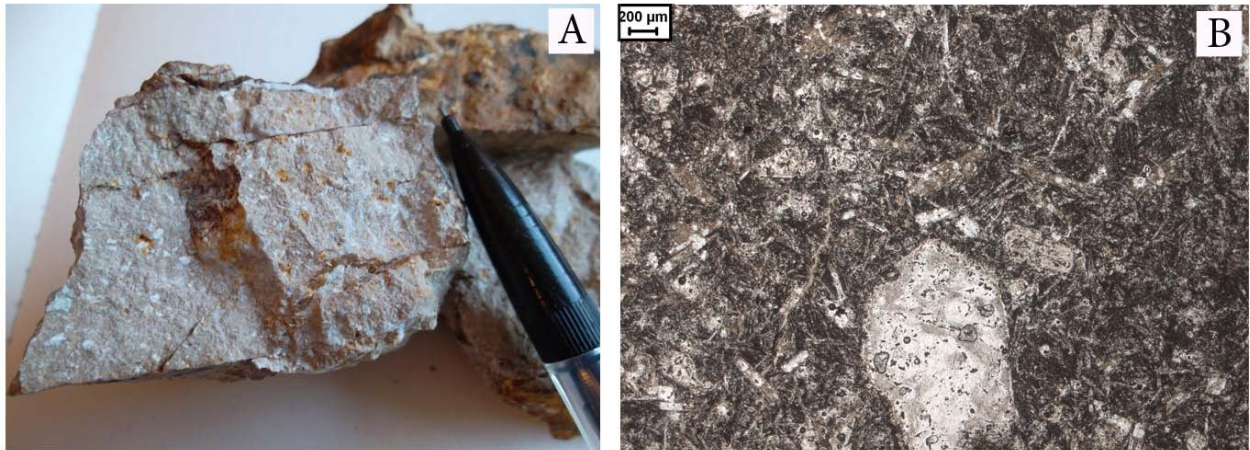


Figure 9. (a) Fine grained grey dyke from the center of the Guarda Structure with angular white and brown fragments in it. Those are not directly identifiable. The dyke is located next to a greenish mafic dyke as described in Figure 8c. (b) Plane polarized light image of the dyke. The matrix exists of small elongated crystals and the white fragments are probably weathered crystals.

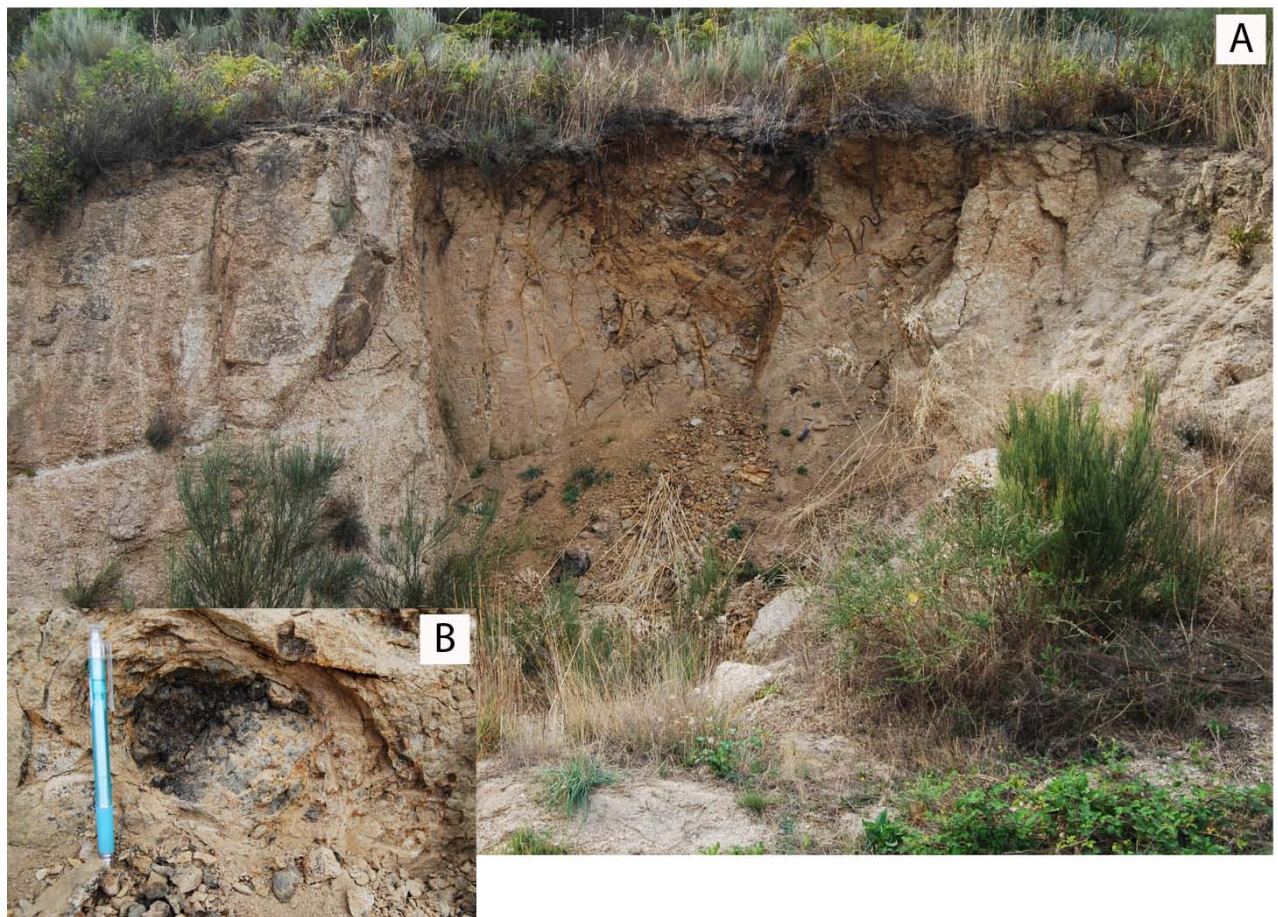


Figure 10. (a)  $\pm$  4 m wide dyke, near the village of Cadafaz, (b) composed of circular structures that are full of little black spheroids.

In the lower elevated ring, 10 km from the center, near the village of Menoita, three dark-brown veins are present in heavily fractured and soft T-granite (figure 11). The granite outcrop is

comparable to the description of figure 6. The veins seem very weathered and material is not directly recognizable. There is some black soft soil-like material in this vein.



Figure 11. (a) Brown vein in weathered T-granite near the village Menoita. The vein starts directly beneath the vegetation and extends  $\pm 7$  m downward, becoming wider when with depth. Black soft material is found within the vein.

## 1.5 Discussion

### 1.5.1 Maximum age of alleged crater

Before discussing the implications of our field observations, the maximum age of the alleged impact will be established. The minimum crystallization depth of the currently exposed granitoids ( $\sim 300$ Ma) in the Guarda Structure is 16-18km, mid-crustal levels (Neiva et al. 2011). Based on the following two principles, the maximum age will be established. (1) Before the granitoids in the Guarda Structure can be affected by a meteorite impact, tectonics must bring these rocks closer to the Earth's surface. (2) In order to presently expose these rocks, in total 16-18 km exhumation of the granitoids must have taken place.

#### 1.5.1.1 *Stephanian-Permian extensional uplift*

During the Variscan orogeny continent-continent collision shortening (380-330Ma) was rapidly followed by post-thickening extension tectonics (330-280) (Dias et al., 1998; Vissers, 1992). The onset of extension was followed by a high thermal gradient, due to detachment of the lithospheric root, resulting in melting of the lower crust (Vissers, 1992). This large scale melting resulted in granitic intrusions in many parts of the European crust (Dias et al., 1992; Neiva et al., 2011; Vissers, 1992).

Lithospheric root detachment resulted in a strongly anomalous thermal structure of the Variscan crust, and enhanced gravitational potential energy driving uplift, ongoing extension and tectonic denudation (Vissers, 1992). Vissers (1992) found late-Variscan uplift/exhumation data for the Pyrenees; the middle to upper crustal section was subjected to Stephanian-Permian (300-245Ma) extreme uplift and denudation of >10 km. According to Vissers (1992) the dynamics of the Pyrenean Variscan cannot be isolated from tectonics of the West European Variscan as a whole. The Variscan extension affected large parts of the CIZ as well (figure 9 in Vissers, 1992). Uplift and denudation in the Pyrenees, during Stephanian –Permian, can probably be applied to the granite intrusions in the CIZ. During Stephanian and Permian the granitoids were probably uplifted to a depth of 6-8 km, ~10 km above their crystallization depth.

#### **1.5.1.2 Structural uplift during meteorite impact**

Deep drilling has been done in the Puchezh-Katunki complex crater (~165 Ma), East European Platform, Russia (Masaitis, 1999). The Puchezh Katunki has a rim crater diameter of ~40 km (Ivanov et al., 1994). The drilling went through the central uplift towards a depth of 5374 m. The rocks at the top of the central uplift record shock pressures up to 45 GPa. The crystalline rocks at ~5 km depth were brecciated and faulted and experienced shock pressures between 15-20 GPa. These rocks were initially located at ~11 km below the Earth's surface. The rocks at ~600 m were originally located at a depth of ~5 km depth (Masaitis, 1999). This gives a structural uplift of ~5 km for the Puchezh-Katunki crater. Ferrière et al. (2008) found a structural uplift of 1.2 -1.5 km for the ~10.5 km in diameter Bosumtwi complex crater, Ghana. The rocks in the central uplift for the Bosumtwi crater experienced shock pressures below 30 GPa.

The Guarda Structure (35km in diameter) is slightly smaller than the Puchezh-Katunki crater and 3 times larger than the Bosumtwi crater. The structural uplift in a crater with  $\approx D$  35km is probably  $\gg 1.2-1.5$  km and  $< 5$  km. Since rocks at an original depth of ~11 km were affected during the Puchezh-Katunki impact, the granitoids in the Guarda Structure, located at 6-8 km below Earth's surface (at 245 Ma), were probably close enough to the surface to be shocked by a meteorite impact. In order to affect the granitoids in the Guarda Structure by an impact, the maximum age of the alleged crater must be  $>245$  Ma -  $<300$  Ma. During an impact these rocks may have experienced a structural uplift of ~4 km. This structural uplift together with the Stephanian –Permian uplift potentially brings the granitoids to a depth of 2-4 km.

#### **1.5.1.3 Tertiary erosion and denudation**

As discussed in the previous paragraph, the granitoids will be located 2-4 km below Earth's surface after Stephanian-Permian uplift and a meteorite impact. Since an impact, at least 2-4 km denudation must have taken place to currently expose the granitoids in the Guarda Structure. Unfortunately not much is known about post-Paleozoic denudation rates in the area of the Guarda Structure. However, there are data about denudation in the Spanish Central System (SCS) that is located in the CIZ as well.

The SCS is an ENE-WSW trending 500 km long, 50 km wide intraplate mountain range of mainly Variscan basement (granite and gneiss), extending from Portuguese coast to central Spain. The E-W trending Sierra de Gredos and the NW-SE trending Sierra de Guadarrama form the central Spanish part (Bruijne and Andriessen, 2002). During Tertiary collision between the European and African plates and the subsequent accretion of Iberia to both the European and African plate, intraplate strain was localized mainly in the Iberian chain and the SCS (Vegas et al., 1990). The thickening of the

crust in the SCS is related to N-S horizontal compressive stress in late Eocene times. Strain was concentrated in the E-W shear zone of central Iberia, which was formed by simple shear deformation caused by left-lateral translation of Iberia in the Late Cretaceous. The N-S horizontal compressive stress caused homogeneous shortening of the lower crust and the uplift of the upper crust involving faulting and rotation of crustal blocks (Vegas, 1990).

Western Sierra de Gredos is located less than 100 km from the Guarda Structure and the Sierra de Guadarrama less than 250 km (figure 2). Since the Guarda Structure is closely located to the SCS and the shear zones where the strain was concentrated during Eocene times (figure 2), the Guarda Structure probably experienced significant shortening as well. Fission track analysis on apatite crystals from SCS indicates an abrupt acceleration in cooling rates from the Middle Eocene to recent (Bruijne and Andriessen, 2001). These accelerated cooling events indicate a sudden change in denudation and/or tectonic activity. Accelerated cooling events occurred across the SCS from the Middle Eocene to recent and reveal periods of tectonic activity or dramatic changes in drainage organization or climate. These accelerated cooling events resulted in  $2.8 \pm 0.9$  km denudation in western Sierra de Gredos,  $3.6 \pm 1.0$  km in the central and eastern Sierra de Gredos and  $5.0 \pm 1.6$  km denudation in Sierra de Guadarrama (Bruijne and Andriessen, 2001). Shifting 100 km from east to west, denudation rates decrease with about 1 km. If the denudation trend is extrapolated to the west, the denudation in the Guarda Structure during the last 50 Ma might be  $\sim 1.8$  km.

$\sim 1.8$  km Tertiary denudation along with an impact and the Stephanian-Permian uplift may be enough to currently expose the granitoids and to remove the upper impact rocks that contain the distinctive shocked materials and melt. The deeper located parautochthonous rocks are probably still present in the field. The next paragraph will discuss this hypothesis.

### **1.5.2 Field observations**

In paragraph 1.5.1.2 it is suggested that the maximum age of the alleged crater lies between  $>245$  -  $<300$  Ma. In this case erosion and weathering processes have quite a long time to destroy the crater. It is not surprising that lithic and suevite breccias were not found in the Guarda Structure and neither were ejecta deposits. Parautochthonous rocks are typified by in situ breccias, dike-like intrusive bodies of allogenic breccias, pseudotachylites and shatter cones. These rocks are less vulnerable to erosion and still found in a circular pattern at deeper erosion levels (French, 1993). However, parautochthonous rocks were not found as well.

Structural uplift during an impact brecciates and fractures rocks (Masaitis, 1999). Many outcrops in the Guarda Structure look brecciated and contain small faults, joints and fractured rocks (figure 6). Even though those outcrops look brecciated, this is probably not due to an impact. The brecciated outcrops are very similar to those described by Braga et al. (2002) and are probably saprolites. Saprolite is material that is generated by chemical weathering of coarse grained rocks, especially granite. In granite, muscovite, biotite and especially feldspar weather to form secondary clay minerals such as kaolinite, metahalloysite, gibbsite and goethite (Braga et al., 2002). The latter is yellow-brownish iron oxy-hydroxide that probably gives the yellow-brownish color to weathered granite (Hurst, 1977). Saprolites are characterized by the preservation of original granitic structure, but can be broken by hand (figure 6a), a characteristic that was clearly observed in some of the outcrops of the Guarda Structure. Most outcrops have harder "corestones" within the saprolites. Those corestones already started to weather, but are harder and can only be broken by a strike of a hammer (figure 6b) (Braga et al., 2002). Braga et al. (2001) also mentioned that the landscapes found

on these rocks are characterized by isolated groups of well-rounded boulders and joint-bounded blocks forming areas of elevated relief, surrounded by deeply weathered bedrocks. The description of the landscape as well as the description of the outcrops is very comparable to what has been found in the Guarda Structure. The "brecciated" outcrops (figure 6 and 11) in the Guarda Structure cannot be linked to parautochthonous rocks in impact craters, but are easily explained by chemical weathering. The brown veins (figure 11) are probably formed by large roots of vegetation that cause chemical and mechanical weathering of the granite.

Quite a few mafic, probably doleritic, dykes (figure 8c) have been found in the structure. The dyke with the spheroidal structures (figure 10a and b) is probably a dolerite dyke as well. The spheroidal structures are most likely caused by spheroidal weathering. Spheroidal weathering is most common in uniform, hard rock which are well jointed, especially granite, dolerite and basalt (Ollier, 1971).

A breccia dyke as described by Monteiro (1991) has not been found in the center of the structure. The grey dyke that was found in the center of the Guarda Structure (figure 9) may resemble very fine breccia with angular fragments in it. However, optical microscope study of this rock shows that the angular fragments are just weathered minerals. The glassy matrix consists of very small elongated crystals. Shocked microstructures were not found in this rock. The dyke probably has a volcanic origin.

Despite intensive fieldwork, heavily brecciated granitoids and other impact rocks were not found in the Guarda Structure. The suggestion that the structure is an impact crater with a maximum age between  $>245 - <300$  Ma is probably incorrect. Some alternatives may explain the lack of impact rocks: (1) The age of the impact structure may be close to the age of the granite emplacement at 16-18 km ( $\sim 300$  Ma) and the currently exposed granitoids were (almost) not affected by an impact. Due to denudation all impact rocks are removed. (2) The Guarda Structure is not a crater and the granitoids are currently exposed due to higher denudation/uplift rates instead of structural uplift during an impact. If one of these alternatives is correct, it remains questionable why the Guarda Structure has a circular topography with an impact character. According to French (1998) the original circular outline will disappear when the impact rocks are completely eroded. This problem will be discussed in the next two paragraphs.

### **1.5.3 Topography and shape**

The circular topography of the Guarda Structure resembles a complex impact structure (appendix 2). The different rings of high and low elevation could be interpreted as a complex series of concentric rings and basins that are quite often found in complex multi-ring craters (French, 1993). The shape of the structure is asymmetric. The west and south side of the structure both have a very circular shape, but at the east side one of the rings is much wider. Post-impact tectonic deformation can deform the original circular shape (French, 1993). From Eocene to Early Miocene, the closely located Sierra de Gredos experienced compression in response to the perpendicular N-S stress field of the Pyrenean compression (Bruijne and Andriessen, 2002). The east side of the structure might have experienced this compression as well, resulting in flattening of the eastern side and an asymmetrical structure. In the north part of the structure the outer rings are missing. The missing parts of the structure could be explained by processes of geological destruction.

#### **1.5.4 Drainage network in the Guarda Structure**

The Rio Côa and its side channels flow from south to north and have a total drainage area of 2520 km<sup>2</sup>. The lithology of the drainage area is dominated by granitoids (73%) and metasediments (24%) (figure 12) (Jorge, 2009). Because the channels mainly incise bedrock, these channels are bedrock channels. The Guarda Structure is located within the drainage area of the Rio Côa. Figure 12a shows the topography of the Guarda Structure. The circular topography is strongly related with the drainage network, having lower elevations at locations where channels incised (Figure 12 and Appendix 2).

##### **1.5.4.1 Anomalous Drainage pattern**

The drainage network of the total drainage area seems to be dendritic (figure 12b). Dendritic patterns are commonly formed on uniformly resistant crystalline rocks (Selby, 1985). In the Guarda Structure the drainage pattern is anomalous; the Rio Côa (I), Rio Noéme (II), Ribeira de Massueime (III), Ribeira das Cabras (IV) and Ribeira da Pega (V) form a circular / arcuate drainage network (figure 12). The design of most drainage networks, and especially of the lower order channels and bedrock channels (both the case in the Guarda Structure), is controlled by regional geological structures, such as faults, folds, joints, domes and craters (e.g. Tinkler and Wohl, 1998; Selby, 1985). Arcuate, circular and centripetal drainage patterns could be related to meteorite impact craters (Selby, 1984; Twidale, 2004). For example in the Neoproterozoic ignimbrites of the Gawler Ranges, South Australia, orthogonal drainage systems are most common, but around the Acraman impact crater, arcuate channels are present (Twidale, 2004). The circular drainage network in the Guarda Structure is compatible with the presence of a multi-ring meteorite crater, having channels incised in the basins. However the lack of any field evidence for an impact more likely points to another geological structure that designed the circular drainage network.

Satellite images show that both types of granitoids contain two dominant sets of joints/fractures; NNE-SSW and NW-SE. Sets of joints and fractures often control the drainage pattern in an area, but generally form an angular drainage pattern instead of circular patterns (e.g. Twidale, 2004; Selby, 1985). The joint sets are probably not the cause of the circular drainage pattern.

##### **1.5.4.2 Dome-like structure**

Around dome-like structures (especially where alternating resistant and weak beds exist), annular drainage patterns develop (Selby, 1985). Annular drainage patterns consist of many curved channels, giving a circular characteristic to the landscape. The granitoids in the Guarda Structure might have a dome-like structure, forcing the channels to incise in a circular pattern. The dome-like structure could have formed after granite emplacement, so <300 Ma. There is no information about <300 Ma deformation in the Guarda Structure. However, there is data of Sierra da Gredos, Sierra da Guadarrama and the Pyrenees (for detailed information see paragraph 1.5.2).

During the Alpine deformation stage, dome-like structures were neither formed in the Sierra da Gredos nor in the Sierra da Guadarrama. E-W-and NE-SW-trending faults in both Sierras mainly control geomorphic features such as elongated depressions and ranges, the high-standing blocks that constitute the ranges or individual sierras and the drainage pattern. The shortening was caused by faulting and rotation of crustal blocks, forming elongated depressions and ranges (e.g. Vegas et al., 1990; de Bruijne and Andriessen, 2001). In areas similar to the Sierra da Gredos, where crystalline and metamorphic rocks are the dominant lithology and different sets of faults intersect, contorted drainage patterns exist (Selby, 1985).

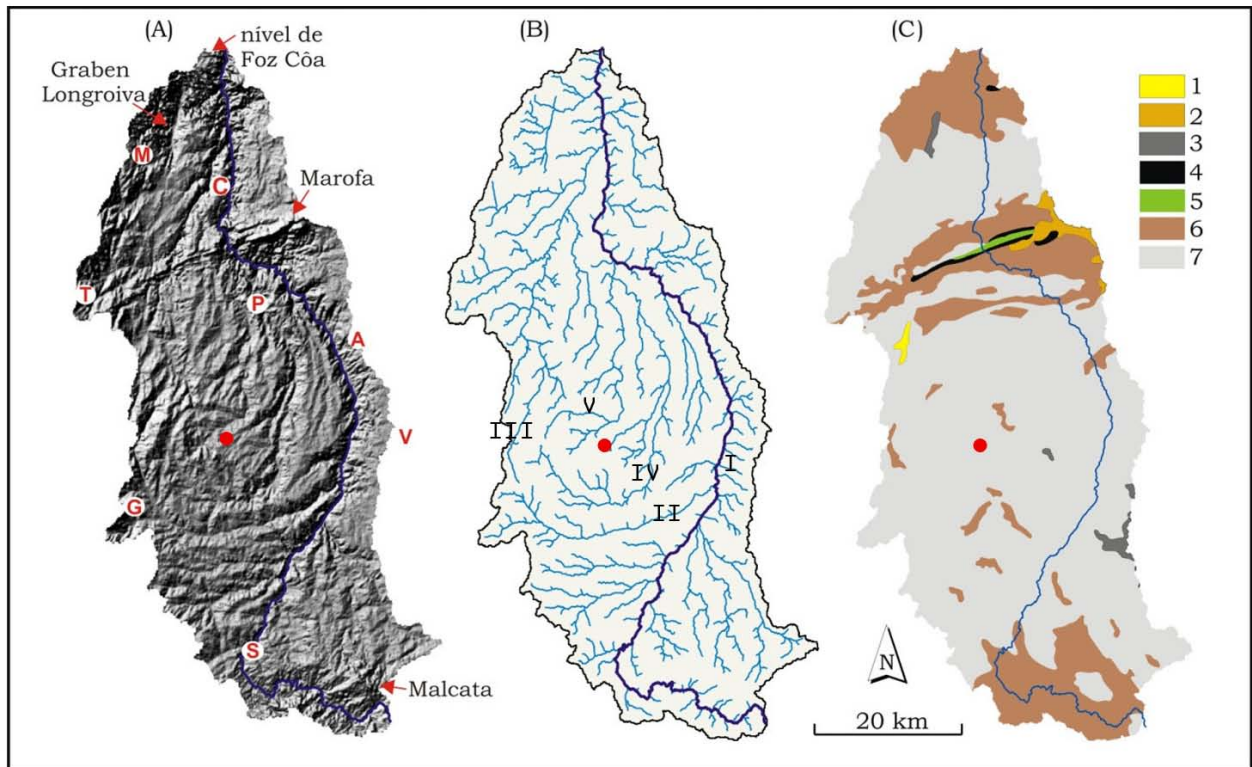


Figure 12. Different maps of the drainage area of the Rio Côa. (a) The topography of the Guarda Structure is visible between Guarda (G), Pinhel (P) and Almeida (A), with the centre of the structure as suggested by Monteiro (1991) shown by a red dot. (b) The drainage network could be correlated to the topography of the Guarda Structure. The dominant channels in the structure are the Rio Côa (I), Rio Noéme (II), Ribeira de Massueime (III), Ribeira das Cabras (IV) and Ribeira da Pega (V). (c) The lithology of the drainage area consists of: Alluvial sediments (1), slope deposits (2, 3), quartzite (4), shales (5), shales and graywackes (6), granitoids (7) (Modified from Jorge, 2009).

The Stephanian – early Permian (300Ma – 280Ma) crustal extension stage (latest stage of the Variscan orogeny) in the Pyrenees lead to extensional deformation, including tilted half grabens, spaced metamorphic domes and gneissic core complexes mantled by crustal scale shear zones (Vissers, 1992). A mantled gneiss dome forms when granite intrudes in metamorphosed sediments and metamorphosed intrusive rocks (Twiss and Moores, 2007). Because the Variscan extension took place in the CIZ as well, a similar dome may have formed in the Guarda Structure. As was deduced from Vissers (1992), the younger T-granite (300Ma) started to uplift immediately after crystallization. The T-granite intruded in pre-Ordovician metasediments, that were deformed during the Variscan collision stage, and in the ++ granite. The transition between ++ granite and T-granite is characterized by chaotic flow patterns. The T-granite intrusion probably melted parts of the older ++ granite. No gneiss is observed at all, probably because at the moment of T-granite intrusion, ++ granite was just ~5 Ma and not deformed at all. The semi-circular form of the T-granite and the pre-Ordovician metasediments in between the two granites may suggest that the T-granite formed a dome-like structure (figure 3). The metasediments might be the last relicts of a dome-like structure. The drainage pattern could be influenced by the dome structure.

### **1.5.4.3 Lithology**

Lithology differences seem to influence the channel pattern (figure 3 and 11) and might have caused the anomalous circular drainage pattern. Channels have a more erratic pattern when incising the shales and graywackes. The anomalous circular channel pattern mainly formed within the inner non phenocrystic T-granite and not within the phenocrystic ++ granite (figure 3). Larger grain sizes and formation of monomineralic aggregates in granite have a negative effect on the quality of the rock (Äkkeson et al., 2001) and compared to quartz crystals, feldspar crystals are more vulnerable to chemical weathering (Braga et al., 2002). The ++ granite, that mainly consists of feldspatic phenocrysts (up to 80%), are probably less resistance than the T- granite that is generally finer grained and consists mainly of feldspar and quartz. Due to the strength differences, the more resistant T-granite could have formed a harder protruding dome-like inner area, forcing the channels to incise around this area.

### **1.5.5 The Guarda Structure and related mass extinctions**

The three largest mass extinctions of the past 500Ma; the Permian-Triassic (~251.4 Ma), Triassic-Jurassic (~199.6 Ma) and Cretaceous-Tertiary (~65 Ma) are often linked to large asteroid impacts (e.g Becker et al. 2001, Becker et al. 2004, Pálffy et al., 2000; Schulte et al. 2010; White and Saunders, 2005). For example, the K-T extinction was triggered by a major asteroid impact that formed the 180-200 km in diameter Chicxulub crater, Mexico (Schulte et al., 2010). However researches still struggle with the explanations for the other two extinction events..

Becker et al (2001) proposed an asteroid impact that caused the P-T extinction, based on trapped noble gases within fullerenes from P-T boundary sediments. Becker et al. (2004) suggested the Bedout High, Australia as possible end-Permian impact structure, although Glikson (2004) questioned this and concluded that the Bedout structure is not an impact crater.

Different explanations were suggested to explain the T-J extinction including meteorite impacts, but there is still no convincing explanation (e.g. Hodych & Dunning, 1992; Schmieder et al., 2010) The Manicouagan Crater of Quebec, Canada, was dated  $214 \pm 1$  Ma and failed to explain this mass-extinction (Hodych & Dunning, 1992). The Rochechouart impact structure in the NW Massif Central, France is determined to be  $201 \pm 2$  Ma and could be perfectly correlated to the Triassic-Jurassic extinction (Schmieder et al., 2010). Since the Chicxulub crater is ~200 km in diameter, the Rochechouart, 25-50 km in diameter, seems too small to cause such a worldwide mass-extinction. Since the Guarda Structure has a maximum age of >245 - <300 Ma, it might be linked to one of the mass-extinctions

Suggestions that impacts are the primary cause of significant global mass extinctions are deficient (White and Saunders, 2005). White and Saunders (2005) suggest: "There could have been as many as 18 Chicxulub-sized impacts and 60  $D \geq 100$  km impacts during the Phanerozoic. This does not rule out impacts as being a contributory factor in some mass extinctions, but it does suggest that the outcome is strongly dependent upon the condition of the system at the time of impact, i.e., whether the biosphere was already in a stressed state due to the effects of flood basalts, or other terrestrial processes such as sea level change."

### **1.6 Conclusion and further research**

The circular topography in combination with the circular drainage pattern could easily be interpreted as impact crater phenomena with a maximum age of >245 Ma - <300 Ma. However a dome-like

structure formed during the late-Variscan extension or by lithology differences, could also explain the circular characteristic of the structure and the drainage pattern. Lack of impact rocks might be caused by major denudation, but this remains speculative since data from other locations are used for denudation estimates. Before a definite conclusion can be made about the Guarda Structure, much more research must be done to the rocks from the structure. In Chapter 2, 3 and 4, potential shock microstructures in quartz, zircon and monazite from the Guarda Structure are analyzed and compared to shocked crystals from the Ries Impact Crater, Germany and the Vredefort Dome, South Africa. Shock microstructures in quartz, zircon and monazite could form up to deep levels in the crater (e.g. Masaitis, 1999; Moser, 2011). Although most rocks in the Guarda Structure are very eroded and weathered and possible impact structures might be unrecognizable, microstructures in quartz and zircon could be still present.

## References

- Åkesson, U., Lindqvist, J., Göransson., 2001, Relationship between texture and mechanical properties of granites, central Sweden, by use of image-analysing techniques, *Bulletin of Engineering*, 60, p. 277-284
- Azevedo Do Rosário, M., Valle Aguado, B., 2006, Origem e Instalação de Granitóides Variscos na Zona Centro-Ibérica, p. 107-122
- Becker, L., Poreda, R. J., Hunt, A.G., Bunch, T.E., Rampino, M., 2001, Impact Event at the Permian-Triassic Boundary: Evidence from Extraterrestrial Noble Gases in Fullerenes, *Science*, 291, p. 1530-1533
- Becker, L., Poreda, R. J., Basu, A. R., Pope, K. O., Harrison, T. M., Nicholson, C., and Iasky, R. 2004. Bedout: A possible end-Permian impact crater offshore of Northwestern Australia, *Science* 304, p. 1469–1476
- Braga Sequeira, M.A., Paquet, H., Begonha, A., 2002, Weathering of granites in a temperate climate (NW Portugal): granitic saprolites and arenization, *Catena*, 49, p. 41-56.
- Bruijine de, C.H., Andriessen, P.A.M., 2002, Far field effects of Alpine plate tectonism in the Iberian microplate recorded by fault related denudation in the Spanish Central System, *Tectonophysics*, 349, p. 161-184.
- Dias, G., Letierrier, J., Mendes, A., Simões, P.P., Bertrand, J.M., 1998, U-Pb zircon and monazite geochronology of post-collisional Hercynian granitoids from the Central Iberian Zone, Northern Portugal, *Lithos*, 45, p. 345-369.
- Ferrière, L., Koeberl, C., Ivanov, B.A., Reimold, W.U., 2008, Shock Metamorphism of Bosumtwi Impact Crater Rocks, Shock Attenuation, and Uplift Formation, *Science*, 322, p. 1678-1681.
- French, B.M., 1998, Traces of Catastrophe: *A Handbook of Shock-Metamorphic Effects in Terrestrial Meteorite Impact Structure*, LPI Contribution No. 954, Lunar and Planetary Institute, Houston, 120p.
- Glikson A., 2004, Comment on “Bedout: A possible end-Permian impact crater offshore of Northwestern Australia.” *Science*, 306, p. 613b.
- Grieve, R.A., 1991, Terrestrial impact – The record in the rocks, *Meteoritics*, vol. 26, p. 175-194.
- Hodych, J.P., Dunning G.R., 1992, Did the Manicouagan impact trigger end-of-Triassic mass extinction?, *Geology*, 20, p. 51-54.
- Hurst, V.J., 1977, Visual estimation of iron in saprolite, *GSA Bulletin*, v. 88, 2, p. 174-176
- Ivanov, B. A., Kocharyan, G. G., Kostuchenko, V. N., Kirjakov, A. F., & Pevzner, L. A., 1994, Puchezh-Katunki Impact Crater: Preliminary Data on Recovered Core Block Structure, *Lunar and Planetary Science*, 27, p. 589.
- Jorge, M.A.G., 2009, Geomorfometria da bacia hidrográfica do rio Côa, thesis, 53p.
- Julivert, M., Fontboté, J.M., Ribeiro, A., Conde, L., 1974. Mapa Tectónico de la Península Ibérica y Baleares. Escala 1: 1,000,000. Memoria Explicativa. Instituto Geológico y Minero de España, Madrid, 113 pp.
- Masaitis, V.L., 1999, Impact structures of northeastern Eurasia: The territories of Russia and adjacent countries, *Meteoritics & Planetary Science*, 34, p. 691-711

- Monteiro, J.F., 1991, The Guarda Circular Structure: A Possible Complex Impact Crater (Abstract), ©Lunar and Planetary Institute, NASA Astrophysics Data System.
- Moser, D. E., Cupelli, C. L., Barker I. R., Flowers, R. M., Bowman, J. R., Wooden, J., and Hart, J. R., 2011, New zircon shock phenomena and their use for dating and reconstruction of large impact structures revealed by electron nanobeam (EBSD, CL, EDS) and isotopic U-Pb and (U-Th) / he analysis of the Vredefort dome, *Canadian Journal of Earth Sciences*, 48, p.117–139.
- Neiva Ribeiro, A. M., Ramos, J.M.F., 2010, Geochemistry of granitic aplite-pegmatite sills and petrogenetic links with granites, Guarda Belmonte area, central Portugal, *Eur. J. Mineral*, 22, p. 837-854.
- Neiva Ribeiro, A. M., Silva, P.B., Corfu, F., Ramos, J.M.F., 2011, Sequential melting and fractional crystallization: Granites from Guarda-Sabugal area, central Portugal, *Chemie der Erde*, 71, p. 227-245.
- Neves Ferro, M., Cândido de Medeiros, A., Carvalhosa, A., da Piedade Pilar, L., Andrade Monteiro, P., Caraca Valenta, A.J., Costa Castro, J.F., Isidoro Rodirques, F., Machado L., Pardal Letras, R.M., Remigio da Silva, A., Simões de Carvalho, O., Sousa Soeiro, M.P., 1962, Carta Geológica de Portugal 18A Vila Franca das Naves. Escala 1: 50,000, Instituto Geografico e cadastral.
- Ollier, C. D., 1971. Causes of spheroidal weathering. *Earth-Sci. Rev.*, 7, p. 127-141.
- Pálffy, J., Mortensen, K.J., Carter, E.S., Smith, P.L., Friedman, R.M., Tipper, H.W., 2000, Timing the end-Triassic mass extinction: First on land, then in the sea?, *Geology*, 28, p.39-42.
- Sant’Ovaia, H., Olivier, P., Ferreira, N., Noronha, F. Leblanc, D., 2010, Magmatic structures and kinematic emplacement of the Variscan granites from Central Portugal (Serra da Estrela and Castro Daire areas), *Journal of Structural Geology*, 32, p. 1450-1465.
- Selby, M.J., 1985, *Earth’s changing Surface: An Introduction to Geomorphology*, Clarendon Press Oxford, 607p.
- Schulte, P., Alegret., L., Arenillas, I., Arz, J.A., Barton, J., Bown, P.R., Bralower, T.J., Christeson, G.L., Clages, P., Cockell., C.S., Collins, G.S., Deutsch, A., Goldin, T.J., Goto, K., Grajales-Hishimura, J.M., Grieve, R.A.F., Gulick, S.P.S., Johson, K.R., Kiessling, W., Koeberl, C., Krink, D.A., MacLeod, K.G., Matsui, T., Melosh, J., Montanari, A., Morgan, J.V., Neal, C.R., Nichols, D.J., Norris, R.D., Pierazzo E., Ravizza, G., Rebolledo-Vieyra, M., Reimold W.U., Robin, E., Salge, T., Speijer, R.P., Arthur R. Sweet, Urratia Fucugauchi, J., Vajda, V., Whalen, M.T., Willumsen, P.S., 2010, The Chicxulub Asteroid Impact and Mass Extinction at the Cretaceous-Paleogene Boundary, *Science* 327, p. 1214-1218
- Schmieder, M., Buchner, E., Schwarz, W.H., Trieloff, M., Lambert, P., 2010, A Rhaetian  $^{40}\text{Ar}/^{39}\text{Ar}$  age for the Rochechouart impact structure (France) and implications for the latest Triassic sedimentary record, *Meteoritics & Planetary Science*, 45, p. 1225–1242.
- Tinkler, K.J., Wohl, E.E., Editors, 1998, Rivers Over Rock: Fluvial Processes in Bedrock Channels, Geophysical Monograph 107, American Geophysical Union Washington DC, 323 p.
- Twidale, C.R., 2004, River patterns and their meaning, *Earth-Science Reviews*, v. 67, l. 3-4, p. 259-218.
- Twiss, R.J., Moors, E.M., 2007, *Structural Geology* 2<sup>nd</sup> edition, W.H. Freeman and Company New York, 736p.
- Vegas a, R., Vázquez, J.T., Suriñach E., Marcos, A., 1990, *Tectonophysics*, 184, p. 367-378
- Vissers, R.L.M., 1992, Variscan extension in the Pyrenees, *Tectonics*, v. 11, p. 1369-1384
- White, R.V., Saunders, A.D., 2004, Volcanism, impact and mass extinctions: incredible or credible coincidences?, *Lithos*, 79, p. 299– 316.

## Chapter 2: Planar microstructures in quartz

### 2.1 Introduction

As discussed in chapter 1, typical impact rocks such as shatter cones, suevite breccia and pseudotachylites are not observed in and around the Guarda Structure, but these impact rocks may be eroded and denudated. Other impact criteria must be found to prove whether the Guarda Structure is an impact crater or not. An alternative is to study shock effects on the scale of mineral grains. Stöffler and Langenhorst (1994) suggested quartz as the most important mineral for mineral shock effect studies. Next to feldspar, quartz is the most abundant rock-forming mineral in crustal rocks and quartz exhibits the greatest variety of shock effects compared to other minerals. Shock features in quartz include; high pressure polymorphs (coesite and stishovite), diaplectic glasses, planar fractures (PFs), planar deformation features (PDFs), lechatelierite, mosaicism (e.g. French, 1998; Stöffler and Langenhorst, 1994) and ballen quartz (Ferrière et al., 2009). The most common and most studied shock features in quartz are shock lamellae or planar deformation features (PDFs) (e.g. Stöffler and Langenhorst, 1994; Langenhorst, 2002; Goltrant et al., 1992; Hamers and Drury, 2011). Even on great depths within a crater PDFs are still observed (e.g. Masaitis, 2004 and Ferrière et al., 2008). This chapter focuses on the presence of possible PDFs in quartz grains from the Guarda Structure. The aim is to search for potential planar shock structures in quartz crystals from the Guarda Structure by using an optical microscope and SEM techniques. The results from the Guarda Structure will be compared to shock microstructures from the Ries Impact Crater, Germany.

#### 2.1.1 Shock Lamellae (PDFs)

PDFs in quartz occur as single or multiple closely spaced (<2  $\mu\text{m}$ ) sets of planar thin lamellae penetrating through a whole grain. PDFs do not cut across grain boundaries, fractures or planar fractures, unless these are formed at a later stage than the PDFs (Stöffler and Langenhorst, 1994). PDFs appear remarkably straight, sharp and continuous when detected by the optical microscope (Goltrant et al., 1992). They form parallel to defined crystallographic planes (Vernooij and Langenhorst, 2005). Most important sets are orientated parallel to rhombohedral planes, {1012} and {1013}, and the basal plane (0001) (e.g. Goltrant et al., 1992; Langenhorst, 2002). In total 18 sets of PDFs can be detected, which are

*Table 1. Most abundant PDF orientations in shocked quartz (modified from Langenhorst 2002).*

Miller indices {hkil}, symbol	Form	Azimuth angle
{0001}	Basal pinacoid	0°
{1013}, {0113}	Rhombohedron	30°
{1012}, {0112}	Rhombohedron	30°
{1011}, {0111}, {1010}	Rhombohedron	30°
{1010}	Hexagonal prism	30°
{4041v}, {0441}	Rhombohedron	30°
{5160}, {6150}	Ditrigonal prism	40°
{5161}, {6151}	Trigonal	40°
{6151}, {5161}	Trapezoedron	
{3141}, {4311}	Trigonal	45°
{4131}, {1341}	Trapezoedron	
{2131}, {3211}	Trigonal	50°
{3121}, {1231}	Trapezoedron	
{1122}, {2112}	Trigonal dipyramid	60°
{1121}, {2111}	Trigonal dipyramid	60°
{1120}, {2110}	Trigonal prism	60°
{2241}, {4221}	Trigonal dipyramid	60°

summarized in table 1 (e.g. Langenhorst, 2002).

PDFs are generated at shock pressures between 7-35 GPa. At lower stress regime (<30GPa) PDFs appear to be an excellent barometer, because post-shock annealing converts PDFs in decorated types, but PDF orientations are unaffected (e.g. French, 1998; Langenhorst, 2002). PDFs in directions {1012} and {1013} are critical when determining the shock pressures. Weak to moderate shock stages mainly produce PDFs in the {1013} direction. Sets along the {1012} plane form during (very) high shock stages (Stöffler and Langenhorst, 1994). For more detailed information about the directions of PDFs, I refer to Stöffler and Langenhorst (1994).

Most PDFs are thin (<200-300 nm) lamellae that consists of amorphous silica mixed with various amounts of nanoscale crystallites of quartz (Langenhorst, 2002). The transformation into these amorphous lamellae is probably driven by the front of the shock wave (Goltrant et al., 1992). Goltrant et al. (1992) proposed a simple PDF-formation model, based on the pressure dependence of the shear modulus. PDFs result from elastic instabilities of the shear modulus of the quartz structure at high pressures. This model predicts that the density of PDFs should noticeably increase with shock intensity. The model is in accordance with field observation of for example Ferrère et al. (2008)

PDFs in the basal plane are not amorphous lamellae, but mechanical Brazil twins, probably generated by high deviatoric stresses accompanying the shock wave. (Goltrant et al., 1992). Compared to other PDFs, mechanical Brazil twins form at a relatively low shock pressures (Stöffler and Langenhorst, 1994).

### **2.1.2 PDFs versus Tectonic Deformation lamellae**

As soon as typical impact field evidence is eroded, it's crucial that PDFs are recognized and that they are correctly interpreted. PDFs may be confused with lamellae produced by tectonic deformation, called tectonic deformation lamellae (e.g. Hamers and Drury, 2011; Vernooij and Langenhorst, 2005). Deformation lamellae in quartz form due to slow tectonic processes (Vernooij and Langenhorst, 2005). They are narrow planar microstructures with apparent widths of about 0.5-10  $\mu\text{m}$  and are aligned along sub-basal planes (Drury, 1993). The confusion of deformation lamellae with shock lamellae regularly happened in the past, leading to different interpretation of the same lamellae (e.g. Becker et al., 2004 versus Glikson, 2004; Retallack et al., 1998 versus Langenhorst et al., 2005).

#### **2.1.2.1 Optical Microscopy**

In general, tectonic lamellae develop with a maximum of two sets per grain and are thicker, more curved and more widely spaced than PDFs (Hamers and Drury, 2011), but in some cases both lamellae could look surprisingly similar in the optical microscope (Vernooij and Langenhorst, 2005). Just like PDFs, deformation lamellae, can be decorated with fluid inclusions (Vernooij and Langenhorst, 2005). Although both types of lamellae could look similar in the optical microscope, the origin of PDFs and deformation lamellae are very different. While shock wave produced PDFs consist of amorphous silica (Goltrant et al., 1992), tectonically produced deformation lamellae in quartz are defined by recovered dislocation walls, elongated subgrains or bands of variable dislocation density and inclusion content (Drury, 1993).

#### **2.1.2.2 SEM analyses**

A distinction between PDFs and deformation lamellae can be made with a Scanning Electron Microscope (SEM) (e.g. Gratz et al., 1996; Hamers and Drury, 2011). Gratz et al. (1996) etched natural

shocked and tectonically deformed samples with hydrofluoric acid or hydrothermal alkaline solution, before putting them into a SEM. Gratz et al. (1996) noticed that high-strain-rate shock waves generate PDFs, narrow lamellae of  $<1 \mu\text{m}$  filled with amorphous silica, that are intensely attacked by the etchants. In contrast, slow-strain-rate tectonic deformation produces semi-linear and widely spaced arrays ( $>>1 \mu\text{m}$ ) of dislocation loops that are not glass filled. The deformation lamellae are only weakly and irregularly attacked by etchants.

Hamers and Drury (2011) used a cathodoluminescence (CL)-detector in the SEM to determine the difference between PDFs and deformation lamellae. They showed that both grayscale (limited wavelength) and composite color SEM-CL images provide strong criteria for distinction between PDFs and tectonic deformation lamellae in quartz. Table 2 summarizes the main characteristics of PDFs compared to tectonic deformation lamellae. Figure 1, shows examples of shock and tectonic lamellae.

Table 2. Cathodoluminescence characteristics for planar deformation features and tectonic deformation lamellae (modified from Hamers and Dury, 2011).		
	<b>Planar deformation features</b>	<b>Tectonic deformation lamellae</b>
Number of sets	(usually) multiple	Usually one, rarely two
“Sharpness”	Very well-defined	Hard to distinguish lamellae from host quartz
Thickness	(usually) thin	(usually) much thicker
Spacing	Variable, but usually closely spaced	Closely spaced
Straightness	Straight	Slightly curved, sub planar

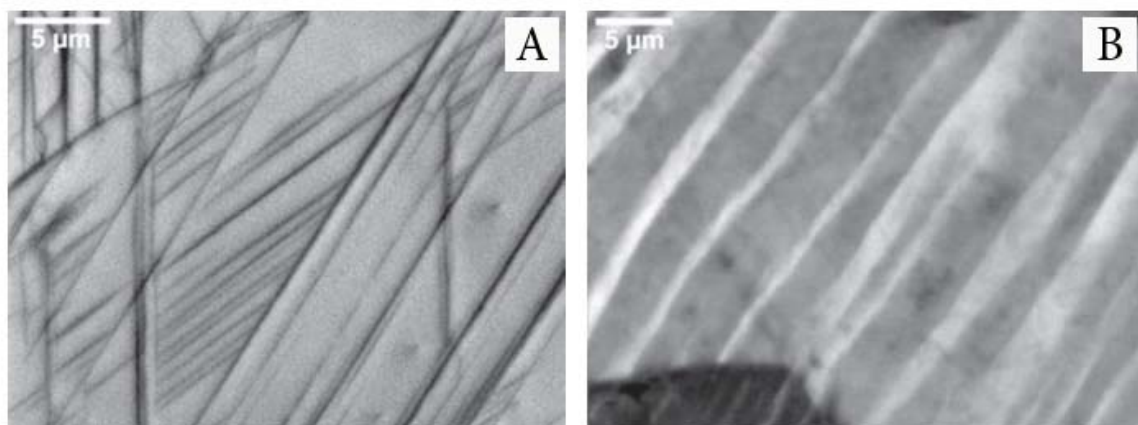


Figure 1. (a) Grayscale CL-image of PDFs in a quartz grain from the Ries Impact Crater, Germany. (b) Grayscale CL-image of tectonic deformation lamellae from the Flinders Range, Australia (Hamers & Drury 2011).

### 2.1.3 Planar Microstructures in quartz from the Guarda Structure

Monteiro (1991) claimed that he found planar elements and decorated planar features (figure 2) in some quartz grains from granite fragments in a breccia dyke (described in chapter 1, paragraph 1.5.2). The breccia dyke is located somewhere in the central area of the structure, containing various fragments of the different lithology present in the Guarda Structure: granites, gabbro, dolerite rocks and pre-Ordovician schists. In the granites from the central region of the structure, Monteiro (1991) found evidence of shock metamorphic features as well. He detected monomict brecciation and remnants of decorated planar elements in quartz. These quartz grains are intensely fractured with some rotation and displacement and the resulting spaces between individual fragments are filled

with matrix of serictic composition. Exact locations of the samples are not known, neither are the methods used to make figure 2.

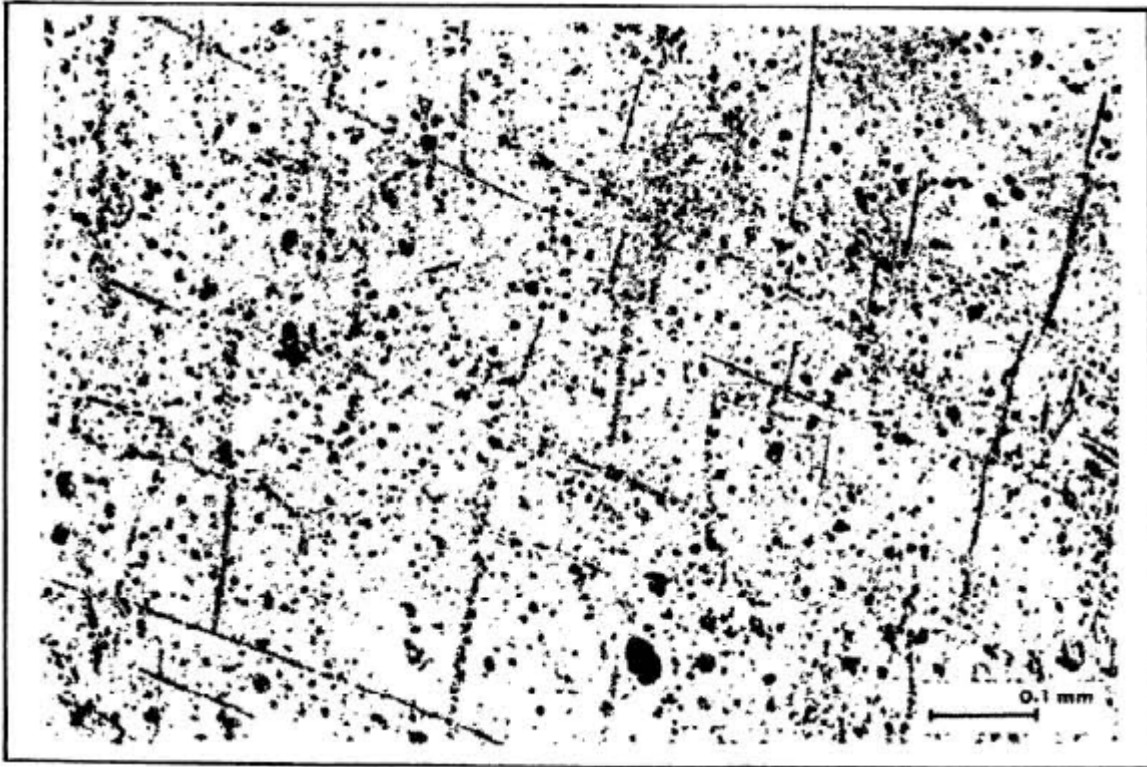


Figure 2. Planar features in a quartz grain from a granite fragment of the breccia dyke found in the central part of the structure. It's not known which method was used to make this image (Monteiro, 1991).

## 2.2 Samples and Methods

To study microstructures in quartz, thin sections have been made of the Portuguese granites. Appendix 1 is an overview of all rocks and thin sections. The thin sections were examined in the light microscope. Samples 3.3b, 2.5a and 1.6g contained quartz with planar microstructures and were selected to be analyzed in the Scanning Electron Microscope (SEM). In total two crystals of sample 3.3b, four of sample 2.5a and six of sample 1.6g were analyzed.

The system used for SEM-analysis is the Philips XL30S FEG SEM. Figure 3 shows the sample holder within the SEM. During analysis a high-energy electron beam is focused on the sample, which leads to emission of light photons, X-rays and electrons that are received by several detectors. During analyses an acceleration voltage of 5 – 20 kV was used. To determine the chemical composition of minerals, energy-dispersive X-ray spectroscopy was used. Cathodoluminescence and backscattered electron images were made of most crystals observed in the SEM. The thin sections were coated with a thin carbon layer to prevent charging during SEM-analyses.

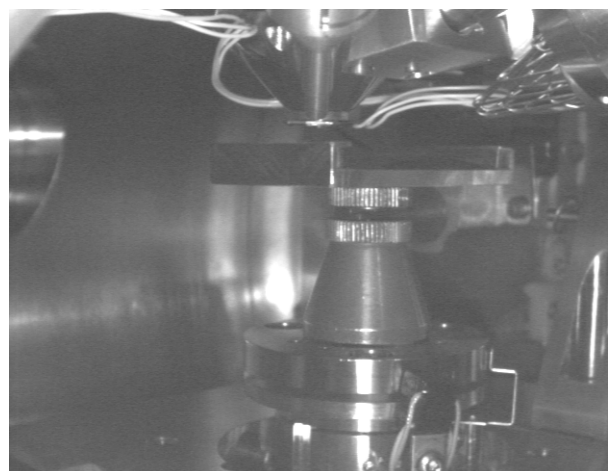


Figure 3. SEM chamber with sample holder and detectors

### **2.2.1 SEM-background**

*Energy dispersive X-ray spectroscopy* - For Energy-dispersive X-ray (EDX-)spectroscopy an EDX-detector has been used. EDX-spectroscopy is done to determine the chemical compositions of individual crystals. A high-energy electron beam is focused on a specific crystal or part of a crystal. The atoms within the crystal contain unexcited electrons in specific electron shells, but due to the incident beam these electrons may be excited and jump into another shell leaving behind an electron hole. This electron hole is filled by another electron from a higher-energy shell. This jump results in an energy difference that is released in the form of an X-ray. The EDX-detector measures these X-rays energies. A specific energy belongs to a specific atom, so the chemical composition of the crystal can be determined.

*Cathodoluminescence* - For cathodoluminescence images a Centaurus CL-detector (K.E. Developments Ltd, Cambridge, UK) has been used. When the high-energy electron beam hits the sample, electrons in atoms get excited to a higher energy level. When those excited electrons return to their ground state, photons with infrared, visible and ultraviolet wavelengths can be emitted. Wavelength and intensity of the emitted photons are different for each mineral composition and can be detected by the CL-detector. The CL-detector used for this research has a wavelength detection range of 300-650 nm with a peak at 420 nm and is thus most sensitive to blue to violet light

*Backscattered electrons* – The back scatter electron (BSE) detector has been used to make BSE-images. High-energy electrons in the electron beam are backscattered by the crystals in the samples. Heavier minerals, such as monazite and zircon, appear brighter in the BSE-image than quartz grains, because heavy elements backscatter the electrons much stronger than lighter elements. So, areas with different grayscale in backscatter images are different minerals.

### **2.3 Results**

Almost all studied thin sections mainly contain feldspar and quartz with minor biotite and muscovite (Chapter 1, figure 5). The quartz crystals in most samples contain randomly orientated cracks and healed fractures. Planar microstructures in quartz were only observed in samples 2.5a, 3.3b and 1.6g, which are schist and granites respectively. A detailed overview of the optical microscope and SEM results of sample 2.5a, 3.3b and 1.6g is given in table 3. Most relevant results are summarized below.

*2.5a (figure 4)* – Planar microstructures detected in the optical microscope are sharp, straight and often decorated. EDX analyses indicate that these crystals with observed planar microstructures are plagioclase grains.

*3.3b (figure 5)* – grayscale CL-images exhibit quartz crystals with two sets of sub planar/ slightly curved lamellae with a spacing of 2-7 $\mu$ m. All crystals have planar microstructures within the same direction and it is difficult to distinguish the lamellae from host quartz. Plane polarized light-images show some planar structures crossing the grain boundary.

*1.6g (figure 6)* – grayscale CL-images show one set sub-planar microstructures with a spacing of 2-7  $\mu$ m that crosscut zoning, but not the grain boundaries. It is hard to distinguish the lamellae from host quartz. This description is similar to the description of deformation lamellae given by Hamers and Drury (2011) (table 2).

Table 3. Detailed overview of light microscope observations and SEM analyses of sample 2.5a, 3.3b and 1.6g. (ppl = plane polarized light, xpl = crossed polarized light). The figure numbers correspond to the numbers of the figures below this table.

Sample	Location	Rock	Optical observations	EDX-analyses	CL-imaging (grayscale)
2.5a  Figure 4	40°39'33"N 7°04'45"W ~5 km from the center of the GS.	Very fine grained pre-Ordovician schist.	<p><i>ppl</i> – Very fine grained schist with grains having a weak preferred orientation. Several crystals show straight dark colored sharp planar structures that do not cross the grain boundary. Some planar features are decorated by tiny bubbles.</p> <p><i>xpl</i> – Planar features are better visible in xpl and are very straight. Some lamellae have a different extinction angle than the host grain. In one crystal two sets of planar features are observed. Due to small grain sizes, it's hard to observe whether the crystals are feldspar or quartz.</p>	The grains with planar features are plagioclase crystals.	
3.3b  Figure 5	40°36'49"N 7°10'49"W ~7 km from the center of the GS.	Weathered fine grained T-granite.	<p><i>ppl</i> – Lighter colored sub-planar features observed in the quartz crystal. All quartz crystals have planar features in the same two orientations. The planar features do cross the grain boundary in some areas. Two sets of planar structures are observed. Some planar features are decorated by tiny bubbles. A lot of non planar fractures in crystals as well.</p> <p><i>xpl</i> – Planar features not visible.</p>	Grains with planar features are <u>quartz</u> grains	<p><u>Sub-planar features</u> – Slightly curved lamellae with a spacing between 2-7µm. Difficult to distinguish the lamellae from the host mineral. Two sets of lamellae do not cross each other. Hard to observe whether the lamellae cross the grain boundaries.</p> <p><u>Dark bands</u> – Dark bands randomly cut through crystals with sub-planar features. Lamellae crosscut these dark bands.</p>

<p>1.6g</p> <p>figure 6</p>	<p>40°36'17"N 7°01'54" W ~7 km from the center of the GS.</p>	<p>Greenish fine grained weathered T-granite with a lot of quartz veins and fractures.</p>	<p><u>pp/</u> – Quartz vein with 5 quartz crystals with 1 set of planar features. The planar features appear to be fine parallel lamellae that are lighter colored than host grain and do not cross grain boundaries.</p> <p><u>xpl/</u> – The lamellae have a slightly different refractive index than the host grain. It's very difficult to distinguish lamellae from host grain.</p>	<p>All grains with planar features are <u>quartz</u> grains.</p>	<p><u>Zoning</u> – Dominant structure in most grains; non-planar alternated bands of brighter and darker luminosity that is mainly present at the rims of crystals.</p> <p><u>Sub-planar features</u> - Sub-planar lamellae as observed in the optical microscope are only observed at higher magnification and limited to just a few crystals. The spacing of the lamellae range between 2-7µm and it's hard to distinguish the lamellae from the host mineral. Whereas the lamellae do not crosscut the grain boundary, they do crosscut zoning structures.</p>
-----------------------------	---	--	--	--	---

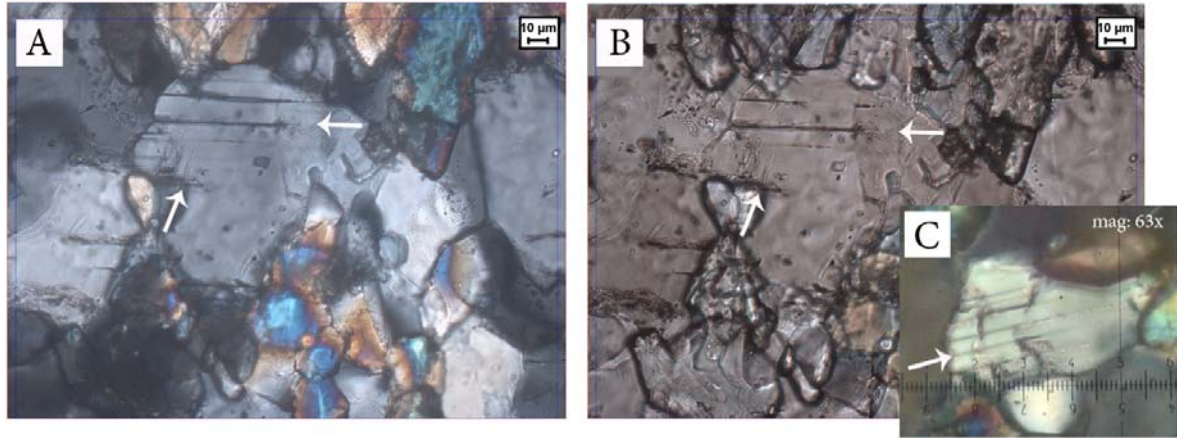


Figure 4. (a,c) The arrows point to planar microstructures in plagioclase grains in sample 2.5a in crossed polarized light and (b) plane polarized light. In both light types the grain could easily be interpreted as quartz. The horizontal set of planar lamellae is probably twin lamellae, because of the different extinction angle of the lamellae in crossed polarized light. The less clear other set of planar microstructures could be cleavage of sub-planar fractures.

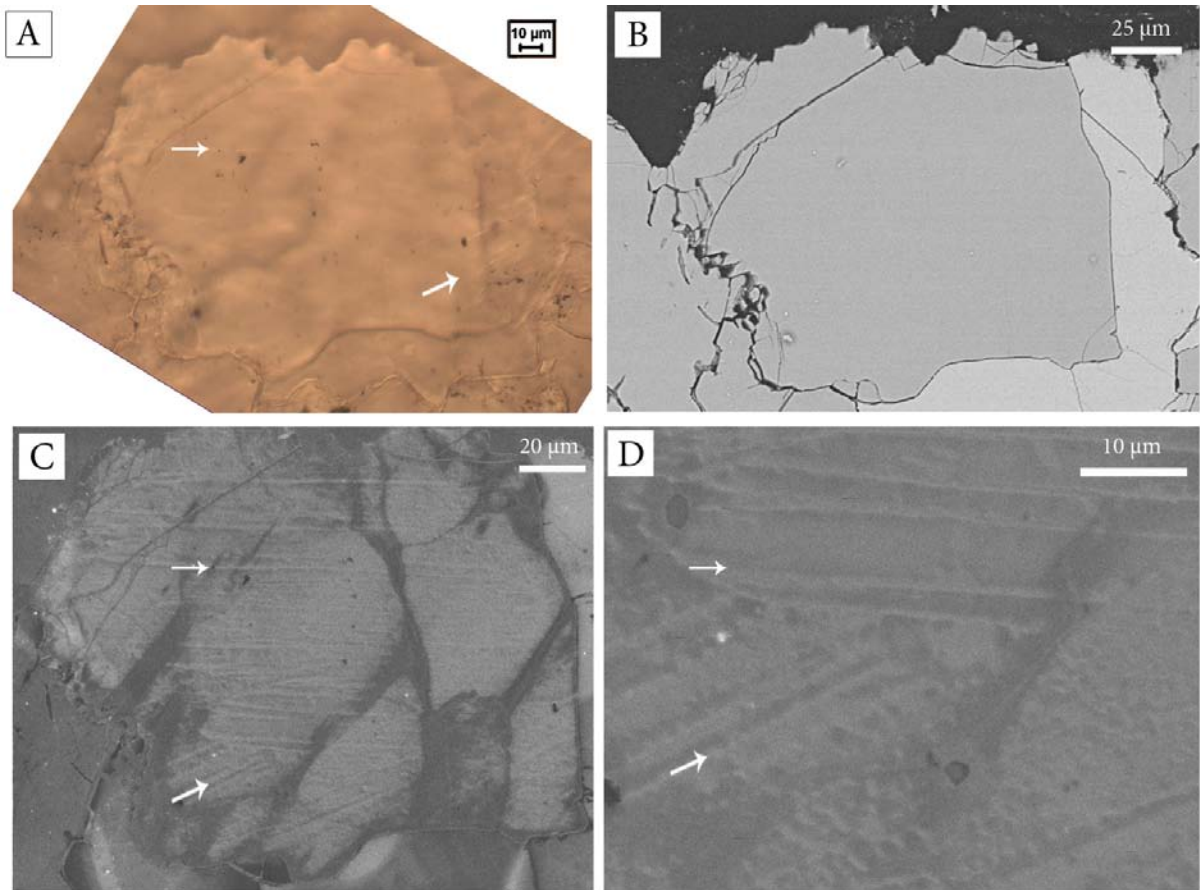


Figure 5. Several images of planar microstructures in a quartz crystal formed during thin section preparation in sample 3.3b. Arrows point into the direction of the planar microstructures. (a) The planar microstructures are not clearly visible in ppl, but at the right side of the grain one set of planar microstructures cross the grain boundary and continues in a feldspar crystal. (b) BSE-image of the quartz crystal and the lighter colored feldspar crystal at the right side. (c) Grayscale CL-image of sub-planar microstructures and black, non-planar bands. (d) Higher magnification grayscale CL-image of planar microstructures.

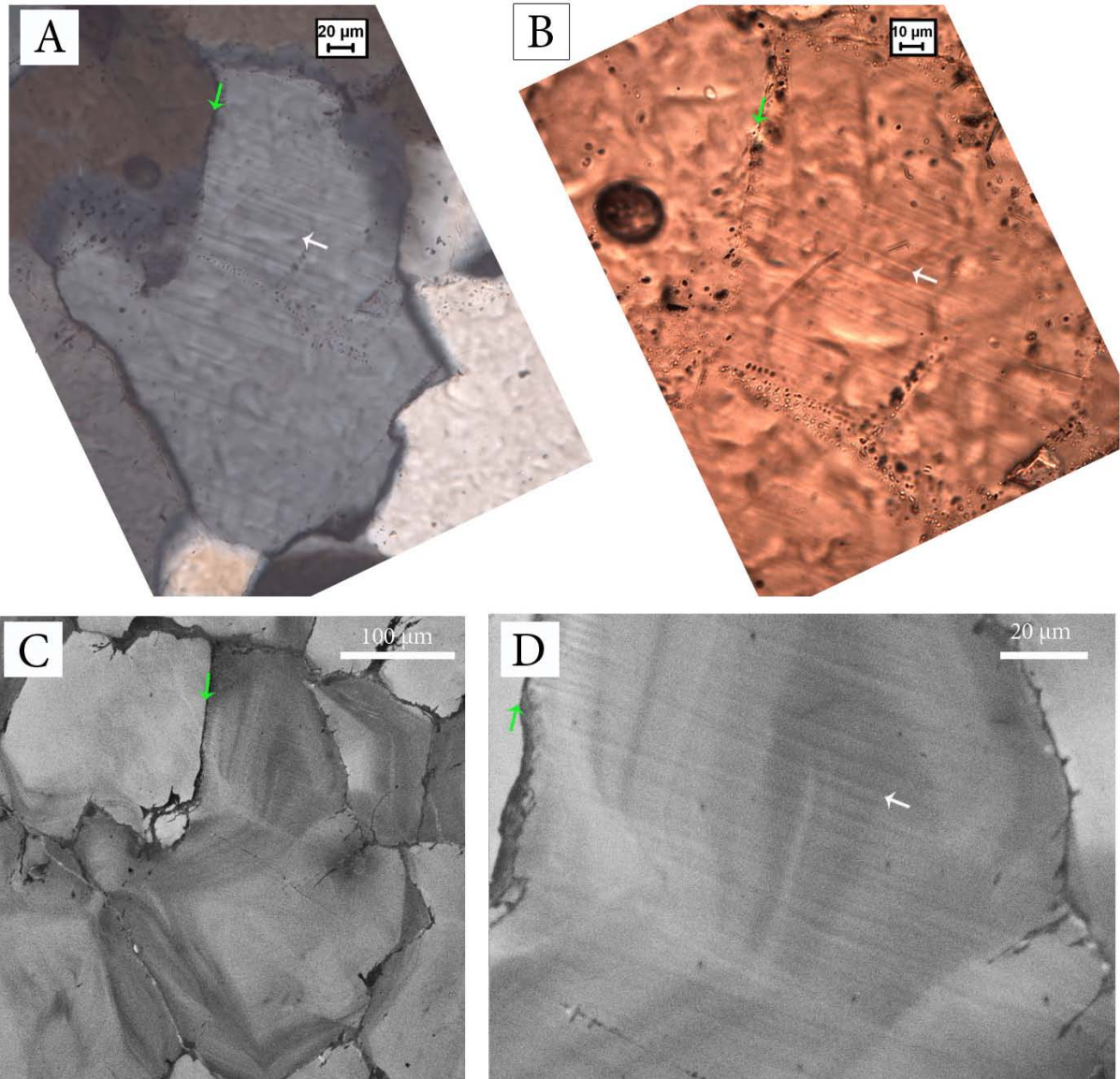


Figure 6. Several images of a quartz grain in sample 1.6g. The green arrows point to the same grain boundary and the white arrows point in the direction of the deformation lamellae. (a) Lamellae in quartz are clearly visible in cross polarized light having bands of alternating darker and lighter color. (b) The lamellae are also visible in plane polarized light. (c,d) The dominant feature present in CL-images is zoning, but at higher magnification it's clear that the planar lamellae crosscut the zoning.

## 2.4 Discussion

Planar microstructures will be discussed per sample. Afterwards the results are compared to PDFs in quartz from the Ries Crater, Germany and the results from Monteiro (1991).

### 2.4.1 Sample 2.5a

In the light microscope the crystals with straight decorated planar microstructures resemble quartz (figure 4), but EDX analysis point out that the crystals are plagioclase. Observations with just an optical microscope could easily lead to wrong interpretations. In crossed polarized light some planar microstructures have other extinction angles, indicating that the features might be twin lamellae or planar fractures filled with other material.

### 2.4.2 Sample 3.3b

Although the observed planar lamellae in the CL-image are quite similar to the description of deformation lamellae in table 2, it's remarkable some planar microstructures cross the grain boundary, all grains have planar microstructures in the same direction and the planar microstructures are not visible in xpl (figure 5). To check whether these features were not formed during preparation of the thin sections, the sample is studied in the reflected light optical microscope. The planar microstructures appear to be scratches formed during the polishing process. Preparation scratches could resemble deformation lamellae in CL-images. This example shows again how easy it is to make misinterpretations when studying microstructures in quartz, but it also illustrates the importance of good sample preparation.

### 2.4.3 Sample 1.6g

#### 2.4.3.1 Hydrothermal veins and zoning

Before discussing the planar microstructures observed in sample 1.6g (figure 6), the present zoning will be discussed. The quartz vein from sample 1.6g may be a hydrothermal vein, because the granitoids in the Guarda Structure underwent two hydrothermal alteration processes. Na/K-, H- and Ca-rich fluids altered the Guarda granitoids by adding and removing chemical elements (metasomatism) (Bobos et al., 2005). The first alteration stage occurred around 245 Ma and is related to an alkaline (Na, K) metasomatism. During this stage moderately saline fluids with a temperature higher than 300°C have migrated along microcrack networks in granitic rock. Progressive cooling of the fluids was probably promoted by a dilution process with a poorly aqueous saline fluid. The second alteration stage, 225 – 209 Ma, is associated with highly saline fluids of slightly lower temperatures (<200). Both alteration events were related to post -Variscan metallogenesis (Bobos et al., 2005).

During the hydrothermal events, quartz veins may have formed in granites from the Guarda Structure. Zoning, as present in grayscale CL-images, is abundant in hydrothermal quartz (Jourdan et al. 2009). Zoning is represented by the alternation of brighter and darker luminosity, which are caused by fluctuating trace element content (Landtwing & Pettke, 2005). Al, Ti, K, Li, Na and Fe are considered to be the most likely substitutes in hydrothermal quartz (Jourdan et al., 2009). Bright luminosity in quartz correlates with a high total abundance of trace elements (e.g. Jourdan et al., 2009; Landtwing & Pettke, 2005).

There are two types of zoning. (1) Sector zoning; compositional differences among coeval parts of crystallographically non-equivalent growth sectors within a single crystal and (2) Growth zoning: concentric zoning defined as a change in composition measured along a growth vector of a single sector (Jourdan et al., 2009). It is suggested that the presence of growth and sector zoning is related to relatively low temperatures, 300°C or less, during formation of the crystal. Quartz formed at temperatures close to 400°C does not have sector-and growth zoning (Jourdan et al., 2009).

Quartz crystals from sample 1.6g clearly show growth zoning (figure 3c and d). Sector zoning is not directly visible from the CL-images, but according to the sector-zoning model of Dowty (1976), sector zoning can be present in quartz. Prism faces in quartz have interstitial sites that easily incorporate cations such as Li, Al, Fe<sup>3+</sup> etc., whereas just a small number of cations may be adsorbed and incorporated on rhombohedral faces. The various rhombohedral sites in quartz also differ in exact

face structure and presumably in their capacity for adsorption of cations (Dowty, 1976). Quartz from sample 1.6g contain growth and probably sector zoning, therefore the vein must be formed at a temperature below 300°C. This means that the vein may be linked to the cooling episode of the first hydrothermal stage or the second hydrothermal alteration stage. Therefore the zoning probably has a minimum age of ~209 Ma.

#### **2.4.3.2 Deformation lamellae**

The sub-planar microstructures in sample 1.6g appear to be deformation lamellae, since the sub-planar lamellae are quite similar to the description of deformation lamellae given by Hamers and Drury (2011) (table 2 and figure 1). To check this result, the orientation of the lamellae can be determined. As mentioned in paragraph 2.1.2, deformation lamellae form in sub-basal planes (Drury, 1993). According to Vernooij and Langenhorst (2005) energetically favorable  $1/3 \langle 110 \rangle$  dislocations in the (0001) plane are activated during slow tectonic processes. Subsequent climb of dislocations result in a movement out of the (0001) plane, rotating away from the basal plane. The speed of dislocation glide and climb control the degree of rotation. Due to such dislocation climb process, dislocations are arranged in subgrain walls in sub-basal planes (Drury, 1993; Vernooij and Langenhorst, 2005).

By using an optical microscope, the orientation of sub-planar lamellae with respect to the trace of the basal plane in quartz can be estimated. When using crossed polarized light a quartz crystal is completely extinct (black) when the trace of the basal plane (dip of basal plane is unknown) is parallel to one of the two vibration directions of the polarized light. Because the vibration directions of polarized light are known, it's possible to measure the angle between the lamellae and the trace of the basal plane. Since a quartz crystal turns black twice during one complete rotation you can measure an obtuse and an acute angle.

The acute angles between the sub-planar lamellae in six quartz crystals and the basal trace are measured in an optical microscope. The angles vary between 10° and 27° from the trace of the basal plane, indicating that the sub-planar lamellae are probably in sub-basal planes. This result in combination with the CL-images implicate that the sub-planar lamellae from sample 1.6g are probably deformation lamellae.

#### **2.4.3.3 Age of deformation lamellae and possible involved tectonics**

Higher magnification CL-image shows deformation lamellae crosscutting growth zoning. A deformation event forming these deformation lamellae must have occurred after the formation of the hydrothermal quartz vein, so < 209 Ma. The deformation lamellae may have formed during the Tertiary accretion of Iberia to both the European and African plate (e.g. Vegas et al., 1990; Bruijne and Andriessen, 2002). The influence of this tectonic event on the Guarda Structure was discussed in chapter 1, paragraph 1.5.3. However, it seems obscure that deformation lamellae are observed in just six quartz grains of one sample. To draw conclusions about deformation lamellae in the Guarda Structure and the involved tectonics, more research must be done on other microstructural deformation features throughout the Guarda Structure.

#### **2.4.4 Guarda Structure versus Ries Crater**

In the Guarda Structure, PDFs were not observed at all and deformation lamellae were observed in just one sample. Monteiro (1991) claimed he found decorated planar microstructures in rocks from

the Guarda Structure. To make a comparison between PDFs, deformation lamellae and the decorated planar microstructures found by Monteiro (1991), figure 7 is designed. Decorated planar microstructures of Monteiro (1991) neither resemble PDFs from the Ries Crater nor deformation lamellae from the Guarda Structure. The first remarkable difference is the spacing of the several planar microstructures; the decorated planar microstructures of Monteiro (1991) have a spacing of  $>100\ \mu\text{m}$ , while the deformation lamellae have spacing between  $2\text{--}7\ \mu\text{m}$  and the PDFs  $<5\ \mu\text{m}$ . The planar microstructures of Monteiro are also sub parallel and less continuous compared to PDFs from the Ries Crater.

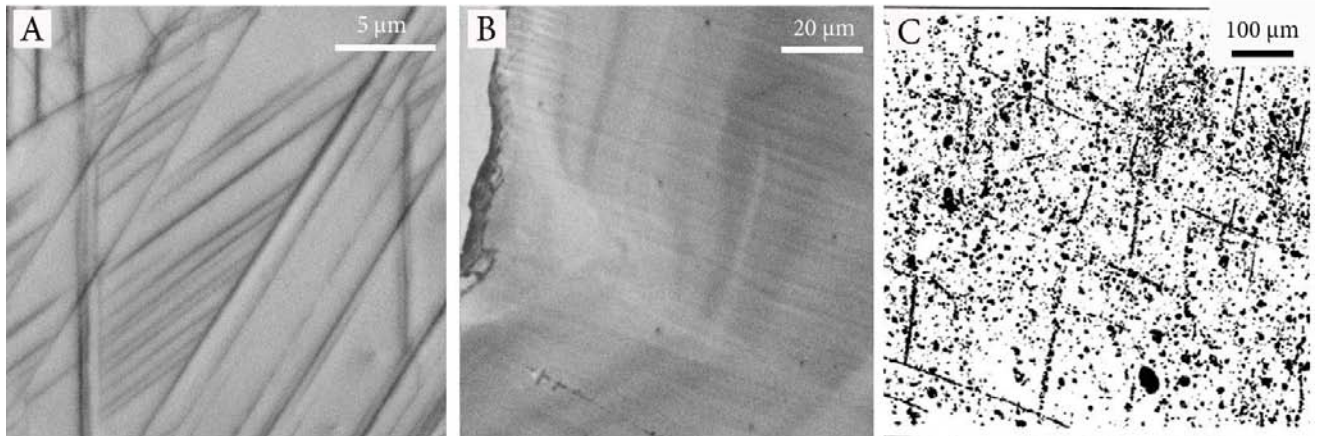


Figure 7. (a) Grayscale CL-image of PDFs in quartz from the Ries Crater, Germany and (b) deformation lamellae in quartz from the Guarda Structure. (c) Decorated planar microstructures in quartz from a breccia dyke in the center of the Guarda Structure (Monteiro, 1991). Note the different scales of the images.

#### 2.4.5 Post shock annealing of PDFs in quartz

Planar shock structures in quartz were not found in and around the rocks from the Guarda Structure and Monteiro (1991) decorated planar microstructures strongly deviate from PDFs. In some impact structures, especially in large old eroded ones, PDFs could have been annealed by post-impact thermal and hydrothermal processes (e.g. Grieve et al., 1990; Goltrant et al., 1991; Goltrant et al., 1992; Leroux et al., 1993). Only in quartz from younger impact craters like the 50,000 Ma Meteor Crater, Arizona or the 15 Ma Ries impact Crater, Germany, all PDF microstructures are preserved (Goltrant et al., 1992).

A clear example of affected PDFs in quartz is the 2.02 Ga Vredefort Dome in South Africa (Leroux et al., 1993 and Grieve et al., 1990). Both studies pointed out that the PDFs in quartz from the Vredefort structure were anomalous when compared with those from other impact structures. The PDFs are almost always decorated with tiny fluid inclusions and almost all PDFs lie in the basal plane (mechanical brazil twins), whereas in other well characterized impact sites PDFs in  $\{10\bar{1}n\}$  planes are the most usual ones (Grieve et al., 1990; Leroux et al., 1993). Leroux et al. (1993) suggested, in agreement with Grieve et al. (1990), that the anomalies in PDF-occurrence can be explained by intense post-impact thermal overprint (intense metamorphism) of  $\approx 900^\circ\text{C}$ . The efficient recovery of the PDFs in the  $\{10\bar{1}n\}$  planes is caused by high-temperature diffusion and only thin mechanical brazil twin lamellae in the basal plane will survive (Goltrant et al., 1991).

The tiny water bubbles decorating PDFs in shocked quartz from the Vredefort Dome stem from water precipitation as result of a post-shock thermal event. The shocked quartz could have been initially wet and precipitated its water during the thermal event or some aqueous fluid phase has

been circulated through a network of cracks and fractures which healed later (Goltrant et al., 1992). Annealing quartz for one week at moderate pressure and moderate temperature  $\approx 400^{\circ}\text{C}$  induces nucleation of large density of very tiny bubbles (Goltrant et al., 1991). Goltrant et al. (1992) suggested that annealed PDFs lack the original fine structure, but could still be detected by light microscope. However, according to the observations of Leroux et al. (1993) original PDFs could be completely vanished.

As discussed in paragraph 2.4.3, the Guarda granite underwent a series of hydrothermal alteration processes. It started with K/Na – exchange and was followed by alteration of the rocks due to circulation of H- and Ca-enriched fluids. During the first alteration stage temperatures were elevated to  $>300^{\circ}\text{C}$  (Bobos et al., 2005). Because the Guarda Structure did experience hydrothermal stages with moderate temperatures, post-shock annealing of PDFs in quartz might have taken place. It is not impossible that PDFs were once present in quartz, but have since been healed and are no longer visible. If this is true, the hydrothermal events give younger age constraints for a possible impact. This implicates that the minimum age of the alleged crater must be  $\sim 209$  Ma.

The decorated planar microstructures found by Monteiro (1991) may be relicts of annealed PDFs in quartz. This conclusion remains very unlikely, because no relicts of PDFs have been found at any location in the Guarda Structure during this research. Annealed PDFs are often planar arrays of inclusions (e.g. figure 2 and 11 in Leroux et al., 1993; figure 2 in Grieve et al., 1990) and not sub-planar as showed by Monteiro (1991).

## 2.5 Conclusion and further research

Although several types of (sub-)planar microstructures are present in quartz grains from the Guarda Structure, none of these shows the typical characteristics of PDFs. It therefore seems unlikely that the planar microstructures found by Monteiro (1991) are the result of shock.

Because post-impact thermal and hydrothermal processes could anneal or even completely vanish PDFs in quartz (e.g. Grieve et al., 1990; Goltrant et al., 1991; Goltrant et al., 1992; Leroux et al., 1993) and the Guarda Structure experienced two episodes of hydrothermal alternation (Bobos et al., 2005), it is useful to study shock effects in other minerals that are more refractory and resistant to alteration. Zircon and monazite are good candidates, because they also show a wide range of shock features that seem to survive extreme metamorphism, erosion and hundred millions of years (e.g. Kusaba, 1985; Bohor et al., 1993; Leroux et al., 1999; Wittman et al., 2006; Cavosie et al., 2010; Cintrón et al., 2011; Moser et al., 1997). Chapter 3 and 4 will investigate the microstructures of zircon and monazite from the Guarda Structure. Potential microstructures in zircon and monazite from the Guarda Structure will be compared to shocked crystals from the Vredefort Dome.

## References

- Becker, L., Poreda, R. J., Basu, A. R., Pope, K. O., Harrison, T. M., Nicholson, C., and Iasky, R. 2004. Bedout: A possible end-Permian impact crater offshore of Northwestern Australia, *Science* 304, p. 1469–1476.
- Bobos, I., Jaques, L., Noronha, F., Clauer, N., Liewig, N., 2005, Geochemistry, geothermometry, and K-Ar dating of episyenitic rocks associated with the Guarda uraniferous granites, Portugal, *8th Biennial SGA Meeting*, Beijing-China, p. 225-228.
- Bohor, B. F., Betterton, W. J., Krogh, T. E., 1993, Impact-shocked zircons: Discovery of shock-induced textures reflecting increasing degrees of shock metamorphism, *Earth and Planetary Science Letters* 119, p. 419–424.

- Cavosie, A. J., Quintero, R. R., Radovan, H. A., Desmond, E. M., 2010, A record of ancient cataclysm in modern sand: Shock microstructures in detrital minerals from the Vaal River, Vredefort Dome, South Africa, *Geological Society of America Bulletin* 122, 1968–1980.
- Cintrón, N. O., Cavosie, A. J., Gibbon, R.J., Radovan, H. A., Moser, D. E., Wooden, J., 2011, In Situ U-Th-Pb Geochronology of detrital shocked monazite in Pleistocene fluvial deposits along the Vaal River, South Africa, *42nd Lunar and Planetary Science Conference* (Abstract).
- Drury, M. R., 1993, Deformation lamellae in metals and minerals. In *Defects and processes in the solid state: Geoscience applications*, edited by Boland, J. N. and Fitz Gerald, J. D. Amsterdam: Elsevier Science Publishers B. V. p. 195–212.
- Dowty, E., 1976, Crystal structures and crystal growth: II, sector zoning in minerals, *American Mineralogist* 61, p. 460-469.
- Ferrière, L., Koeberl, C., Libowitzky, E., Reimold, W. U., Greshake, A., and Brandstätter, F., 2010, Ballen quartz and cristobalite in impactites: New investigations, *Geological Society of America Special Papers* 465, p. 609–618.
- French, B.M., 1998, Traces of Catastrophe: A Handbook of Shock-Metamorphic Effects in Terrestrial Meteorite Impact Structure, LPI Contribution No. 954, Lunar and Planetary Institute, Houston, 120p.
- Glikson A., 2004, Comment on “Bedout: A possible end-Permian impact crater offshore of Northwestern Australia.” *Science* 306, p.613b.
- Goltrant, O., Leroux, H., Doukhan, J. C., Cordier, P., 1992, Formation mechanisms of planar deformation features in naturally shocked quartz, *Physics of The Earth and Planetary Interiors* 74, p. 219–240.
- Goltrant, O., Cordier, P., Doukhan, J.-C., 1991, Planar deformation features in shocked quartz; a transmission electron microscopy investigation, *Earth and Planetary Science Letters* 106, p. 103-115.
- Gratz, A. J., Fidler, D. K., and Bohor, B. F., 1996, Distinguishing shocked from tectonically deformed quartz by the use of the SEM and chemical etching, *Earth and Planetary Science Letters* 142, p. 513–521.
- Grieve R. A. F., Coderre, J. M., Robertson, P. B., Alexopoulos, J., 1990, Microscopic planar deformation features in quartz of the Vredefort structure: Anomalous but still suggestive of an impact origin, *Tectonophysics* 171, p. 185–200.
- Hamers, M.F., Drury, M.R., 2011, Scanning electron microscope-cathodoluminescence (SEM-CL) imaging of planar deformation features and tectonic deformation lamellae in quartz, *Meteoritics & Planetary Science*, p. 1-18.
- Jourdan, A-E., Vennemann, T.W., Mullis, J., Ramseyer, K., Spiers, C.J., 2009, Evidence of growth and sector zoning in hydrothermal quartz from Alpine veins, *Eur. J. Mineral* 21, p. 219–231.
- Kusaba, K., Syono, Y., Kikuchi, M., Fukuoka, K., 1985, Shock behaviour of zircon: Phase transitions to scheelite structure and decomposition, *Earth and Planetary Science Letters* 72, p. 433– 439.
- Langenhorst, F., 2002, Shock metamorphism of some minerals: Basic introduction and microstructural observations, *Bulletin of the Czech Geological Survey* 77, 4, p. 265–282.
- Langenhorst, F., Kyte, F. T., Retallack, G. J., 2005, Reexamination of quartz grains from the Permian-Triassic boundary section at Graphite Peak, Antarctica (abstract #2358). 36th Annual Lunar and Planetary Science Conference: League City, Texas.
- Landtwing, M.R., Pettke, T., 2005, Relationships between SEM-cathodoluminescence response and trace-element composition of hydrothermal vein quartz, *American Mineralogist* 90, p. 122 -131.
- Leroux, H., Reimold, W.U., Doukhan, J.-C., 1993, A TEM investigation of shock metamorphism in quartz from the Vredefort dome, South Africa, *Tectonophysics* 230, p. 223-239.
- Leroux, H., Reimold, W. U., Koeberl, C., Hornemann, U., Doukhan, J.-C., 1999, Experimental shock deformation in zircon: A transmission electron microscopic study, *Earth and Planetary Science Letters* 169, p. 291–301.
- Monteiro, J.F., 1991, The Guarda Circular Structure: A Possible Complex Impact Crater (Abstract), ©Lunar and Planetary Institute, NASA Astrophysics Data System

- Moser, D.E., 1997, Dating the shock wave and thermal imprint of the giant Vredefort impact, South Africa: *Geology* 25, p. 7–10.
- Retallack, G. J., Seyedolali, A., Krull, E. S., Holsen, W. T., Ambers, C. P., and Kyte, F. T., 1998, Search for evidence of impact at the Permian-Triassic boundary in Antarctica and Australia. *Geology* 26, p. 979–982.
- Stöffler D., and Langenhorst F., 1994, Shock metamorphism of quartz in nature and experiment: I. Basic observation and theory, *Meteoritics* 29, p. 155–181.
- Vernooij, M. G. C., and Langenhorst, F., 2005, Experimental reproduction of tectonic deformation lamellae in quartz and comparison to shock-induced planar deformation features, *Meteoritics & Planetary Science* 40, p. 1353–1361.
- Wittmann, A., Kenkmann, T., Schmitt, R.T., and Stöffler, D., 2006, Shock-metamorphosed zircon in terrestrial impact craters: *Meteoritics & Planetary Science* 41, p. 433–454.

## Chapter 3: Shock Microstructures in Zircon

### 3.1 Introduction

As discussed in Chapter 2, in cases of an old impact structure and/or post-impact (hydro)-thermal events, PDFs in quartz could be highly annealed and may be no longer visible (e.g. Grieve et al., 1990; Goltrant et al., 1991; Goltrant et al., 1992; Leroux et al., 1993). It's useful to look at shock effects in other minerals than quartz. Zircon is a mineral which is much more refractory and resistant to alteration than most other minerals, such as quartz or feldspar (Leroux et al., 1999). Zircon is one of the last minerals that succumb to high shock pressures and the following high temperatures (El Goresy, 1965). Shock features in experimentally shocked and naturally shocked zircons are increasingly studied and seem to be a very useful tool for the determination and characterization of a meteorite impact. There are four well-known shock features in zircon; planar microstructures, high pressure polymorph reidite, granular texture and decomposition of zircon. (e.g. Kusaba, 1985; Bohor et al., 1993; Leroux et al., 1999; Wittman et al., 2006; Cavosie et al., 2010).

#### 3.1.1 Planar and non-planar microstructures

There are several types of planar microstructures present in shocked zircons; micro-twin lamellae, planar deformation features (PDFs), planar fractures (PFs).

*Micro-twin lamellae* - Synthetic twins, similar to Brazil twins in shocked quartz, were found in experimentally shocked zircons (Leroux et al., 1999). The twins were produced at pressures >40 GPa and had {112} orientation (figure 1). These twins form along with the high-pressure polymorph (reidite) of zircon. Micro-twin lamellae are also observed in naturally shocked zircon. The micro-twin lamellae in zircon form as angle-axis pairs with an angle of 65° about the [110] axis as represented in figure 1. They can form at shock pressures >20 GPa (Moser et al., 2011). Moser et al. (2011) suggested that the synthetic and natural twins could be the same type.

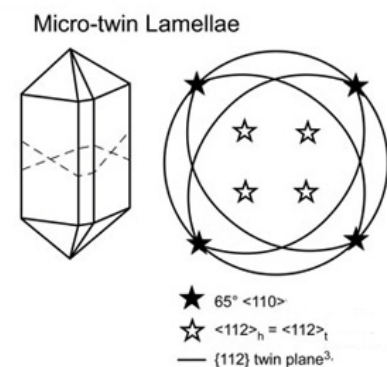


Figure 1. Orientations of micro-twin lamellae (modified from Timms et al., 2011)

#### Planar Deformation Features (PDFs)

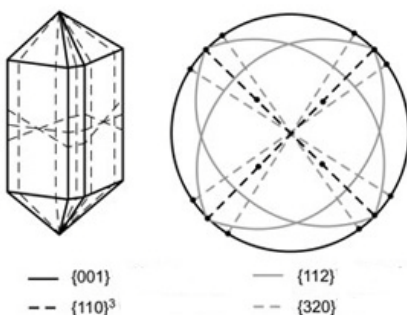


Figure 2. PDF-orientations in zircon (Modified from Timms et al., 2011)

#### PDFs - Bohor et al. (1993)

was the first who noticed PDFs in shocked zircons during SEM-analyses using edging techniques. Leroux et al. (1999) did shock experiments on zircons and found PDFs in zircons that were experimentally shocked to 40GPa and 60GPa. According to Leroux (1999), these PDFs were not visible in a light microscope (only visible in TEM) and consist of thin (~10 nm) planar defects filled with amorphous zircon. PDFs were observed close to the {320} planes and in the {110}, {001} and {112} planes (figure 2) (Leroux et al., 1999; Moser et al. 2011; Timms et al 2011).

Micro cleavage / PFs - During zircon shock experiments, optically identifiable planar defects in 20GPa and 40GPa shocked zircon were found as well (Leroux et al., 1999). On optical microscopic scale, many straight sets of fractures mainly formed parallel to {201}, {211}, {221}, {111}, {100} and {hk0} planes (figure 3). These micro-fractures are <50 nm wide and interpreted as shock-induced micro-cleavage planes or planar fractures (PFs) developed due to brittle deformation (Leroux et al., 1999). Newly grown minerals or melt can occupy these PFs at the highest shock conditions (Timms et al., 2011). Leroux et al. (1999) found also evidence for plastic deformation in these zircons and suggested that the cracks are areas of stress concentration and seem to be nucleation sites for the generation of dislocations. The high dislocation density at the crack tips suggest that plastic deformation was initiated by the micro-cracking process. According to Leroux et al. (1999), there is no evident increase in the number of dislocations in the 40 GPa sample compared to the 20 GPa sample.

Cavosie et al. (2010) also found those PFs in naturally shocked zircons from the Vredefort Dome, South Africa. They observed at least five orientations of planar fractures; (100), (001), (010) (figure 3) and two unindexed (hkl) orientations, with a variable spacing of 5-20  $\mu\text{m}$ . Some grains show planar fractures that offset igneous growth zoning in the zircon.

Although some research is done on PFs in zircon, the number of possible crystallographic orientations for PFs in zircons is unknown. It is also unknown in which way the number and orientations of PFs is related to the intensity of shock metamorphism (Cavosie et al., 2010).

NPFs - Irregular or nonplanar fractures (NPFs) also occur in shocked zircons (Leroux et al., 1999; Cavosie et al., 2010). The density of nonplanar fractures increases with shock intensity (Leroux et al. 1999). However, NPFs are not exclusively formed by impact shock, and could be formed by other processes (e.g. Leroux et al., 1999; Cavosie et al., 2010; Timms et al., 2011).

### 3.1.1.1 Terminology of planar microstructures; PDFs and PFs in quartz versus PDFs and PFs in zircon

To make correct observations and interpretations about planar microstructures in minerals, it's very important that the terminology is used consistently. Especially planar deformation features (PDFs), planar fractures (PFs) and a general term such as planar features could be easily confused. To avoid confusion and to make sure PDFs in zircon and in quartz are equivalent features, the characteristics of PDFs in both quartz and zircon are listed in table 1. The same has been done for PFs (also table 1).

PDFs in zircon and quartz both correspond to shock-induced amorphization along crystallographically determined planes (Leroux et al., 1999). The thickness of PDFs in zircon is 20-30 times smaller than the PDFs in quartz. The difference in thickness might be the reason why PDFs in quartz are visible in light microscopy and PDFs in zircon are not. However, Bohor et al. (1993) developed an etching technique that allowed the SEM to visualize the nanoscale PDFs.

PFs in quartz are shock features which appear identical to cleavage (French and Koeberl, 2010). PFs in zircon are also interpreted as shock induced micro-cleavage planes (Leroux et al., 1999). PFs in both minerals could appear as open fractures and/or be filled with secondary minerals (French and Koeberl, 2010; Cavosie et al., 2010). Therefore, it seems likely that PFs in zircon and quartz are similar

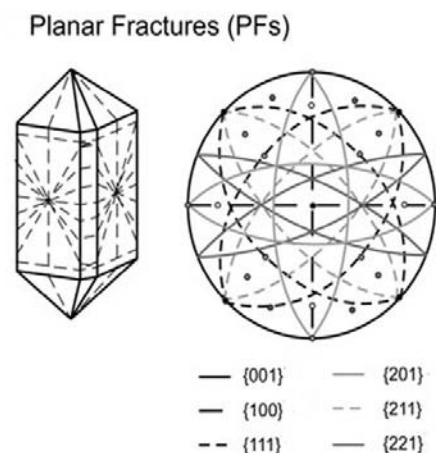


Figure 3. PF-orientations in zircon (modified from Timms et al. 2011).

features as well. The main difference between PFs/PDFs in quartz and zircon is the spacing and thickness.

To avoid any confusion about the terminology, all types of planar structures in zircon will be called **planar microstructures (PMs)** (term also used in chapter 4). The general term PM was introduced by French and Koeberl (2010) to designate any type of (quasi-)planar or structure within a quartz grain.

Table 1. The main characteristics of PDFs and PFs in zircon and quartz (French and Koeberl <sup>1</sup> , 2010; Leroux <sup>2</sup> et al., 1999; Bohor <sup>3</sup> et al., 1993; Langenhorst <sup>4</sup> , 2002; Cavosie <sup>5</sup> et al. 2010).		
PDFs	Quartz	Zircon
Type/Consist of	Lamellae filled with amorphous silica <sup>1</sup>	Lamellae filled with amorphous zircon <sup>2,3</sup>
Thickness	<200-300 nm <sup>4</sup>	~10 nm <sup>2</sup>
Spacing	<2 μm <sup>4</sup>	<1 μm <sup>3</sup>
Pressure range	7-35 GPa <sup>1,4</sup>	>40 GPa <sup>2</sup>
PFs	Quartz	Zircon
Type	Fractures <sup>1</sup> (sometimes open/filled)	Fractures <sup>2</sup> (sometimes open/filled)
Thickness	3–10 μm <sup>1</sup>	<50 nm <sup>2</sup>
Spacing	>20 nm <sup>1</sup>	5-20 μm <sup>5</sup>
Pressure range	<10 GPa <sup>1</sup>	>20-40 GPa <sup>2</sup>

### 3.1.2 High Pressure Polymorph Reidite

During shock experiments on zircon, the crystal undergoes a phase transition from the zircon structure to the high pressure polymorph reidite with a scheelite structure (e.g. Kusaba et al., 1985; Fiske, 1999). The high-pressure phase, reidite, forms at 20-50 GPa (Fiske, 1999). Reversion of reidite into zircon structure occurs after rapid heating to 1200°C at room pressure (Kusaba et al., 1985). Kusaba et al. (1985) suggested that this strongly indicates that the transition from zircon into reidite has a displacive nature rather than reconstructive. The main change during the phase transition is the *c/a* ratio; 0.9052 for zircon and 2.219 for reidite. Due to this change reidite is 10% more dense than zircon (Kusaba et al., 1985). The zircon-reidite transition induced under shock compression does not reverse after the release of shock pressure and the high-pressure polymorph reidite is completely retained (Kusaba et al., 1985).

### 3.1.3 Granular texture

Zircons with a granular texture are frequently observed in naturally shocked zircons (e.g. Bohor et al., 1993; Cavosie et al., 2010) and represent crystallites of zircon in a glassy ZrSiO<sub>4</sub> matrix (figure 4). Such polycrystalline grains result from shock-induced amorphization and the following recrystallization (Bohor et al., 1993). Bohor et al. (1993) suggested that granular texture in shocked zircons is formed by a greater shock pressure than that is responsible for the development of PDFs, because granular structures overprint PDFs. A series of textural changes in shocked zircons has been observed, going from low to high shock pressures and temperatures. The series started with grains showing no shock features, to grains showing only PM, than PMs with superimposed granular texture, to a well-developed granular texture and even melting phenomena (Bohor et al., 1993). According to Wittman et al. (2006), granular texture in zircon forms at shock pressures >50 GPa.

### 3.1.4 Decomposition of Zircon

After shock experiments on zircon, Kusaba et al. (1985) observed decomposition of  $ZrSiO_4$  to  $ZrO_2$  and  $SiO_2$ . These decomposition products are a metastable form of tetragonal  $ZrO_2$  and  $SiO_2$  glass. Decomposition is primarily determined by temperature, rather than by pressure of shock loading (Kusaba et al., 1985). Decomposition of zircon into  $ZrO_2$  and  $SiO_2$  takes place under atmospheric pressure at temperatures  $> 1667^\circ C$  (El Goresy, 1965).

### 3.1.5 Overview shock microstructures in zircon

Wittmann et al. (2006) studied the occurrence and stability of the different shock features in zircon by combining results from their own research and of many other researches (most referred paragraph 1.3). They used results from naturally shocked zircon, experimentally shocked zircon and all other types of shock indicators to make figure 5; a diagram of zircon shock microstructure against shock pressure and post-shock temperature. The term planar microstructures used in figure 5 incorporate micro-twin lamellae, PDFs and PFs.

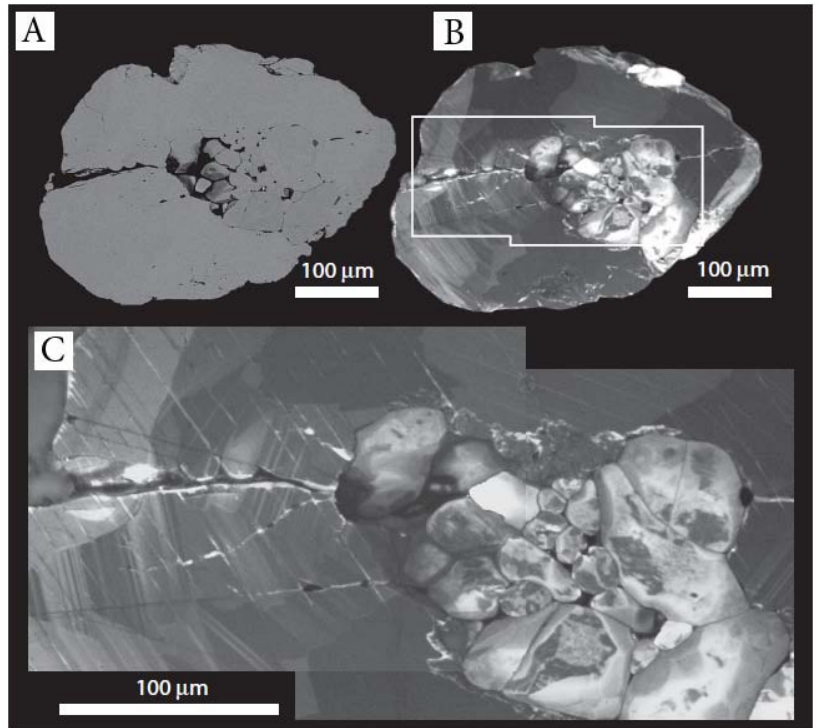


Figure 4. (a) A BSE-image and (b,c) two CL-images of a zircon with growth zoning, granular texture and PMs (modified from Cavosie et al. 2010).

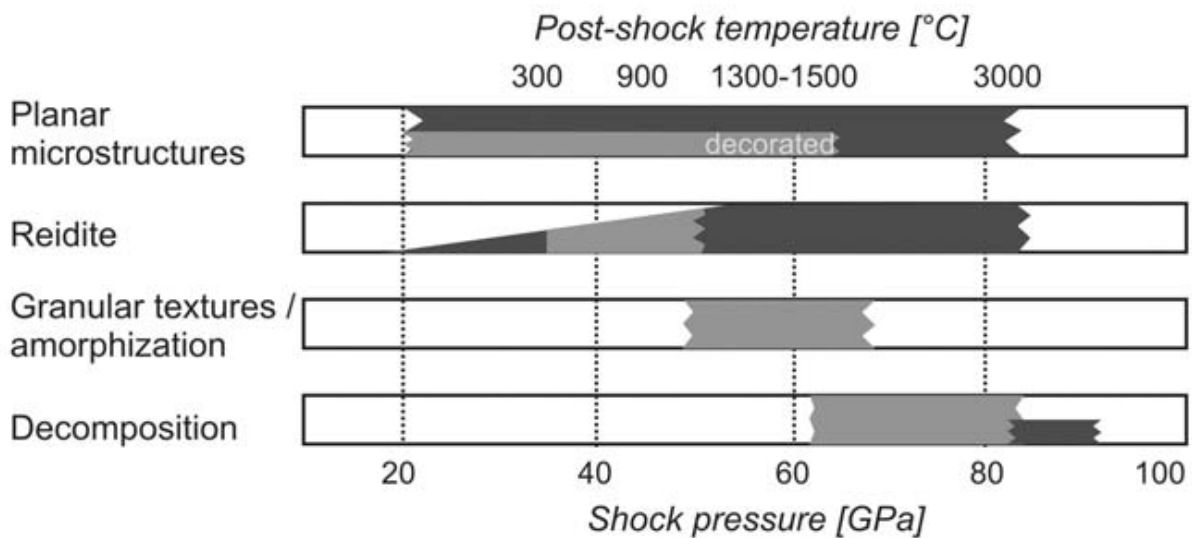


Figure 5. The relation between shock microstructures in zircon, shock pressure and post-shock temperature. The grey shading results from naturally shocked zircon and the black shading from experimentally shocked zircon. Below 20 GPa zircon exhibits no clear shock features (modified from Wittmann et al., 2006).

The aim of this study is to find potential shock structures in zircon from the Guarda Structure. Analyses were done with a light microscope and a SEM. The focus will be on the optically observable

PMs and granular texture. Results from the Guarda Structure are compared to shocked zircons from the Vredefort Dome. The usability of shock structures in zircon will be studied and the shock pressures range for PMs in zircon will be established.

### 3.2 Background of the Vredefort Dome

The Vredefort Structure is the oldest recognized impact structure on Earth (ca. 2.02 Ga; Moser, 1997). The structure is located within the Witwatersrand basin in the eastern Kaapvaal craton, South Africa (Moser et al., 2011). Based on shock microstructure distribution, the crater diameter is estimated to be as large as 300km (Grieve et al., 2008). Post-impact erosion of the structure is estimated to be 8 to 10 km (Gibson and Reimold, 2008 as referred in Moser et al., 2011).

The central part of the structure is known as the Vredefort Dome (figure 15); an uplifted area 80-90km in diameter (Grieve et al., 2008). The center of the Vredefort Dome consists of Archean basement granulites that are surrounded by sub-vertical to overturned supracrustal late Archean - early Proterozoic metasediments and metavolcanic strata (Grieve et al., 2008).

### 3.3 Methods and Samples

15 thin sections of Portuguese granitoids were studied in the optical microscope (appendix 1), all thin sections contain zircon. Due to the small grain sizes (<10  $\mu\text{m}$ ) of the zircon, most samples are not suitable for this study. Samples 6.5 and 2.6 contain zircon grains >50  $\mu\text{m}$  and were selected to study.

16 granulite samples from the Vredefort Dome were studied in the optical microscope. The granulites contain mainly feldspar, quartz and minor micas and oxides. 10 of these granulite samples contain one or more zircon grains. Sample H11, J11, K5, V1407b, V288, V251b and V284a were selected to study in more detail. Appendix 3 show scans of the 2 thin sections from the Guarda Structure and the 7 thin sections from the Vredefort Dome. In a table below each scan, the size and internal structure of each zircon are listed.

SEM analyses have been done on zircon grains in samples 6.5, 2.6, H11, J11, K5 and V1407b. The same SEM techniques have been used as described in chapter 2 (paragraph 2.1.2). Sample V288, V251b and V284a were used as test group and were not analyzed in the SEM.

### 3.4 Results

The most representative zircons were selected from sample 6.5, 2.6, H11, J11, K5 and V1407b. All characteristics of these zircons are listed in table 2 and presented in figure 6 to 13. A short description of all zircons per sample is given below.

*Sample 6.5* – 5 zircons are studied in the optical microscope and contain growth zoning and some NPFs. Two zircons of  $\sim 90 \mu\text{m}$  were analyzed in the SEM.

*Sample 2.6* – This sample contains relatively small zircons. 4 zircons are large enough to study in the optical microscope and contain NPFs. The largest zircon of  $\sim 100 \mu\text{m}$  is analyzed in the SEM.

*Sample H11* – In total 20 zircons were detected in the optical microscope. All zircons contain NPFs. 6 out of 20 zircons contain 1-3 sets of PMs. All zircons containing PMs are  $>100 \mu\text{m}$ . Zircons  $<100 \mu\text{m}$  do not contain PMs. 4 zircons were analyzed in the SEM. In the center of one of the zircons granular texture might be present.

*Sample K5* – 3 zircons were studied in the optical microscope as well as in the SEM. All 3 zircons contain NPFs, at least one set of PMs and are  $\geq 200 \mu\text{m}$ . Grayscale CL-images show most NPFs and PMs, but not all.

*Sample J11* – 7 zircons were detected in the optical microscope and contain NPFs. 2 zircons are  $>100 \mu\text{m}$  and contain PMs. The 5 other zircons are  $<100 \mu\text{m}$  and do not contain PMs. 2 zircons are studied in the SEM.

*Sample V4107b* – 13 zircons were studied in the optical microscope. 4 zircons were analyzed in the SEM. Compared to H11, K4 and J11, the zircons contain more (wider) NPFs, holes, inclusions and show more “damage”. 5 out of 14 zircons have 1-2 sets of PMs, one of these five zircons is  $<100 \mu\text{m}$ . Most fractures were filled with material. EDX-analysis pointed out that this material has a zirconic composition.

Sample V288, V251b and V284a were used as test group. A summary of the locations, rock types and optical observations is given below (Appendix 3 for a complete overview).

*Sample V288* – Granulite,  $26^{\circ}56'28''\text{S}$   $27^{\circ}24'03''\text{E}$ , Vredefort Dome, South Africa. This sample contains 2 zircons that are  $>200 \mu\text{m}$  and contain PMs.

*Sample V284a* – Granulite,  $26^{\circ}56'22''\text{S}$   $27^{\circ}30'33''\text{E}$ , Vredefort Dome, South Africa. This sample contains 2 zircons (one is  $<100 \mu\text{m}$  and the other  $>100 \mu\text{m}$ ) that contain no PMs.

*Sample V251a* – Granulite,  $26^{\circ}56'59''\text{S}$   $27^{\circ}30'33''\text{E}$ , Vredefort Dome, South Africa. In total 3 zircons are observed. The zircons are  $>100\mu\text{m}$  and contain 1 set of PMs.

Table 2. Optical microscope and SEM results of a few representative zircons from sample 6.5, 2.6, H11, J11, K5 and V1407b. The grain numbers correspond to the grain numbers in appendix 3. The figure numbers correspond to the figures below this table.

Sample	location	rock	Optical microscope	CL- and BSE-imaging
6.5 (grain 1) Figure 6	$40^{\circ}37'35''\text{N}$ $7^{\circ}02'02''\text{W}$ Guarda Structure, Portugal	++ granite	- $\sim 90 \mu\text{m}$ - Growth zoning. - Some NPFs.	- Fine growth zoning. - Some NPFs (core to rim).
2.6 (grain 2) Figure 7	$40^{\circ}38'12''\text{N}$ $7^{\circ}05'27''\text{W}$ Guarda Structure, Portugal	T granite	- $\sim 100 \mu\text{m}$ - A few NPFs.	- No clear growth zoning. - A few NPFs.
H11 (grain 2) Figure 8	$26^{\circ}58'15''\text{S}$ $27^{\circ}23'19''\text{E}$ Vredefort, South Africa	Granulite	- $\sim 200 \mu\text{m}$ - Very dark colored in ppl and xpl. - Hard to observe PMs and growth zoning.	- Clear growth zoning. - Three sets of PMs. Spacing between individual PMs varies between 1-10 $\mu\text{m}$ . PMs are $<0.5\mu\text{m}$ wide. - some PMs offset growth zoning and displace the crystal. - NPFs quite abundant, wider spaced than PMs. - crystallographic control on PMs orientation and displacement direction.

H11 (grain 4) Figure 9	26°58'15" S 27°23'19" E Vredefort, South Africa	Granulite	- ~60 $\mu\text{m}$ - Weak growth zoning. - No PMs. - Some NPFs.	- Some NPFs. - A few sub-planar fractures are present, but no distinct sets. - Granular structure might be visible on BSE-image in the center of the crystal.
K5 (grain 1) Figure 10	26°58'15" S 27°23'19" E Vredefort, South Africa	Granulite	- ~200 $\mu\text{m}$ - Two clear sets of closely spaced PMs. - Many NPFs. - One side looks ruptured.	- Two sets of PMs with spacing between 1-4 $\mu\text{m}$ . - NPFs. - No BSE-image .
K5 (grain 4) Figure 10	26°58'15" S 27°23'19" E Vredefort, South Africa	Granulite	- ~200 $\mu\text{m}$ - One set of PMs. - Major fracture crosscut through the crystal. - NPFs at rim of crystal.	- PMs not visible in CL-image. - Major non-planar fracture through the crystal displacing the crystal a few $\mu\text{m}$ . - No BSE-image.
J11 (grain 3) Figure 11	26°58'15" S 27°23'19" E Vredefort, South Africa	Granulite	-~90 $\mu\text{m}$ - NPFs	- Clear growth zoning. - NPFs
V4107b (grain 2) Figure 12	27°02'52" S 27°29'36" E Vredefort, South Africa	Granulite	- Two accreted zircons, both > 200 $\mu\text{m}$ . - Many NPFs. - Some PMs observed, but no clear sets. - Some areas in crystal remain black during rotation in crossed polarized light.	- Disrupted growth zoning. - Many NPFs. - Holes in the zircon. - Two sets of PMs with spacing between 7-10 $\mu\text{m}$ . - NPFs and PMs filled with material. - Crystals extremely fractured in some areas. - One area very fine and closely spaced <1 $\mu\text{m}$ PMs.
V4107b (grain 4) Figure 13	27°02'52" S 27°29'36" E Vredefort, South Africa	granulite	- Two zircons of ~100 $\mu\text{m}$ and ~200 $\mu\text{m}$ . - PMs and NPFs. - Surrounding rock is very fractured.	- Holes in crystal. - Many NPFs. - 2 sets of PMs. - NPFs and PMs filled with material. - Crystal fractured at rim.

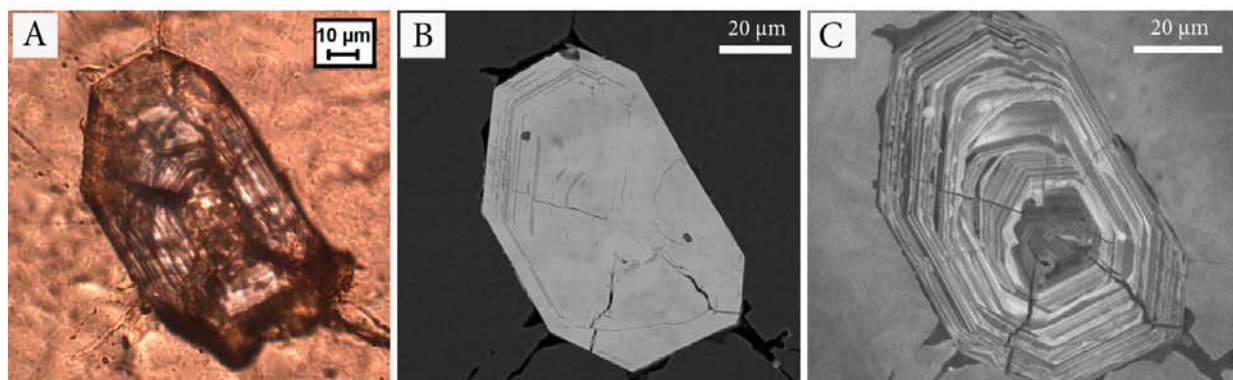


Figure 6. Zircon (grain 1) of ~90  $\mu\text{m}$  in sample 6.5, Guarda Structure. The zircon contains NPFs and growth zoning, visible in (a) a plane polarized light image, (b) BSE-image and (c) grayscale CL-image.

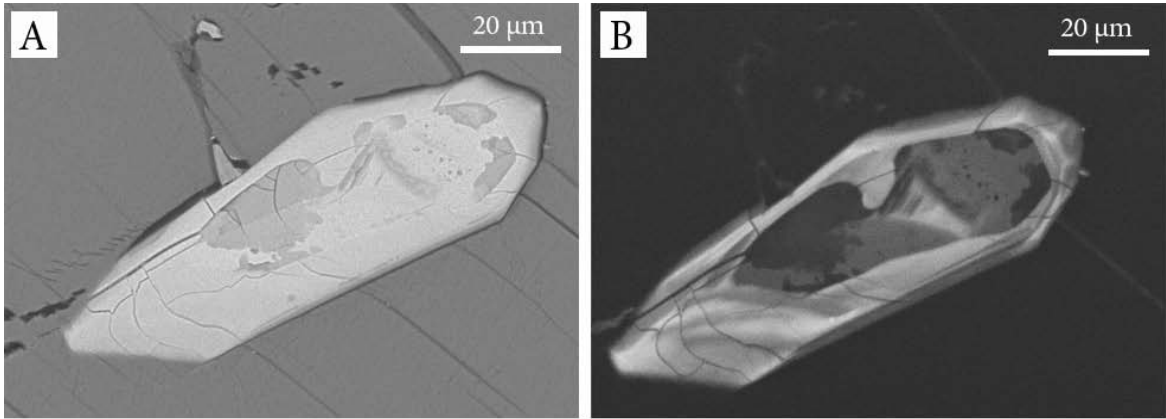


Figure 7. Zircon (grain 2) of  $\sim 100 \mu\text{m}$  in sample 2.6, Guarda Structure. The zircon contains NPFs that are visible in (a) BSE-image and (b) grayscale CL-image

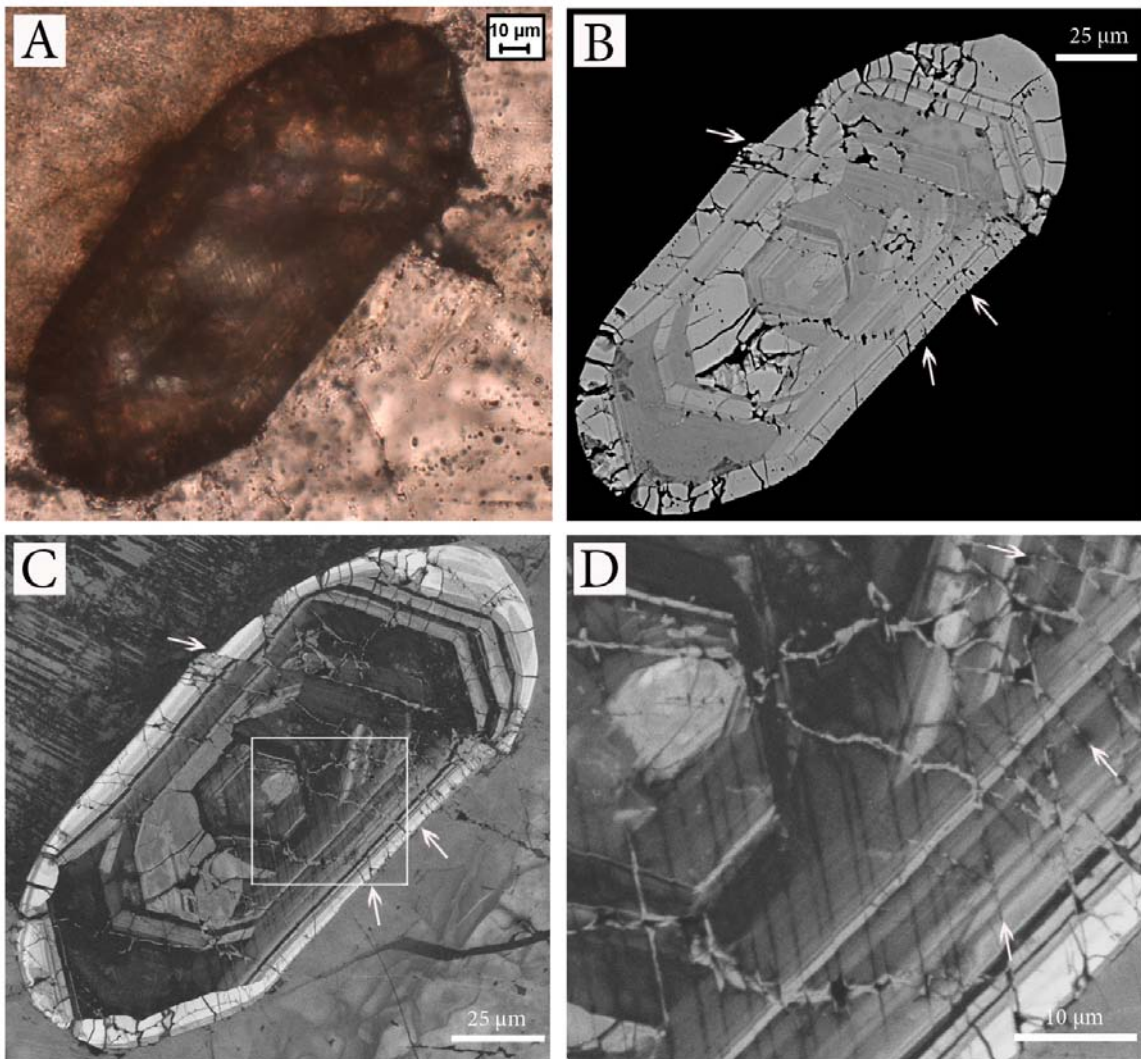


Figure 8. A shocked zircon (grain 2) of  $\sim 200 \mu\text{m}$  with NPFs and PMs in sample H11, Vredefort Dome. The white arrows point in the direction of three different sets PMs. (a) The internal structures aren't clearly visible in optical microscope images. (b) In the BSE-image the widest PMs and NPFs are visible. (c, d) Three distinct sets of PMs with a spacing between  $1\text{-}10 \mu\text{m}$  and width of  $<0.5 \mu\text{m}$  are present in the grayscale CL-images. Some PFs and PMs are filled with lighter colored material. Some PMs cause mineral displacement. Note the crystallographic control on PMs and apparent shear displacement.

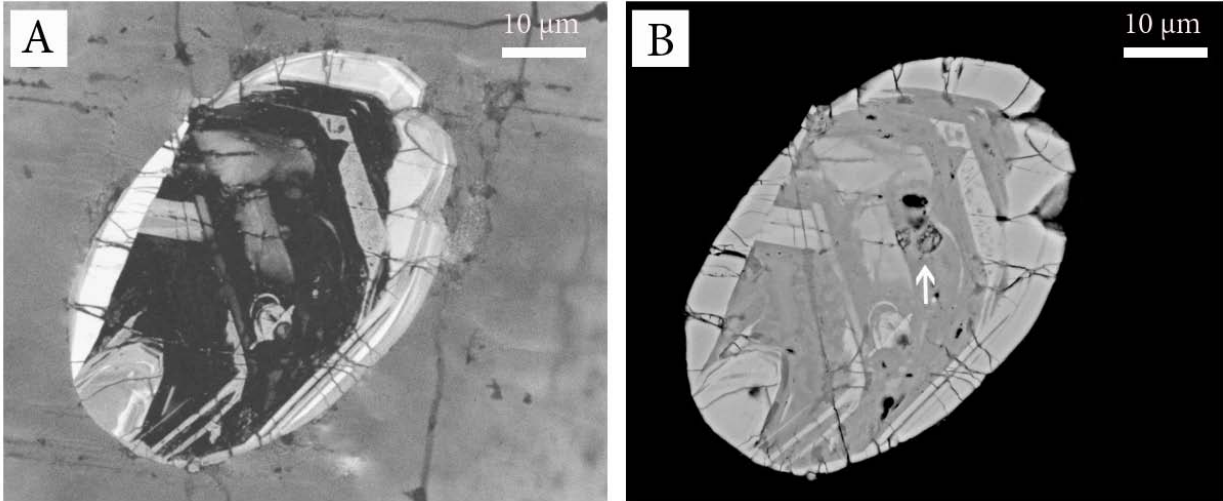


Figure 9. Zircon (grain 4) of  $\sim 60 \mu\text{m}$  in sample H11, Vredefort Dome. (a) In the grayscale CL-image some NPFs are visible. Planar features are mainly caused by growth zoning. (b) In the center of the BSE-image of the zircon granular structure may be visible.

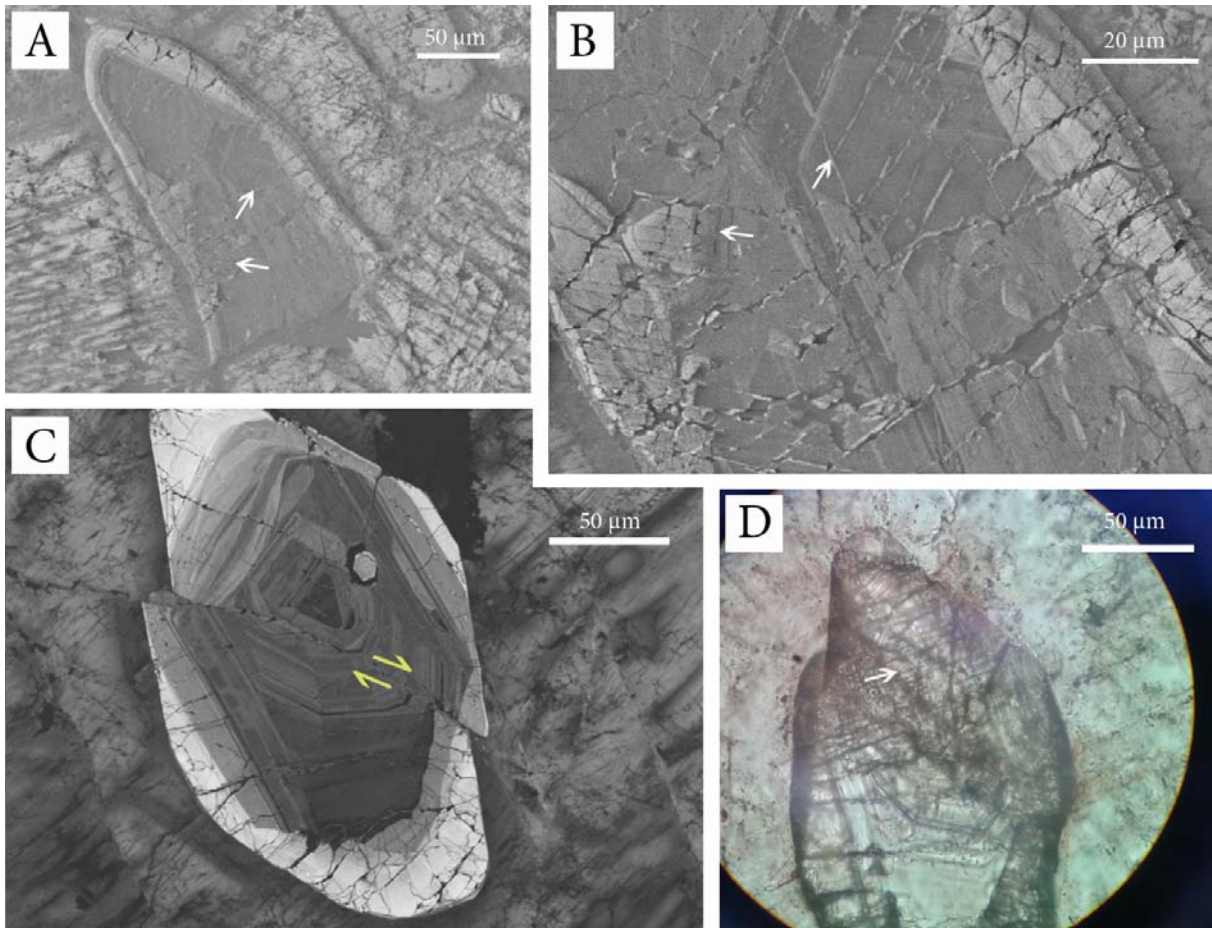


Figure 10. (a,b,c) Grayscale CL-images of two shocked zircons in sample K5, Vredefort dome. (a,b) Zircon (grain 1) contain two distinct sets of PMs with spacing between  $1\text{-}4 \mu\text{m}$ . White arrows point in the direction of the PMs. (c) Grayscale CL-image of the other zircon (grain 4) show a large fracture displacing the zircon. The yellow arrows give the 2D displacement direction. PMs are not visible in the CL-image. (d) However, a plane polarized light image does show one set of PMs in this zircon (white arrow).

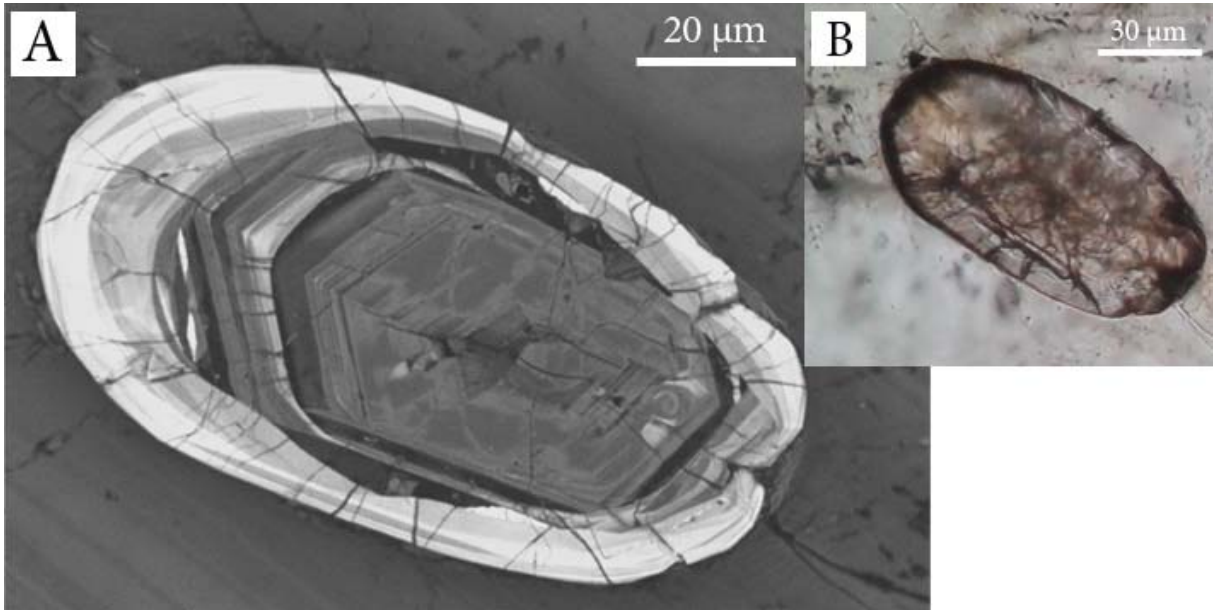


Figure 11. A zircon (grain 3) of  $\sim 90 \mu\text{m}$  in sample J11, Vredefort Dome. (a) Grayscale CL-image showing some NPFs. (b) The NPFs are better visible in plane polarized light.

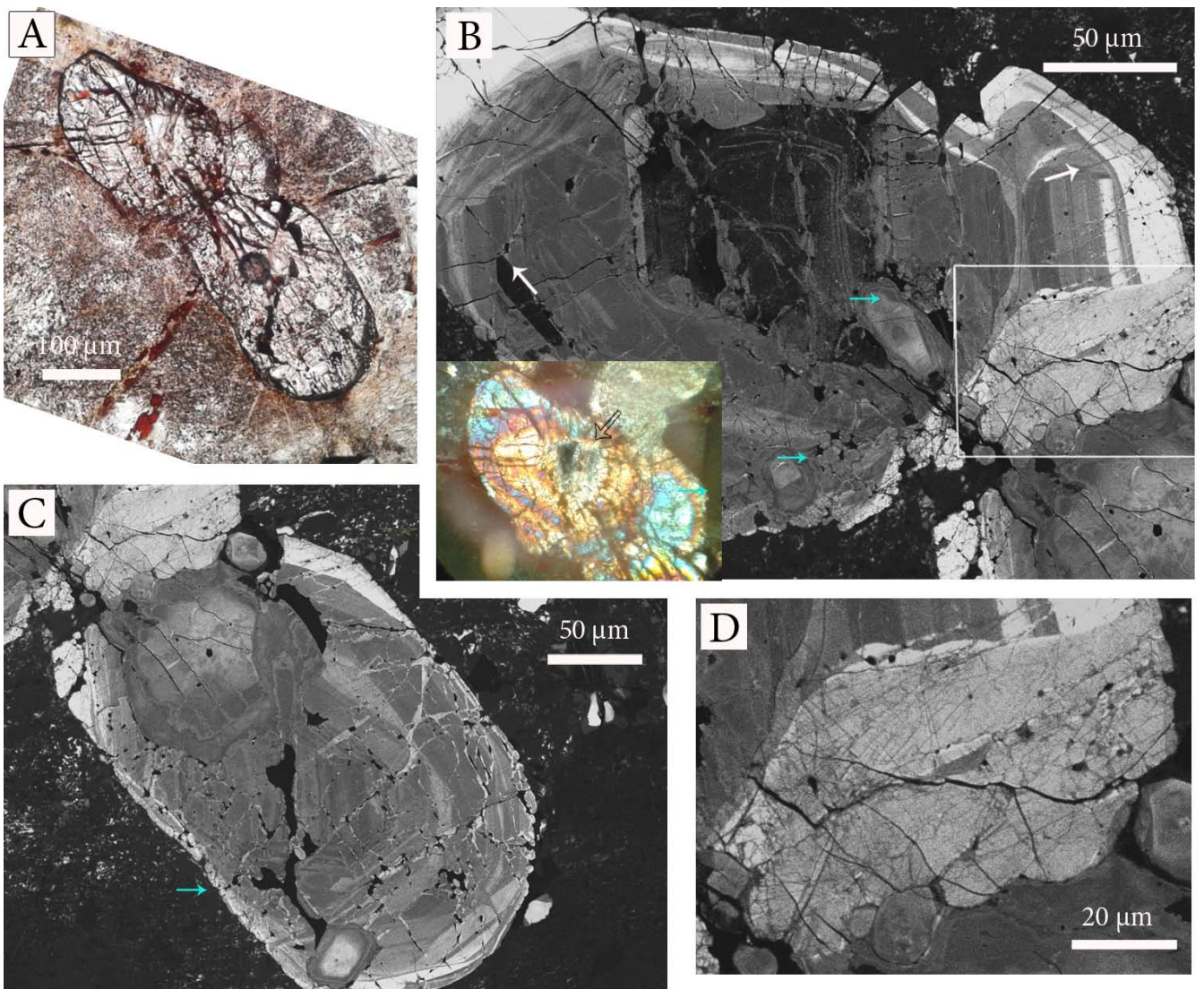


Figure 12. Two accreted zircon crystals (grain 2) of  $>200\ \mu\text{m}$  in sample V1407b, Vredefort Dome (a) Plane polarized light image of the accreted zircons, both contain many NPFs. (b) grayscale CL-image of the upper zircon containing many NPFs and two sets of PMs (white arrows) with spacing between  $7\text{--}10\ \mu\text{m}$ . A crossed polarized light image of the upper zircon is shown in the left corner. The transparent arrow points the inner part of the zircon with no birefringence color. This area remains black during rotation of the stage. (c) grayscale CL-image of the lower zircon containing wide NPFs and many holes. Quite a lot NPFs are filled with lighter colored material. The blue arrows point to areas where the zircons are extremely fractured to small pieces. (d) This grayscale CL-image is a higher magnification view of the white square in figure b. Note that in this lighter colored area, the zircon contains very closely spaced ( $<1\ \mu\text{m}$ ) PMs.

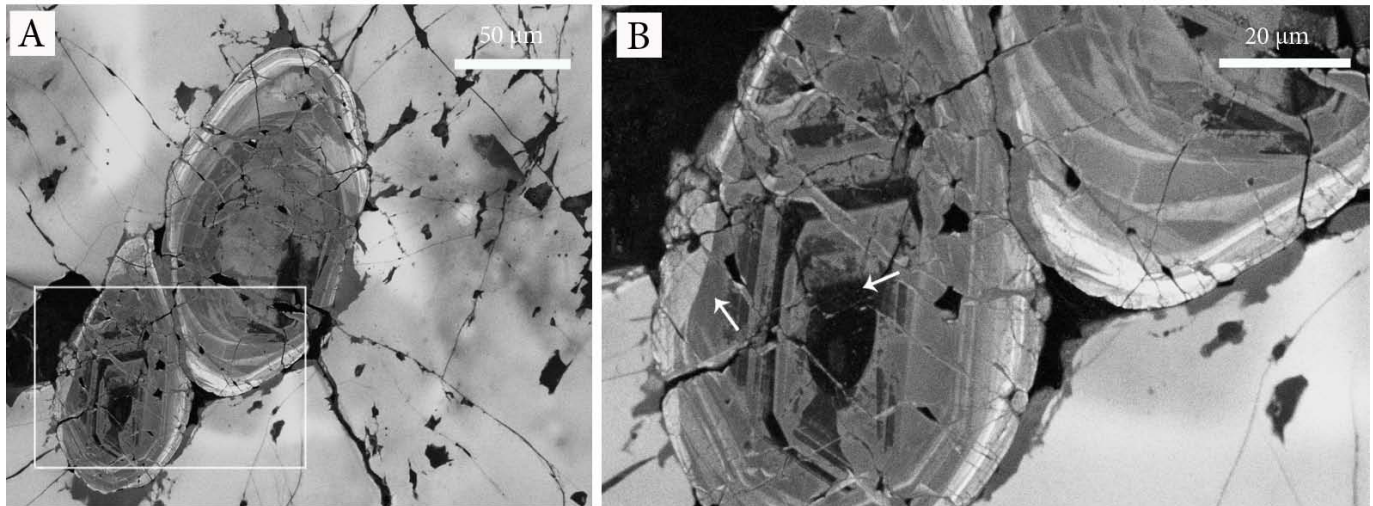


Figure 13. Two accreted zircons (grain 4) of  $\sim 100\ \mu\text{m}$  and  $\sim 200\ \mu\text{m}$  in sample V1407b, Vredefort Dome. (a) Grayscale CL-image showing filled fractures and holes in the zircons. The surrounding minerals are also intensely fractured. (b) A higher magnification view of the white square in figure a. Two sets of PMs (white arrows) that are mainly filled with material. EDX analyses pointed out that the fractures are filled with zirconic material. At the left side, the zircon starts to fall apart.

### 3.4.1 Summary of the results

The zircons from the Guarda Structure contain some NPFs and no PMs (figure 6 and 7). All studied zircons in samples H11, K5, J11 and V1407b from the Vredefort Dome contain NPFs and  $\sim 40\%$  of the zircons contain one or more sets of PMs (figure 8-11). PMs in zircon have been mainly developed in zircons  $>100\ \mu\text{m}$  and there is a clear crystallographic control on most PMs (figure 8). Many PMs are filled with (secondary) material. Not all PMs are visible in grayscale CL-images, but are visible in plane polarized light (figure 10). Zircons from sample v1047b contain finer, more closely spaced PMs, more (filled) NPFs, holes, inclusions and show more “damage” compared to the other shocked zircons (figure 12). One zircon in sample H11 (figure 9) may contain some granular texture in the center of the grain. Zircons from the test group samples, V288, V251b and V284a, contain NPFs and some zircons contain PMs as well.

### 3.5 Discussion

Before the results of the Guarda Structure are compared to the results of the Vredefort Dome, the nature and main characteristics of the PMs in the shocked zircons from the Vredefort Dome will be discussed.

### 3.5.1 Nature of planar microstructures in zircon

40% of the zircons in sample H11, K5, J11 and V1407b contain PMs. The PMs could be PFs, PDFs or micro-twin lamellae. According to Leroux et al. (1999) only PFs are observable during light microscopy. As mentioned in paragraph 3.1.1.1, PDFs in zircon are probably too small (~10 nm) to be observed and micro-twin lamellae can only be observed with the help of electron backscatter diffraction (EBSD-)techniques (Moser et al., 2011). The PMs in zircon observed during this study often appear as open or filled structures with spacing between 1-10  $\mu\text{m}$  (figure 8, 10, 12 and 13). Sometimes an individual PM causes mineral displacement (figure 8). The orientations of the PMs are strongly correlated to specific crystallographic planes. As visible in figure 8 and 13, the PMs are often parallel to the growth zoning of some crystallographic planes. Because the growth zoning shows the tetragonal crystal structure (figure 8) of the zircon, the approximate crystallographic planes of PMs (dip of PMs remains unknown, because all images are 2D) could be determined. PMs are mainly observed perpendicular and oblique to the main crystal length (c-axis) (figure 8). The corresponding crystal planes might be {001} and {011}. As represented in figure 3, PFs in zircon form parallel to specific planes, including {001} and a few planes oblique to c-axis. Most PMs observed during this study have the characteristics of PFs (table 1) and the same orientation of PFs in zircon (figure 3). Therefore most PMs observed in the zircons are probably PFs.

The PMs observed in a specific area of a zircon from sample V1407b (figure 12d) appear to be different from the previous described PMs. These PMs are finer and more closely spaced (<1  $\mu\text{m}$ ) which are typical characteristics for PDFs (table 1). My hypothesis is that these PMs might be PDFs. This implicates that PDFs in zircon are observable during light microscopy, but only at high magnifications and probably in lighter colored areas of grayscale CL-images.

### 3.5.2 Relation crystal size and PM development

In total ~40% of the studied zircons in sample H11, K5, J11 and V1407b from the Vredefort Dome contain one or more sets PMs (Appendix 3). However, it is quite remarkable that 96% of this 40% has a size >100  $\mu\text{m}$ . Just one zircon <100  $\mu\text{m}$  contains PMs. The test group with sample V288, V251b and V284a is used to test whether this zircon size-PM relation is present in other samples as well. 9 zircons were observed in the three test samples. 5 zircons contain PMs and all zircons were >100  $\mu\text{m}$ . Two zircons from the test group were <100  $\mu\text{m}$  and don't contain PMs. The test group also confirms this size-PM relation.

My hypotheses is that PMs preferably develop in crystals >100  $\mu\text{m}$  because there is a clear size-PM relation within all samples from the Vredefort. The zircons with PMs that are shown by Cavosie et al. (figure 3-7, 2010) and Moser et al. (figure 2-4, 2011) are also > 100 $\mu\text{m}$ . Only Flowers et al. (2003) shows one zircon with PMs that is <100  $\mu\text{m}$ . Since all zircons from the Guarda Structure are <100  $\mu\text{m}$  it is questionable whether the PMs in zircon can be used as impact criteria. To compare the results from the Guarda Structure and the Vredefort Dome it is probably more useful to look at NPFs. NPFs form in zircons of all sizes.

### 3.5.3 Guarda Structure versus Vredefort Dome

NPFs are present in zircon from the Guarda Structure as well as in the samples from the Vredefort Dome. The density of NPFs increases with shock intensity (Leroux et al., 1999). Figure 14 confirms this suggestion; with increasing shock pressure the NPFs cause more damage to the zircon. (Detailed information about the shock pressures is given in paragraph 3.5.4).

The appearance of NPFs in zircon from the Guarda Structure does not have to indicate that the zircon is shocked. NPFs can form at low strain rate processes during tectonic activity (Timms et al., 2011). As discussed in chapter 1 (paragraph 1.5.3), Tertiary accretion of Iberia to both the European and African plate might have influenced the Guarda Structure (e.g. Vegas et al., 1990; Bruijne and Andriessen, 2002). NPFs can also develop due to cooling and volume change associated with metamictization in zircon (Timms et al., 2011). Metamictization is the crystalline conversion of a crystal into an amorphous mineral, due to alpha decay. Differential expansion of individual layers due to variations in alpha-decay causes a systematic pattern of fractures (Chakoumakos et al., 1987).

If the zircons from the Guarda Structure are shocked, they experienced clearly lower shock pressures than sample H11 and V4107b. However, due to the fact that NPFs can be produced by other processes than a meteorite impact, it's not possible to make a definite conclusion about the Guarda Structure.

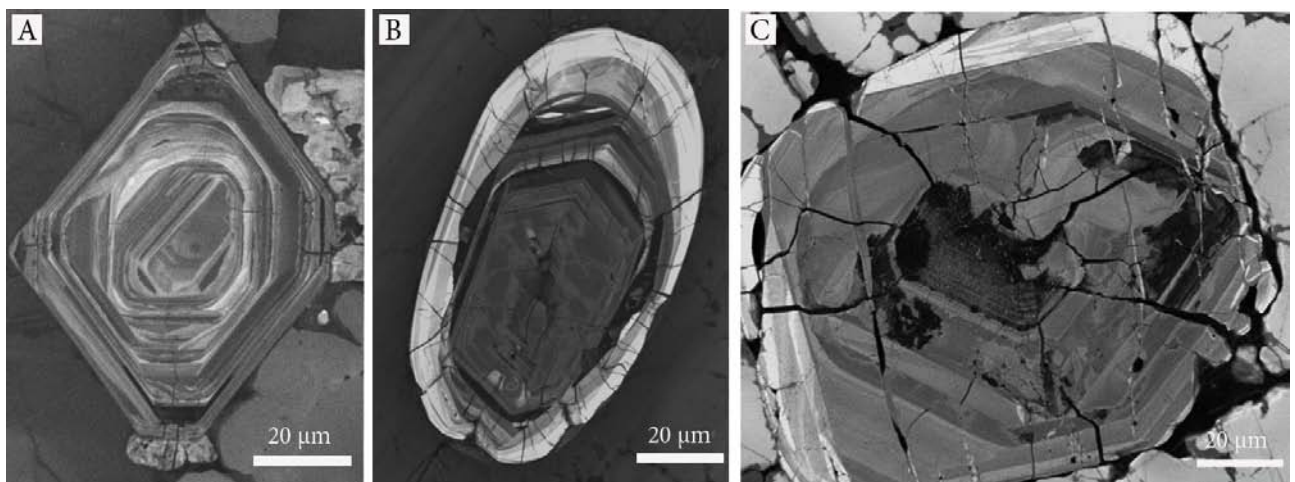


Figure 14. Three grayscale CL-images of zircons with a comparable size. (a) A zircon from the Guarda Structure with a few NPFs at the rim. (b) Zircon in sample H11 from the Vredefort Dome (10-15GPa) containing more NPFs than the zircon in figure a. (c) Zircon in sample V4107b from the Vredefort Dome (>30GPa), compared to figure a and b the NPFs are wider, often filled and disrupt growth zoning. At the right the zircon falls apart.

### 3.5.4 Shock pressures forming PMs

As discussed in the previous paragraphs, the zircons from the Vredefort contain PMs. The shock pressure range for PMs could be determined, because the shock pressure distribution in the Vredefort (Gibson and Reimold, 2005) and the sample locations are known.

#### 3.5.4.1 Previous work

According to Wittman et al. (2006) PMs do not develop at shock pressures <20 GPa (figure 5). Wittman et al. (2006) didn't discuss the formation of PFs separately from PDFs and micro-twin lamellae. Leroux et al. (1999) observed PFs in zircon shocked experimentally to 20 GPa and 40GPa, but did no experiments with lower shock pressures. PDFs were found in zircons shocked to 40GPa and 60GPa. The shock pressure range for the development of PMs in zircon is thus quite uncertain.

#### 3.5.4.2 Shock pressure distribution in the Vredefort Dome

Gibson and Reimold (2005) determined the shock pressure distribution in the Vredefort Dome by looking at shock microstructures in quartz, feldspar and ferromagnesium minerals (figure 15). H11,

J11 and K5 are granulite samples that were sampled from zone II; representing shock pressures between 10-15 GPa (Gibson and Reimold, 2005). ~36% of the zircons in these samples contain one or more sets of PMs. This may implicate that PMs in zircon form at lower shock pressures than 20 GPa. However, Gibson and Reimold (2005) also determined pressure heterogeneity on a hand specimen-scale and even mineral grain-scale. The distance between the sample locations of samples H11, J11 and K5 is just a few meters and all samples contain at least two zircon crystals with PMs. The PMs could be formed due to shock heterogeneity in this area or within the different samples. Therefore, the zircons containing PMs must have experienced shock pressures >20 GPa. Nevertheless, it is also possible that PMs are not formed due to pressure heterogeneity.

To test this latter hypothesis, a test group of three other samples, V288, V251b and V284a from the Vredefort Dome were analyzed with an optical microscope (Appendix 3). The samples in this test group are also located in zone II, 10-15 GPa (figure 11). Samples V288 and V251b contain zircons with PMs as well. Sample V284a doesn't contain zircon with PMs, but just two zircons were observed in this sample. In total 34 zircons >100  $\mu\text{m}$  are observed in the 7 samples from the Vredefort Dome. 61% of the 34 zircons contain PMs. I suggest this high percentage indicates that PMs do not develop due to pressure heterogeneity.

Zircons from five different locations in zone II contain PMs. If the pressure distribution of Gibson and Reimold is correct, PMs in zircon probably form at shock pressures between 10 and 15 GPa. This implicates that PMs in zircon form during lower shock pressures than was suggested before by Wittmann et al. (2006). However, it is questionable whether the shock pressure distribution of Gibson and Reimold (2005) is correct. The shock pressure in zone II (10-15GPa) is based on PDFs in quartz. As discussed in chapter 2 (paragraph 2.4.5) PDFs in quartz from the Vredefort Dome are highly annealed and in some cases no longer visible (Leroux et al., 1993 and Grieve et al., 1990). Nevertheless, the upper limit (15 GPa) of zone II is determined by PDFs in plagioclase. According to Huffman and Reimold (1996) the formation of PDFs in plagioclase occurs at ~15 GPa and is independent of pre-shock temperatures. If this upper limit is correct, PMs (probably PFs) most likely start to form at pressures <15 GPa.

The possible granular structure observed in a zircon in sample H11 (figure 9) may be caused due to pressure heterogeneity, because it is observed in just one sample. However, granular texture in zircon forms at pressures >50 GPa (Wittmann et al., 2006). A local shock pressure increase of >30GPa may be unlikely. It is also possible that the structure is formed by some dense NPFs.

Sample V4107b is located in the center of the Vredefort Dome, zone IV. The center experienced shock pressures >30-35 GPa. The shock pressure range for zone IV was determined by development of diaplectic feldspar and quartz glass above ~30–35 GPa. PMs are also observed in zircons from V4017b. Some of these PMs are more widely spaced and often filled with zirconic material. Due to non-adiabatic decay of the impact shock wave, the center of the structure exceeds temperatures of 900-1000°C and locally even exceeds 1350°C (Gibson, 2002). These temperatures may not initiate the melting and recrystallization in the fractures, since the melting temperature of zircon is about ~2750°C. Local melting of the zircon may be initiated by the high shock pressures. Also PMs that had characteristics of PDFs were observed in zircons from this sample. If these PMs are PDFs they probably form already at pressures between 30-35 GPa.

Some areas within zircons from sample V4107b remain black in crossed polarized light. The mineral structure within these areas is probably (partly) damaged due to the high shock pressures. However, granular texture was not observed, so according to Wittmann et al. (2006) the shock pressure was

<50 GPa. I therefore conclude that PMs probably developed in zircons from the Vredefort Dome within the pressures range of >10-35 GPa. Leroux et al. (1999) even found PMs in zircons that were experimentally shocked to 60 GPa.

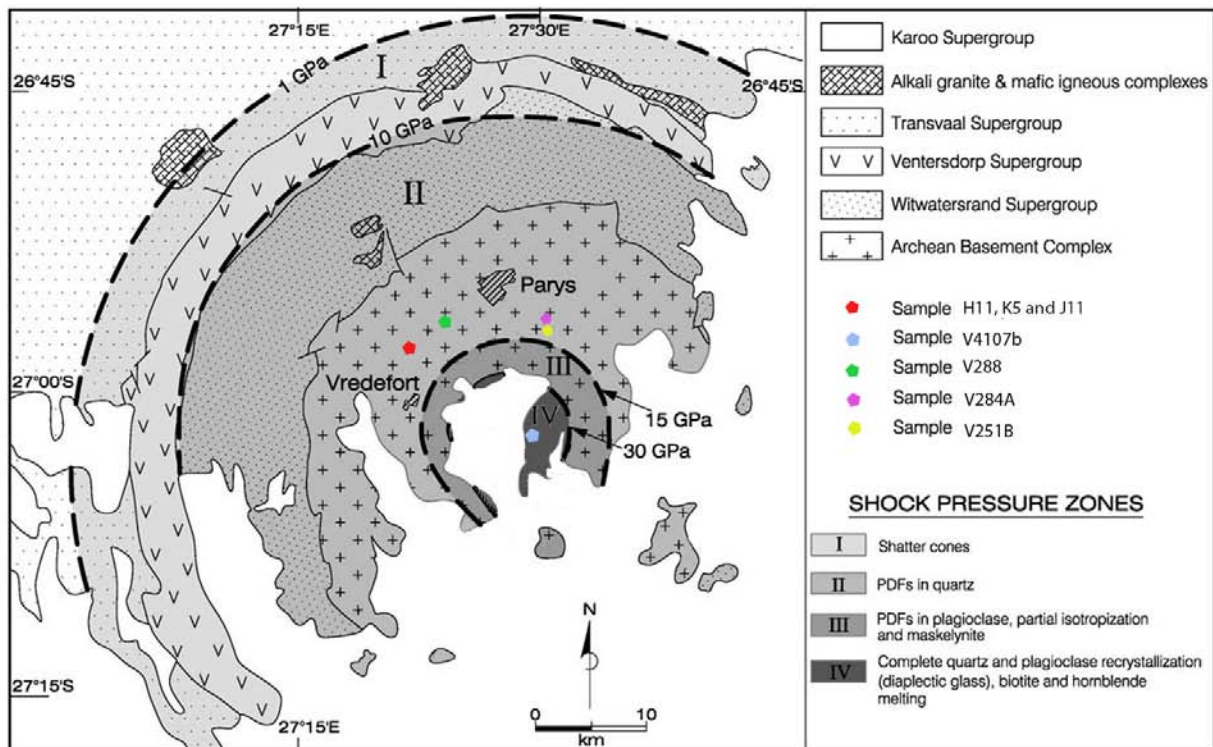


Figure 15. Pressure distribution in the Vredefort Dome, South Africa. The colored dots are the samples and their locations. All samples come from zone II, 10-15 GPa, excluding sample v4107b. Sample v4107b is located in zone IV representing shock pressures >30 GPa (Modified from Gibson and Reimold, 2005).

### 3.6 Conclusion and further research

Optical microscope study in combination with SEM analysis is a good method to analyze PMs in zircon. In some CL-images PMs are hard to observe, while they are clearly present in the optical microscope. On the other hand growth zoning could resemble PMs in the optical microscope, but PMs and growth zoning are easy to distinguish in CL- and BSE- images.

PMs observed in most zircons have characteristics and orientations similar to PFs described in previous studied. Only a few finer more closely spaced PMs from sample V1407b could be PDFs.

There's a clear relation between the zircon crystal size and the development of PMs in shocked zircons. Zircons from the Vredefort Dome that are >100  $\mu\text{m}$  predominately contain distinct sets of PMs. None of the observed zircons from the Guarda Structure contain PMs, but all zircons in the Guarda Structure are <100  $\mu\text{m}$ . Due to the size-PM relation observed in the Vredefort samples, it's impossible to conclude whether the zircons in the Guarda Structure are shocked or unshocked. The amount and thickness of NPFs increase with increasing shock pressures. Compared to the Vredefort zircons, the zircons from the Guarda Structure contain less and thinner NPFs. These NPFs can be formed due to processes other than meteorite impact. To determine whether the Guarda Structure is an impact crater, zircons >100  $\mu\text{m}$  must be collected and analyzed or potential shock microstructures in monazites from the Guarda Structure can be analyzed (chapter 4).

Based on the shock distribution of Gibson and Reimold (2005) PMs in zircon develop over a wide range of shock pressure >10 GPa up to 40 GPa and can probably form at lower pressure than assumed previously. PMs in zircon could be used as shock indicator for relatively low and high shock stages. It is still unknown whether PMs with a specific orientation preferentially develop at particular shock pressures. More zircons must be collected from craters with a known pressure distribution and the orientation of the PMs must be determined. The U-stage might be a good instrument to determine the different orientations of PMs.

## References

- Bohor, B. F., Betterton, W. J., Krogh, T. E., 1993, Impact-shocked zircons: Discovery of shock-induced textures reflecting increasing degrees of shock metamorphism, *Earth and Planetary Science Letters* 119, p. 419–424.
- Cavosie, A. J., Quintero, R. R., Radovan, H. A., Desmond, E. M., 2010, A record of ancient cataclysm in modern sand: Shock microstructures in detrital minerals from the Vaal River, Vredefort Dome, South Africa, *Geological Society of America Bulletin* 122, 1968–1980.
- Chakoumakos, B.C., Murakami, T., Lumpkin, G.R., Ewing, R.C., 1987, Alpha-Decay--Induced Fracturing in Zircon: The Transition from the Crystalline to the Metamict State, *science*, 236, p. 1556-1559.
- Cintrón, N. O., Cavosie, A. J., Gibbon, R.J., Radovan, H. A., Moser, D. E., Wooden, J., 2011, In Situ U-Th-Pb Geochronology of detrital shocked monazite in Pleistocene fluvial deposits along the Vaal river, South Africa, 42nd Lunar and Planetary Science Conference (Abstract)
- El Goresy, A., 1965, Baddeleyite and Its Significance in Impact Glasses, *Journal of Geophysical research*, 70, p. 3453-3456.
- Fiske, P.S., 1999, Shock-induced phase transitions of ZrSiO<sub>4</sub>, reversion kinetics, and implications for impact heating in terrestrial craters, American Physical Society, Conference on Shock Compression of Condensed Matter. June, Snowbird, Utah (abstract)
- French, B.M, Koeberl, C., 2010, The convincing identification of terrestrial meteorite impact structures: What works, what doesn't, and why *Earth-Science Reviews*, 98, p. 123–170.
- Gibson, R.L., 2002, Impact-induced melting of Archaean granulites in the Vredefort Dome, South Africa, I: Anatexis of metapelitic granulites, *Journal of Metamorphic Geology*, 20, p. 57–70.
- Gibson, R.G., Reimold, W.U., 2005, Shock pressure distribution in the Vredefort impact structure, South Africa, *Geological Society of America Special Paper*, 384, p. 329-249.
- Goltrant, O., Leroux, H., Doukhan, J. C., Cordier, P., 1992, Formation mechanisms of planar deformation features in naturally shocked quartz, *Physics of The Earth and Planetary Interiors* 74, p. 219–240.
- Goltrant, O., Cordier, P., Doukhan, J-C., 1991, Planar deformation features in shocked quartz; a transmission electron microscopy investigation, *Earth and Planetary Science Letters* 106, p. 103-115.
- Grieve R. A. F., Coderre, J. M., Robertson, P. B., Alexopoulos, J., 1990, Microscopic planar deformation features in quartz of the Vredefort structure: Anomalous but still suggestive of an impact origin, *Tectonophysics* 171, p. 185–200.
- Grieve, R.A.F., Reimold, W.U., Morgan, J., Riller, U., and Pilkington, M., 2008, Observations and interpretations at Vredefort, Sudbury and Chicxulub: Towards a composite Kinematic model of terrestrial impact basin formation, *Meteoritics & Planetary Science*, 43, p. 855–882.
- Huffman, A.R., and Reimold, W.U., 1996, Experimental constraints on shock-induced microstructures in naturally deformed silicates, *Tectonophysics*, 256, p. 165–217.
- Kusaba, K., Syono, Y., Kikuchi, M., Fukuoka, K., 1985, Shock behavior of zircon: phase transition to scheelite structure and decomposition, *Earth and Planetary Science Letters*, 72, p. 433-439.
- Leroux, H., Reimold, W.U., Doukhan, J-C., 1993, A TEM investigation of shock metamorphism in quartz from the Vredefort dome, South Africa, *Tectonophysics* 230, p. 223-239.

- Leroux, H., Reimold, W. U., Koeberl, C., Hornemann, U., Doukhan, J.-C, 1999, Experimental shock deformation in zircon: A transmission electron microscopic study, *Earth and Planetary Science Letters* 169, p. 291–301.
- Moser, D. E., Cupelli, C. L., Barker I. R., Flowers, R. M., Bowman, J. R., Wooden, J., and Hart, J. R., 2011, New zircon shock phenomena and their use for dating and reconstruction of large impact structures revealed by electron nanobeam (EBSD, CL, EDS) and isotopic U-Pb and (U-Th) / he analysis of the Vredefort dome, *Canadian Journal of Earth Sciences*, 48, p.117–139.
- Timms, N.E., Reddy, S.M., Healy, D., Nemchin, A.A., Grange, M.L., Pidgeon, R.T., Hart, R., 2011, Resolution of impact-related microstructures in lunar zircon: A shock-deformation mechanism map, *Meteoritics & Planetary Science*, p. 1–22.
- Wittmann, A., Kenkmann, T., Schmitt, R. T., Stöffler, D., 2006, Shock-metamorphosed zircon in terrestrial impact craters, *Meteoritics & Planetary Science*, 41, p. 433–454.

## Chapter 4: Shock microstructures in Monazite

### 4.1 Introduction

PMs in zircon appear to be a valuable shock indicator for relatively high as well as low shock pressures. However, the PMs in zircon may be limited as shock indicator for the Guarda Structure, due to the crystal size – PM relation proposed in chapter 3 (paragraph 3.5.2). This final chapter deals with shock microstructures in monazite.

Monazite is a REE-containing phosphate mineral that is often present in granitic rocks. Next to zircon, monazite is also quite durable in impact environments (e.g. Cavosie et al., 2010 and Cintrón et al., 2011). Besides quartz and zircon, monazite could also contain shock microstructures, but to date not much has been published about monazite as shock indicator (Cavosie et al., 2010). Monazite appears to be a valuable mineral to date impacts (Moser et al., 1997 and Cintrón et al., 2011).

In this chapter shock microstructures in monazites from the Vredefort Dome will be studied. These monazites are compared to monazites from the Guarda Structure. The usability of shock structures in monazites will be studied and the shock pressures range for several shock microstructures in monazite will be established.

#### 4.1.1 Shock Microstructures in monazite

Planar microstructures (PMs) have been observed in shocked monazite (e.g. Schärer and Deutsch, 1990; Flowers et al., 2003; Cavosie et al., 2010; Cintrón et al., 2011). Schärer and Deutsch (1990) were the first who reported weak PMs in a SEM-image of a shocked monazite from the Houghton impact structure, Canada. Flowers et al. (2003) observed PMs in BSE-images of shocked monazites from the Vredefort Dome, South Africa. PMs in shocked monazite from the Vredefort Dome were recorded as well (Cavosie et al., 2010). Up to four orientations of PMs are found in shocked monazite grains from the Vredefort Dome (Cavosie et al., 2010; Cintrón et al., 2011). The PMs have a variable spacing of 1 to 20  $\mu\text{m}$  (Cavosie et al., 2010). The orientations of the PMs have never been determined.

Moser et al. (1997) was the first who reported polycrystalline monazite in rocks from the Vredefort Dome; where monazite occurs as an aggregate of 5-10  $\mu\text{m}$ -wide crystallites. Such polycrystalline monazite is similar to granular texture in shocked zircon. Moser et al. (1997) interpreted the polycrystalline texture as possible shock morphology. The granular structure in zircon was caused by shock-induced amorphization and the following recrystallization (Bohor et al., 1993). This might be the case for monazite as well.

#### 4.1.2 Monazite as impact dating tool

Next to REE, monazite incorporates thorium and uranium, making it an ideal candidate for dating analyzes. Dating analyzes have been done with experimentally and naturally shocked monazites (e.g. Deutsch and Schärer, 1990; Schärer and Deutsch, 1990; Moser et al., 1997; Cintrón et al., 2011).

Deutsch and Schärer (1990) experimentally shocked monazite to pressures up to 35, 47.5 and 59 GPa and corresponding high temperatures (>1200°C). They found that these shock experiments do not measurably affect the U-Pb system. Therefore it appears that the U-Pb system in monazite is not a reliable chronometer to date impact events in moderately to highly shocked rocks. Schärer and Deutsch (1990) dated a monazite with weak PMs (U-Pb method) from the 23-Ma-old Houghton impact crater on Devon Island (Arctic Canada) and found much older high-grade metamorphic ages,

instead of the impact age. On the other hand, Cintrón et al. (2011) did U-Th-Pb age determinations on monazites with 4 distinct sets of PMs and half of the monazite grains formed a discordia that, when regressed through the impact age of 2020 Ma, yield an upper intercept age of  $3005 \pm 62$  Ma. This implies that a part of the monazites lost its Pb during the Vredefort impact and that the U-Pb system in monazite, with several sets of PMs, is usable as chronometer to date impact events.

Moser et al. (1997) showed that a granular monazite from the Vredefort Dome completely lost all its Pb. After U-Pb dating analyzes they found an age of  $2016 \pm 7$  Ma. The error range of the age determination covers the previous determined impact age ( $\sim 2020$  Ma). Moser et al. (1997) suggested that the Pb loss event could be related to the impact event itself, or to the subsequent postimpact metamorphism. They could not resolve which of these mechanisms caused Pb loss, but suggested that the two events were penecontemporaneous.

#### 4.2 Methods and samples

Only sample 6.5 from the Guarda Structure is used to study monazites, because monazites in the other samples were too small  $< 10 \mu\text{m}$ . 2 monazites of  $\sim 60 \mu\text{m}$  were detected in sample 6.5. From the Vredefort Dome 16 granulite samples were studied in the optical microscope. In sample H11, J11, K5, V1407b, V251b and V284a, 1 to 3 monazite grains per sample were observed. Appendix 3 shows scans of the thin sections of the Guarda Structure and the Vredefort Dome. In a table below each scan, the size and internal structure of each monazite is listed.

Each monazite was studied in an optical microscope. SEM analysis has been done on sample 6.5, H11, J11, K5 and V1407b. CL-images were not made, because monazites don't emit light photons. To determine the chemistry of the crystals, EDX-analysis has been done on each monazite. BSE-images have been made as well (chapter 2 for description of methods). Samples V1407b, V251b and V284a were only studied in the optical microscope.

#### 4.3 Results

Table 1 is an overview of the light microscope characteristics of the monazites per sample.

Table 1. Optical microscope and SEM observations of all monazites detected in the samples. Ppl = plane polarized light, xpl = crossed polarized light. The grain numbers per sample correspond with the grain numbers in appendix 3. The figure numbers correspond with the figures below the table.				
Sample	location	rock	Optical microscope	BSE-imaging
6.5 (grain 3 and 4) Figure 1	40°37'35"N 7°02'02"W Guarda Structure, Portugal	++ granite	-Too small to make good observations.	- No planar structures. - Holes and damaged rims.
H11 (grain 4) Figure 2	26°58'15" S 27°23'19" E Vredefort, South Africa	Granulite	- Two sets of PMs visible in ppl and xpl. - Some NPFs. - A reaction rim around the monazite.	- Two set of PMs with spacing between 1-10 $\mu\text{m}$ . - One set seem to be sub-planar fractures. - Some NPFs. - Reaction rim of small crystals.
K5 (grain 2) Figure 3	26°58'15" S 27°23'19" E Vredefort,	Granulite	- Two sets of PMs visible in ppl and xpl. - Birefringence colors	- Three sets of thin PMs visible with a spacing of 1-8 $\mu\text{m}$ . - Some PMs are open fractures.

	South Africa		change from pink to orange to yellow to blue going closer towards PMs. - Clear bands with lower birefringence color. - no NPFs.	- no NPFs. - bands with lower birefringence color in between two PMs forming equally spaced bands of a few micrometer.
J11 (grain 1) (figure 4)	26°58'15" S 27°23'19" E Vredefort, South Africa	Granulite	- Three sets of PMs. - Some PMs are decorated. - Few NPFs.	-Three sets of PMs with spacing between 2-10µm - One set contain PMs that are decorated. - few NPFs.
V4107b (grain 1 and 6) Figure 5	27°02'52" S 27°29'36" E Vredefort, South Africa	Granulite	- Two granular crystals of ~100µm and ~500µm. - Visible in ppl and xpl. - Aggregates are between 10-50 µm.	- Separate aggregates are visible. - No other internal structures.
V284a (grain 1, 2 and 4) Figure 6	26°56'22"S 27°30'33"E Vredefort, South Africa	Granulite	- Contain three sets of PMs. - One set appears as planar bands with other birefringence colors. - PMs visible in ppl and xpl. - Almost no NPFs. - Changing birefringence towards PMs.	-
V251b (grain 1) Figure 7	26°56'59"S 27°30'33"E Vredefort, South Africa	Granulite	- Two sets PMs with regular spacing of ~15µm. - One set has lower birefringence colors than host grain. - The other set is formed by other extinction angle than host grain. - A few large NPFs.	-

#### 4.3.1 Summary of the results

The monazites from the Guarda Structure contain neither NPFs nor PMs. 100% of the studied monazites in samples H11, K5, J11, V251b and V284a contain one, two or three distinct sets of PMs. All PMs are clearly visible during light microscopy. Not all PMs in monazite are the same. PMs include: 1) sharp, thin and straight PMs with a spacing of 1-8 µm, that sometimes appear as open fractures (figure 2, 3, 4, 6, 7). Two of these individual PMs could form a band with different birefringence color than host grain (figure 3, 6 and 7). 2) PMs are visible in crossed polarized light due to other extinction angle than host grain (figure 7). 3) Decorated PMs (figure 4). Sample v1047b contains two monazites with granular texture (figure 5). All studied monazites do not contain any, or a few NPFs.

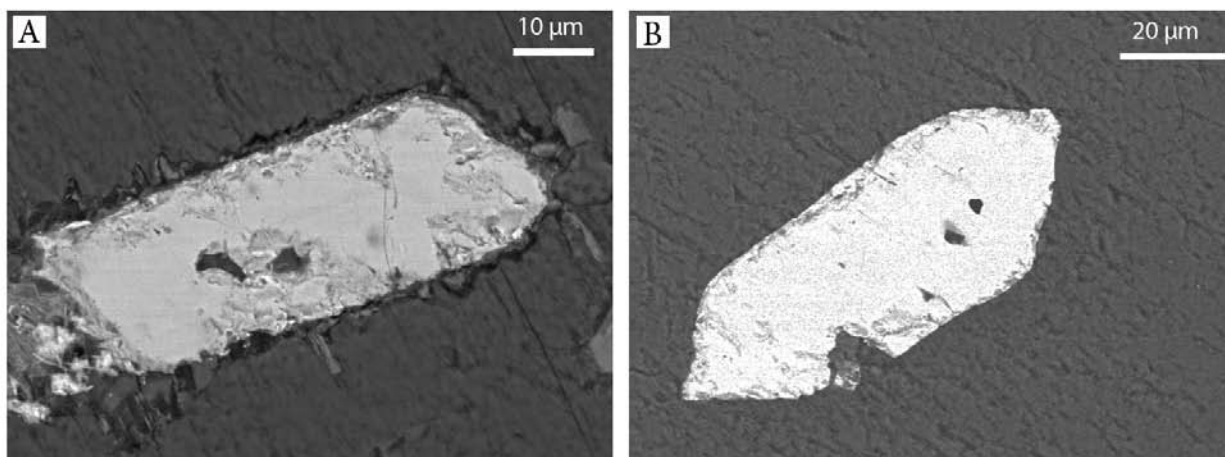


Figure 1. (a,b) Two relatively small ( $\sim 60 \mu\text{m}$ ) monazites in sample 6.5, Guarda Structure. BSE-images show damaged rims and holes in both monazites. No PMs or granular structures are observed in the monazites.

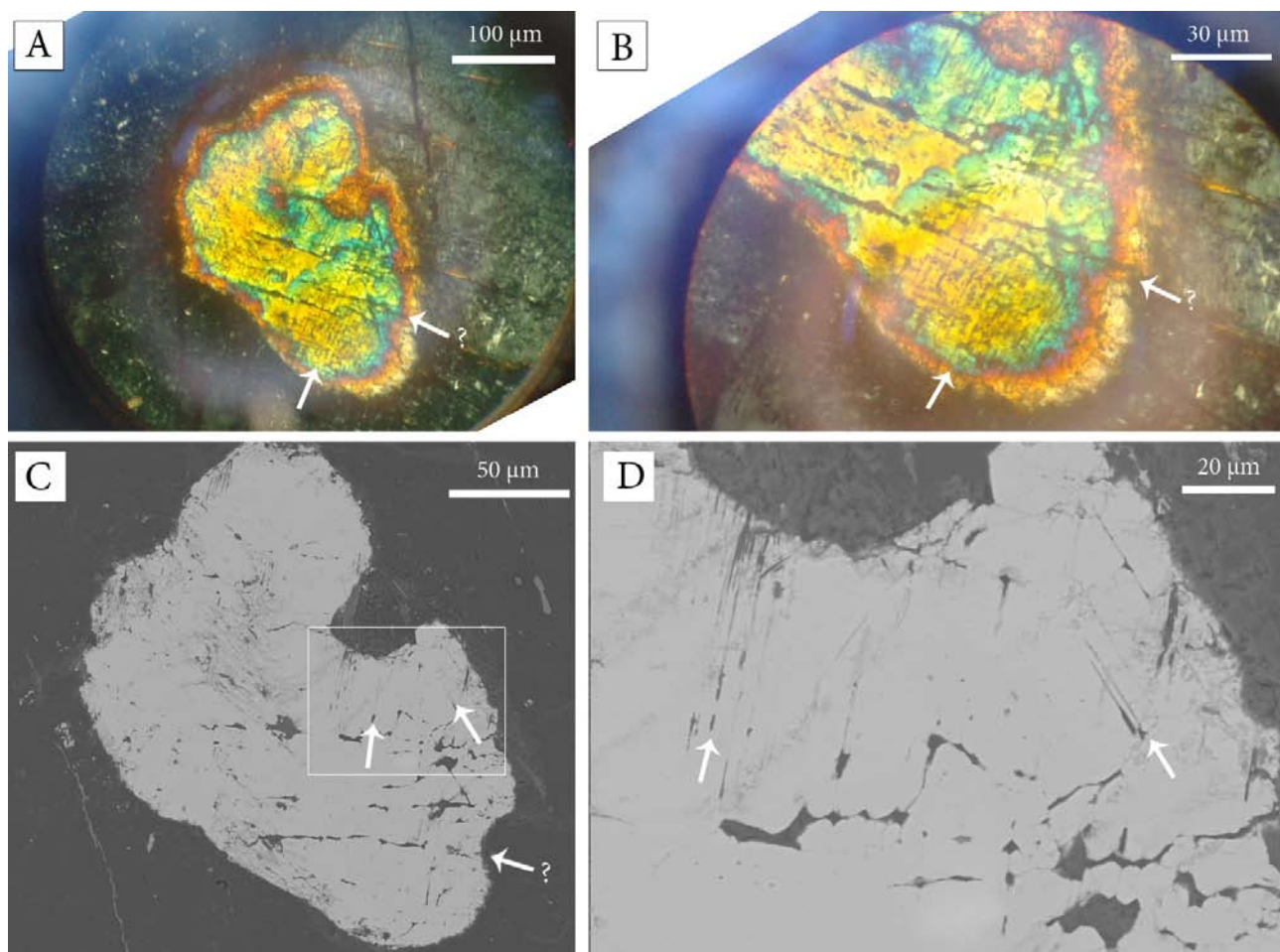


Figure 2. A monazite of  $\sim 200 \mu\text{m}$  in sample H11, Vredefort Dome. (a,b) crossed polarized light images of the monazite containing 2 sets of PMs (white arrows) and some NPFs. There is probably a reaction rim around the monazite. (c) BSE-image showing that there are three sets of PMs, although the set with the question mark appears to be sub-planar/non-planar open fractures instead of PMs. (d) A higher magnification view of the white square in figure c shows the distinct sets of PMs and NPFs. The reaction rim exists of small crystals.

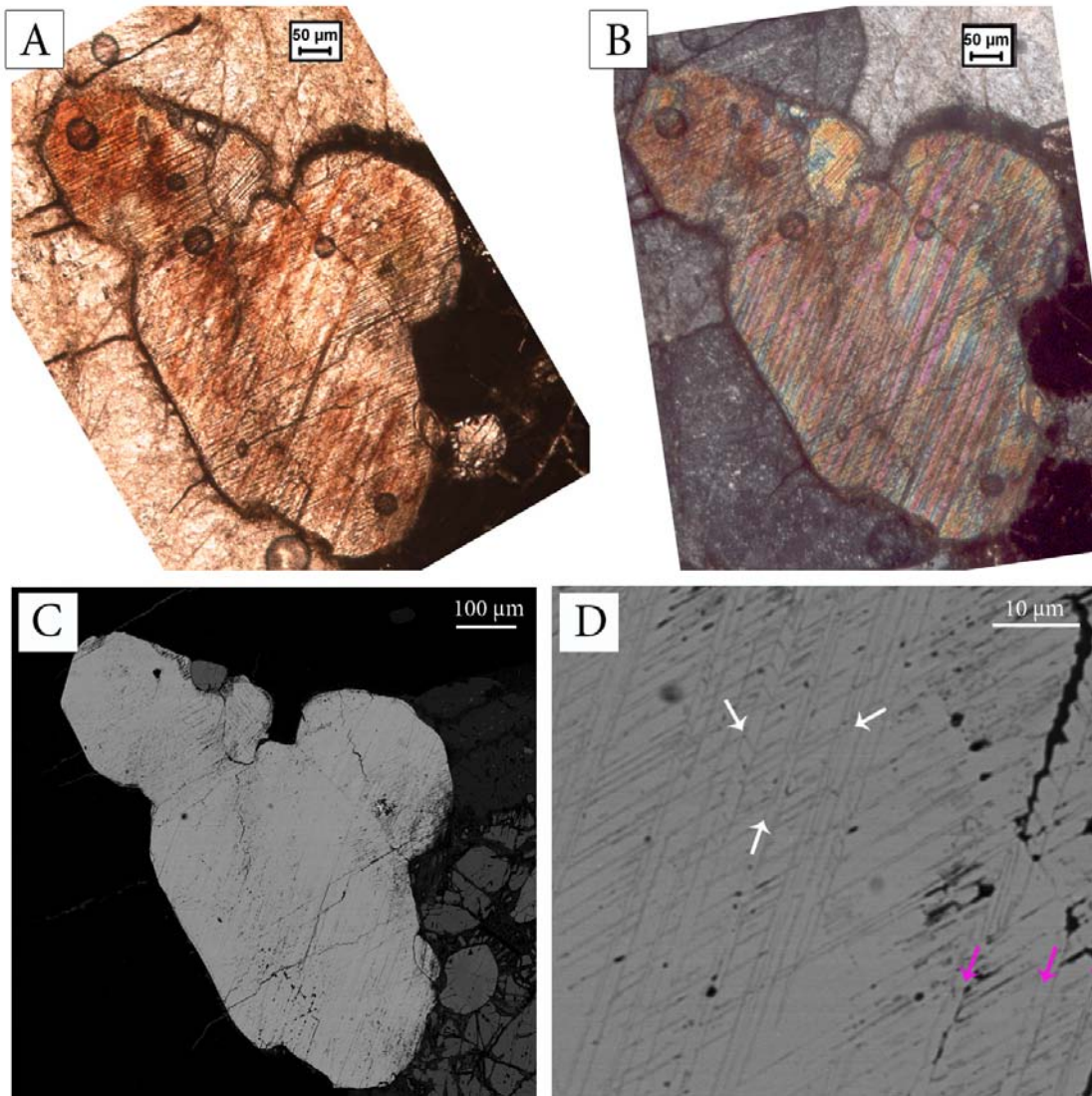


Figure 3. A monazite of  $\sim 550 \mu\text{m}$  in sample K5, Vredefort Dome. (a) Plane polarized light image showing two distinct sets of PMs. (b) Crossed polarized light image showing the same sets of PMs. Birefringence colors change from pink to orange to yellow to blue going closer towards PMs. (c) BSE-image show the same sets of PMs and almost no NPFs. (d) A higher magnification view of the BSE-image show three sets of PMs, some PMs are open structures. The purple arrows point to the bands with clear lighter colored birefringence in crossed polarized light.

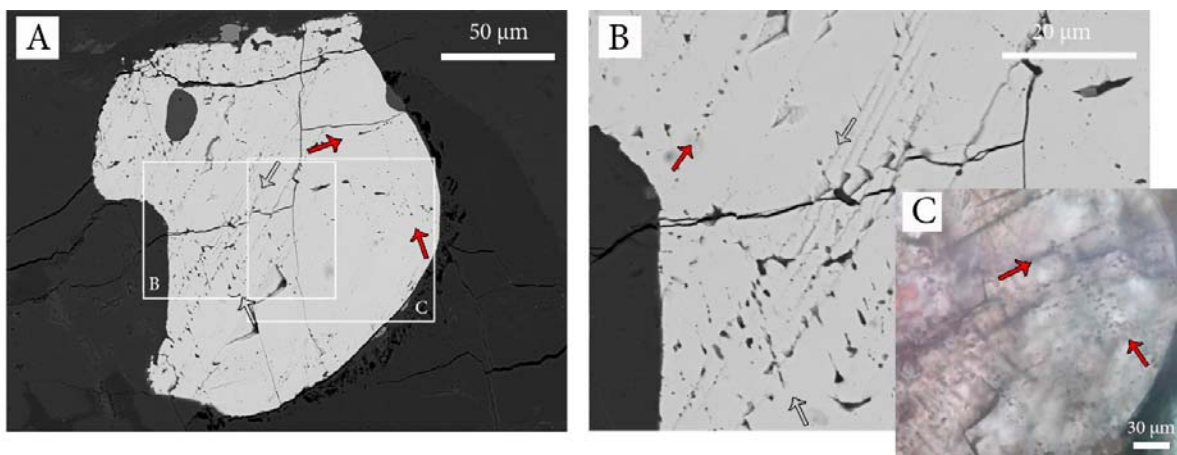


Figure 4. A monazite of  $\sim 200\ \mu\text{m}$  in sample J11, Vredefort Dome. (a) BSE-image of the monazite. The arrows point in the direction of two distinct sets of PMs. The red arrow point to decorated PMs. (b) A higher magnification view of the white square in figure a. (c) A higher magnification view of the other white square in figure a. This is a plane polarized light image showing decorated PMs.

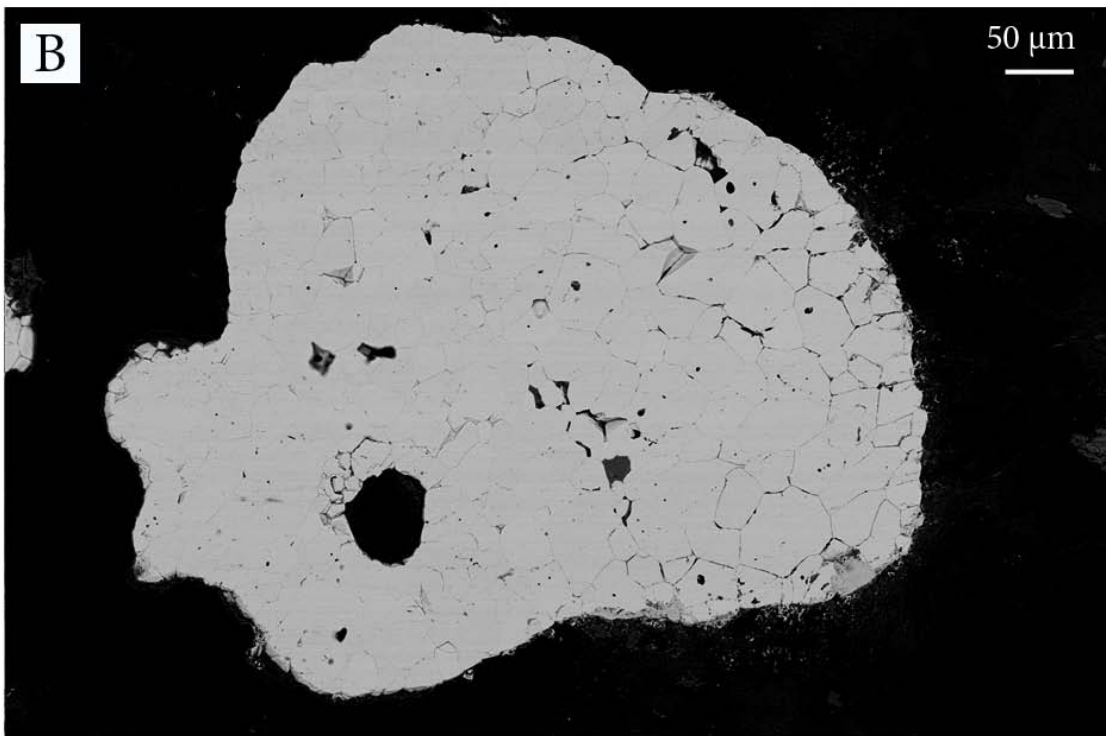
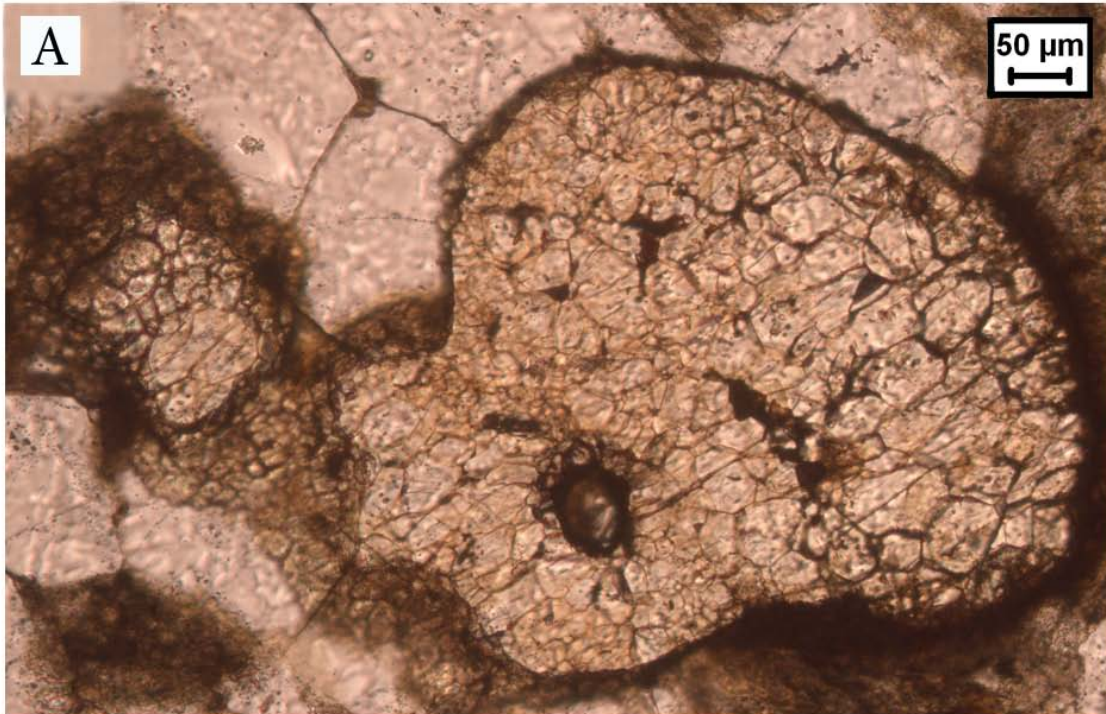


Figure 5. A monazite of  $\sim 500\ \mu\text{m}$  in sample V1407b, Vredefort Dome. (a) plane polarized light image of a monazite with granular texture. (b) BSE-image of the monazite with granular texture. Individual aggregates are 10-50 $\mu\text{m}$ . No PMs in this monazite.

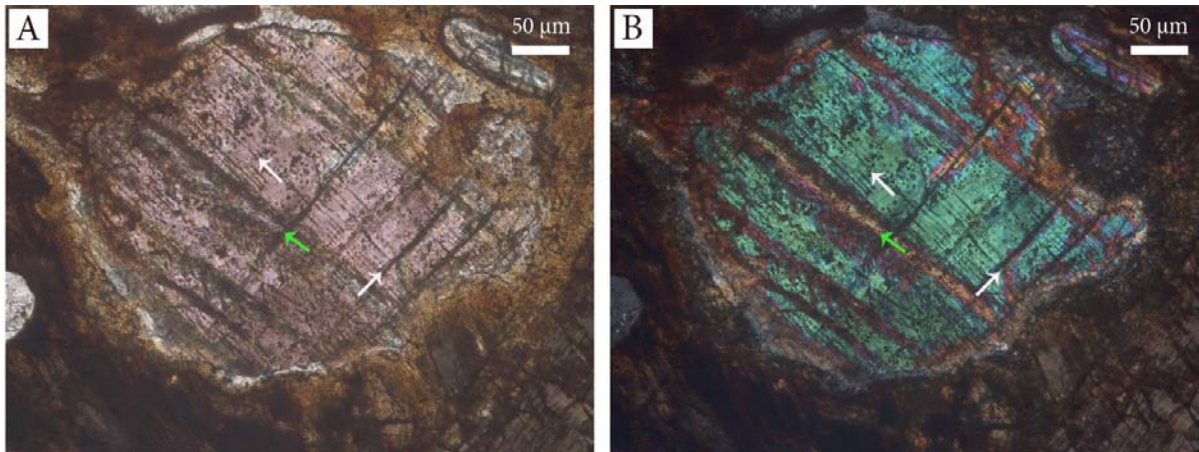


Figure 6. Monazite of  $\sim 500\mu\text{m}$  in sample V284a, Vredefort Dome. (a) plane polarized light (pink color of monazite is caused due to light settings in the light microscope) and (b) crossed polarized light image of a monazite with 3 sets of PMs. The white arrows point in the direction of two sets of dark PMs. The green arrow points in the direction of a  $\sim 10\ \mu\text{m}$  wide bands with different birefringence colors than the host grain.

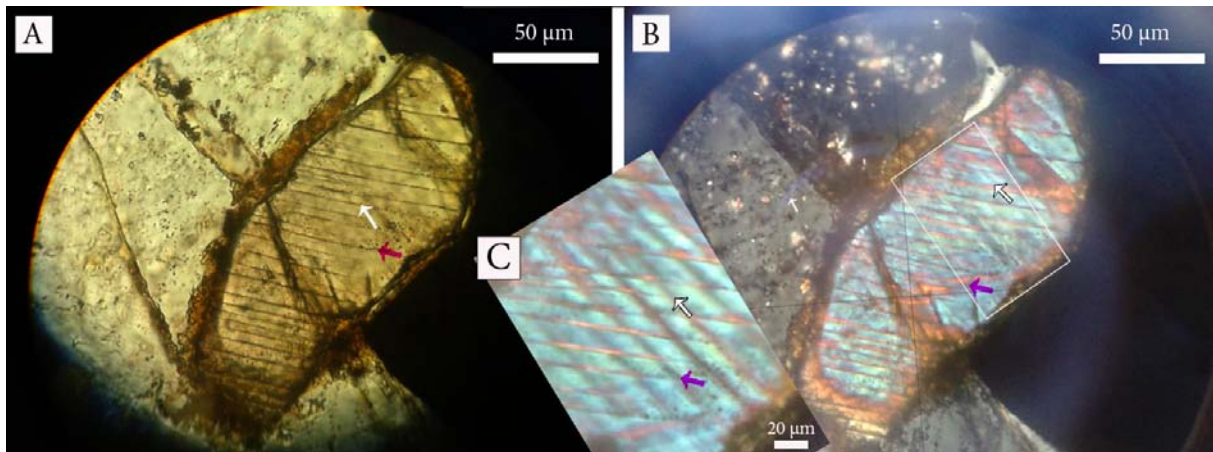


Figure 7. Monazite of  $\sim 175\mu\text{m}$  in sample V251b, Vredefort Dome. (a) Plane polarized light image of the monazite. The arrows point into the direction of two sets PMs. One set consists of very straight and sharp PMs (purple arrow). The other set seems to be decorated with fluid inclusions, but this is very unclear (white arrow). (b) Crossed polarized light image. The purple arrow points in the direction of the set with lower birefringence color. The white arrow points to planar structures that form due to different extinction angles and are similar to twin lamellae. (c) A higher magnification view of the white square in figure b.

## 4.4 Discussion

### 4.4.1 Nature of planar microstructures in monazite

PMs in monazite are hardly discussed in other studies. Flowers et al. (2003) interpreted the PMs in monazite as planar deformation features (PDFs), but didn't discuss why. Cavosie et al. (2010) interpreted the PMs as planar fractures (PFs), because they are notably similar to PFs in zircon (chapter 3). According to Cavosie et al. (2010) the PMs in monazite are open (unfilled) fractures that are visible both on grain surface and grain interiors, just like PFs.

As mentioned in chapter 3 (paragraph 3.1.1.1), fresh PDFs in quartz as well as in zircon characteristically consist of amorphous material, while PFs are, sometimes open or filled, fractures. Transmission electron microscope (TEM)-analysis can point out whether the different sets of PMs in

monazite are filled with amorphous material and could indicate if the features are PDFs, PFs or maybe both. During this research TEM-analysis was not done, so a comparison between light microscope images of the PMs in monazite and PMs in zircon is made. As discussed in chapter 3 (paragraph 3.5.1) most abundant PMs in zircon are probably PFs. The PMs in monazite are compared to these PFs in zircon to look for consistency between the structures. Figure 8 and table 2 show the comparison between PMs in monazite and the PFs in zircon.

Table 2. Comparison between PMs in monazite and PFs in Zircon as observed in BSE-image		
<b>BSE-observations</b>	<b>PMs in Monazite</b>	<b>PFs in Zircon</b>
Width	0.5-1.5 $\mu\text{m}$	0.5–1.5 $\mu\text{m}$
Spacing	1-15 $\mu\text{m}$	1-20 $\mu\text{m}$
Open fractures	A few	A few
Filled/unfilled	Unfilled	Filled and unfilled
Mineral offset by PM	no	yes
<b>Optical observations</b>	<b>PMs in Monazite</b>	<b>PFs in Zircon</b>
PMs have other birefringence colors	Some PMs	no
PMs have other extinction angle in crossed polarized light	Some PMs	no
Decorated PMs	Some PMs	no

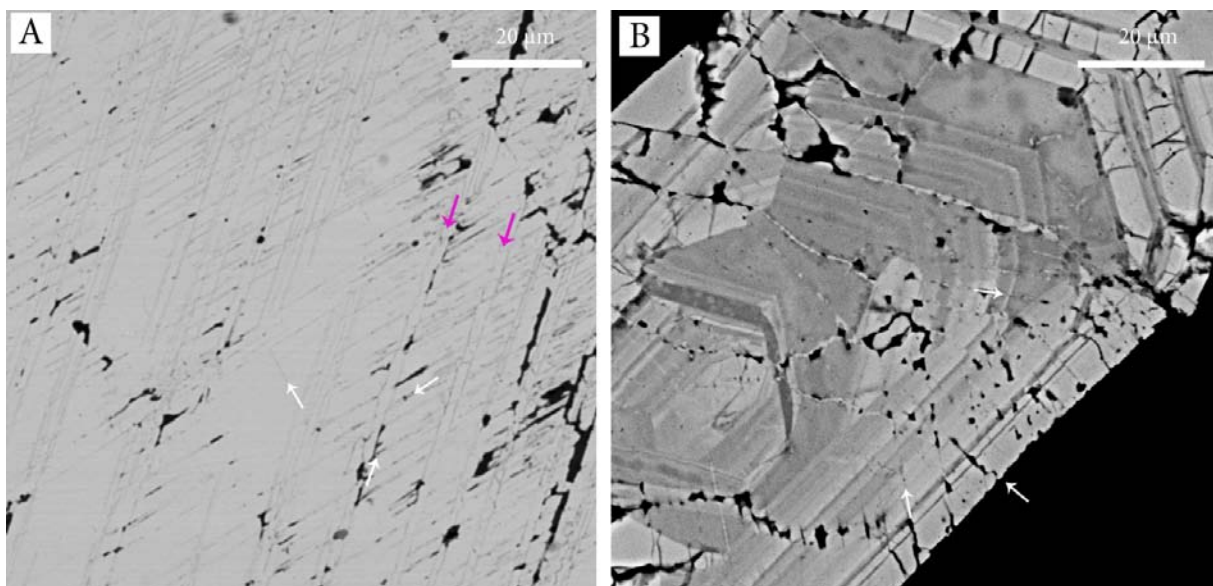


Figure 8. BSE-images with a similar scale of: (a) a shocked monazite with type 1 PMs and (b) a zircon with PFs. Both crystals contain three distinct sets with planar structures. The PMs in monazite are at some places open fractures that are comparable to the open PFs in zircon. In zircon some of these open fractures are filled with (lighter colored) material. This is not observed in monazite. The shocked monazite contains less NPFs. The monazite contain bands of a few micrometer wide (purple arrows) formed by two PMs. These bands have a lower refractive index. Such bands are not observed in zircon.

Most PFs in zircon are quite similar (chapter 3), only the width and spacing of the PFs are different in each zircon. The PMs in monazite show more variation. In general three types of PMs are observed in light microscope images of monazite.

*Type 1* – This type of PMs are similar to PFs in zircon (white arrows in figure 2, 3, 8 and the transparent arrow in figure 4). The PMs in monazite are very straight and sometimes appear as open fractures. The spacing of the PMs in monazite is slightly smaller compared to PFs in zircon. This type was probably observed by Cavosie et al. (figure 8, 2010). The PMs observed by Flowers et al. (figure 4, 2003) also resemble type 1 PMs. In between two individual PMs a band of 3-10  $\mu\text{m}$  with lower birefringence colors than the host grain can form (purple arrows in figure 3 and 7, green arrow in figure 6). The lower birefringence colors could have formed due to damage of the mineral structure. Partial transition of the mineral structure to amorphous material reduces the refractive index. Another possibility is a different crystal orientation between two PMs compared to the host grain. In this case the PMs are comparable to twin lamellae. However, the bright bands do not clearly go extinct during stage rotation in crossed polarized light, while twin lamellae usually do.

*Type 2* – Type 2 is only observed in one monazite (white arrows figure 7). A clear set of PMs is formed due to differences in extinction angle in crossed polarized light. These PMs are comparable to twinning in plagioclase crystals. In plane polarized light the set of PMs is visible as a straight array of fluid inclusions. However, this is not very clear. The crystal showing this type of PMs has not been examined in the SEM. Twins in monazite can form due to tectonic deformation. In total 5 directions, (100), (001), (120), (122) and (120), of twins are reported in the deformed monazite (Hay and Marshall, 2003). According to Hay and Marshall, (2003) these twins are not visible optically in polarized transmitted light, so the twins observed in this study probably have another origin.

*Type 3* - The last type of PMs is shown in figure 4. This monazite contains decorated PMs that show no variation in birefringence color. These decorated features resemble healed PDFs in quartz crystals. This could implicate that PDFs also form in monazites.

Although the NPFs are quite abundant in shocked zircon, shocked monazites contain almost no NPFs. Due to the lack of NPFs and growth zoning in monazite, the PMs are better visible in light microscope images compared to the PFs in zircon.

As discussed in chapter 3 (paragraph 3.5.2) there is a relation between the size of zircon crystals and the development of PMs. PMs predominantly form in zircon crystals  $>100\mu\text{m}$ . Such a relation is not found in the monazite crystals. PMs are present in every monazite that was studied (Appendix 4). However, all monazites studied in this chapter are  $>100\mu\text{m}$ .

#### **4.4.2 Guarda Structure versus Vredefort Dome**

The monazites from the Guarda Structure do not contain NPFs, PMs or granular texture, while the shocked monazites from the Vredefort Dome do contain these shock microstructures. Also zircon and quartz grains from the Guarda Structure lack all types of shock microstructures. Therefore I conclude that it is highly unlikely that the Guarda Structure is a meteorite impact crater.

#### **4.4.3 Pressure range for shock microstructures in monazite**

Pressure ranges for PMs and granular texture in monazite were determined with the help of zircon inclusions in monazite crystals (Cavosie et al., 2010). Monazites with PMs contain zircon inclusions with PMs. To determine the lower pressure constraint of PMs in monazite, Cavosie et al. (2010) used the 20 GPa-limit for PM-development in zircon that was determined by Wittmann et al. (2006). However, in chapter 3 we concluded that PMs in zircon probably already start to develop at pressures between  $<15$  GPa. The original locations of the monazites and zircons used by Cavosie et al. (2010) were unknown, because they used detrital minerals from the Vaal River, Vredefort Dome,

South Africa. The locations of the samples in this study are known. Figure 15 in chapter 3 (paragraph 3.5.4) presents a pressure distribution map (Gibson and Reimold, 2005) of the Vredefort Dome with the locations of all samples containing monazites with PMs (sample H11, J11, K5, V251b and V284a). All samples come from zone II and experienced a shock pressure between 10-15 GPa. Similar to the PMs in zircon, PMs in monazite probably start to develop at pressures between <15 GPa. The reliability of the shock pressure distribution of Gibson and Reimold (2006) is discussed in chapter 3 (paragraph 3.5.4)

Sample v1407b contains two monazites with a granular texture. This sample experienced a shock pressure >30-35GPa (figure 15 in chapter 3, paragraph 3.5.4. and Gibson and Reimold, 2006) and experienced (post)-impact temperatures of 900-1000°C or possible up to 1350°C (Gibson, 2002). Because the melting temperature of monazite is  $2072 \pm 20$  (Hikichi and Nomura, 1987), the granular texture in monazite is probably developed by high shock pressures, just like the granular texture in zircon. In accordance with Cavosie et al. (2010) we found zircon with PMs that occur in a sample with polycrystalline monazite. Cavosie et al. (2010) suggested that this implicates that shock pressures developing granular texture in monazite did not exceed 50GPa, because 50GPa is the minimum pressure required for granular texture in zircon (Wittman et al, 2006). Our results implicate that the granular texture is formed at pressures  $\leq 35$  GPa. This result implies that the upper constraint for PMs in monazite lies between 30-35 GPa.

#### 4.5 Conclusion and further research

Monazites from the Guarda Structure miss all types of shock microstructures, compared to shocked monazite from the Vredefort Dome. This implicates that the Guarda Structure is probably not a meteorite impact crater.

Light microscopy analyses reveal that three types of PMs are common in shocked monazites: 1) PMs similar to PFs in zircon. 2) PMs similar to twinning in plagioclase. 3) Decorated PMs similar to annealed PDFs in quartz. Future TEM-analyses must determine the exact nature of these different PMs. The U-stage might be a good instrument to determine the different orientations of PMs in monazite. Monazites with PMs were not found in samples from the Guarda Structure.

Compared to shocked zircon, shocked monazites show less damage and NPFs. The PMs in monazites are better visible in light microscope images. By combining results of shocked zircons and monazites, pressure ranges can be established.

The PMs in monazites start to develop at pressures between 10-15 GPa. Granular texture in monazites is probably formed at pressures <35 GPa. More monazite grains, from craters with a known pressure distribution, must be analyzed and/or shock experiments on monazites must be done to establish better shock pressure ranges for distinct shock features.

#### References

- Bohor, B. F., Betterton, W. J., Krogh, T. E., 1993, Impact-shocked zircons: Discovery of shock-induced textures reflecting increasing degrees of shock metamorphism, *Earth and Planetary Science Letters* 119, p. 419–424.
- Cavosie, A. J., Quintero, R. R., Radovan, H. A., Desmond, E. M., 2010, A record of ancient cataclysm in modern sand: Shock microstructures in detrital minerals from the Vaal River, Vredefort Dome, South Africa, *Geological Society of America Bulletin* 122, 1968–1980.

- Cintrón, N. O., Cavosie, A. J., Gibbon, R.J., Radovan, H. A., Moser, D. E., Wooden, J., 2011, In Situ U-Th-Pb Geochronology of detrital shocked monazite in Pleistocene fluvial deposits along the vall river, South Africa, *42nd Lunar and Planetary Science Conference (Abstract)*
- Deutsch, A., Schärer, U., 1990, Isotope systematics and shock-wave metamorphism: I. U-Pb in zircon, titanite, and monazite, shocked experimentally up to 59 GPa, *Geochimica et Cosmochimica Acta*, 54, p. 3427-3434.
- Flowers, R.M., Moser D.E., Hart, R.J., 2003, Evolution of the Amphibolite-Granulite Facies Transition Exposed by the Vredefort Impact Structure, Kaapvaal Craton, South Africa, *The Journal of Geology*, 111, p. 455–470.
- Gibson, R.L., 2002, Impact-induced melting of Archaean granulites in the Vredefort Dome, South Africa, I: Anatexis of metapelitic granulites, *Journal of Metamorphic Geology*, 20, p. 57–70.
- Gibson, R.G., Reimold, W.U., 2005, Shock pressure distribution in the Vredefort impact structure, South Africa, *Geological Society of America Special Paper*, 384, p. 329-249.
- Hay, R.S., Marshall, D.B., 2003, Deformation twinning in monazite, *Acta Materialia*, 51, p. 5235–5254.
- Hikichi, Y., Nomura, T., 1987, Melting Temperatures of Monazite and Xenotime, *Journal American Ceramic Society*, 70, p. 252-253
- Moser, D. E., 1997, Dating the shock wave and thermal imprint of the giant Vredefort impact, South Africa, *Geology*, 25, p. 7-10.
- Schärer, U., Deutsch, A., 1990, Isotope systematics and shock-wave metamorphism: II. U-Pb and Rb-Sr in naturally shocked rocks; the Haughton Impact Structure, Canada, *Geochimica et Cosmochimica Acta*, 54, p. 3435-3447.
- Wittmann, A., Kenkmann, T., Schmitt, R. T., Stöffler, D., 2006, Shock-metamorphosed zircon in terrestrial impact craters, *Meteoritics & Planetary Science*, 41, p. 433–454.

## Final conclusions

Monteiro (1991) suggested that the Guarda Structure is a deeply eroded complex multi-ring impact crater. However, convincing evidence was lacking and the origin of the Guarda Structure remained unclear. In order to check whether the Guarda Structure is an impact crater or not, field data and rock samples were collected in the Guarda Structure and detailed optical microscopy and SEM-analyses were done on potential shock microstructures in quartz, zircon and monazite.

The alleged crater must have a maximum age of  $>245 - <300$  Ma and a minimum age of  $\sim 209$  Ma. The circular topography of the structure and the associated circular drainage pattern could easily be interpreted as impact crater phenomena. However, the lack of impact rocks in the Guarda Structure does not support the crater theory. (sub-)Planar microstructures are present in quartz grains from the Guarda Structure, but they don't show the typical characteristics of PDFs. Zircon and monazite grains from the Guarda Structure don't contain shock microstructures as well. Therefore it seems highly unlikely that the Guarda Structure is a meteorite impact crater. The circular characteristic of the structure and drainage pattern are probably formed due to a dome-like structure or lithology differences within the Guarda Structure.

Light microscope studies seem to be a good method to study planar and granular shock microstructures in zircon and monazite. PMs in zircon appear to be a shock indicator for a wide shock pressure range  $>10-35$  GPa. However, zircon has some restrictions as shock indicator, since PMs mainly form in zircons that are  $>100$   $\mu\text{m}$ . Shocked monazites contain three types of PMs: 1) planar fractures, (2) twinning and (3) decorated PMs. All types start to develop at shock pressures between  $>10-15$  GPa. A granular texture in monazites develops at pressures  $<35$  GPa.

## Acknowledgements

I would like to thank Maartje Hamers for all her help, enthusiasm, positive feedback and unconditional support during the fieldwork and the SEM-analyses and for reading and improving my thesis. I enjoyed working with you and your Vredefort samples. I am grateful to Martyn Drury for all his advices, ideas and reviews. Last but not least, thanks also to Reinoud Vissers for finding the abstract about the Guarda Structure and for his advices.

## Appendix 1: Table and map with all collected samples in the Guarda Structure

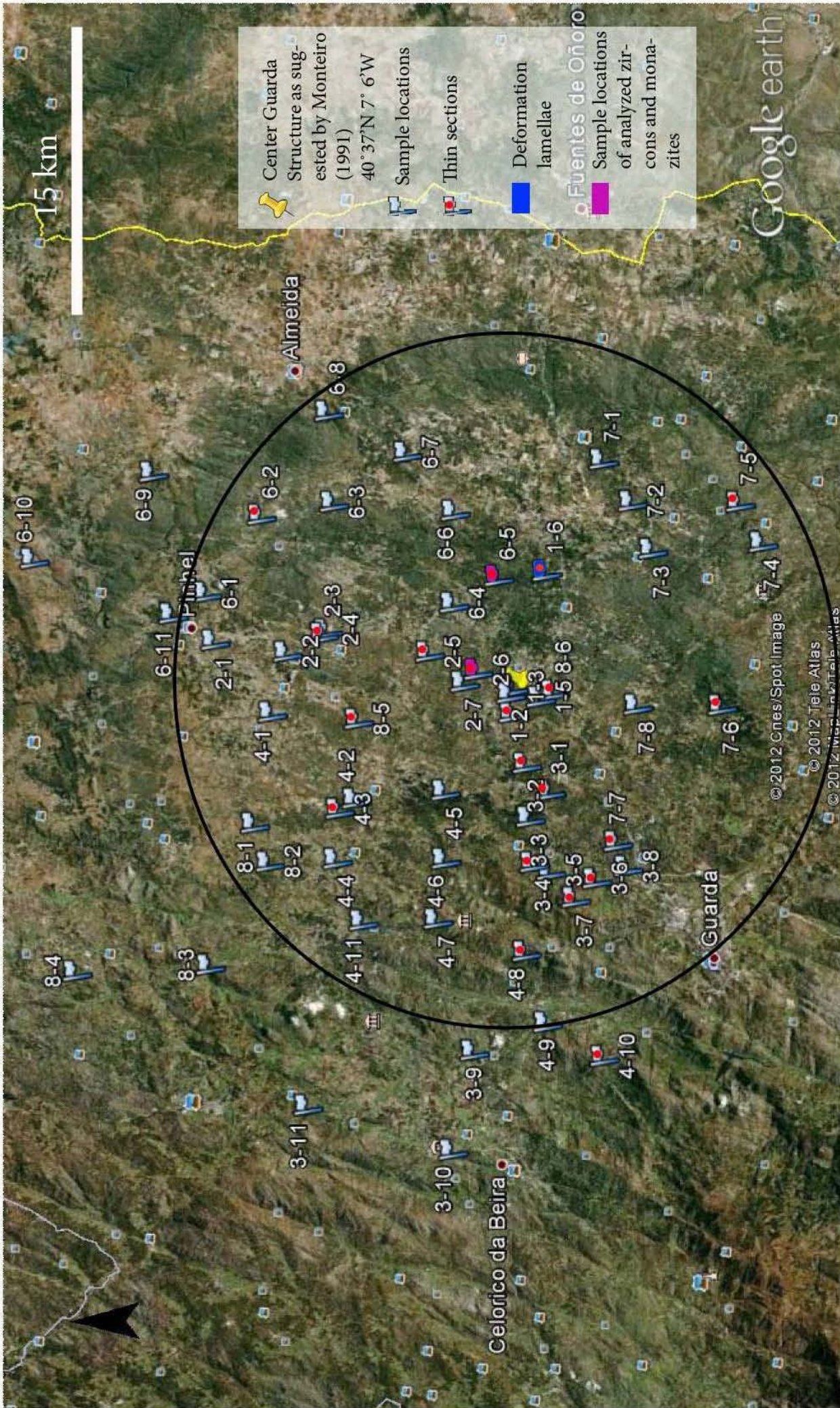
Detailed overview of all collected rocks in and outside the Guarda Structure. ++ Granite: coarse grained granite with between 10-80% feldspatic phenocrysts (up to 10 cm) and often fine dark grained round xenoliths (2-20cm). T-granite: medium-coarse grained granite without phonocrysts. Sometimes with very fine grained granite dykes in it. All sample locations are plotted in a map. The black circle represents the alleged crater.

Sample nr.*	Sample description	GPS-point	Near city	Thin section
1.1	Coarse grained T-granite.		Toito	
1.2 a	Quartz from vein.	0660392/4498706	Toito-Trocheiros	
1.2 e	T-granite with Quartz			x
1.3	Piece from wall, very fine granite with lens of T-granite in it.	0660706/4498584	Trocheiros	
1.4	T-granite with very fine grained minerals and black (biotite) areas.	0660684/4498509	Trocheiros	x
1.5	Grey fine grained rock, soft white spots (weathered minerals), looks like volcanic ash.	0660195/4497173	Old mine between Almeindinha-Trocheiros	x
1.5 b	Same as 1.5			
1.5 c	Very fine grained mafic dyke.			
1.5-2	Grey fine grained rock, soft white spots (weathered minerals), looks like volcanic ash.			x
15-2	Grey fine grained rock, soft white spots (weathered minerals), looks like volcanic ash.			
1.6 a	Very weathered granite (hydrothermal alternation).	0666681/4496911	East of Pinzio	
1.6 b	"			
1.6 c	"			
1.6 d	"			
1.6 e	"			
1.6 f	Pink/orange granite with biotite (very weathered).			
1.6 g	Fine grained granite.			x
2.1 a	Rock from fault gauge.	0663009/4513885	South of Pinhel	
2.1 b	Quartz from vein.			
2.1 c (lost)	T-granite.			
2.2 (2x)	T-granite (from the ground).	0662436/4510158	Voscovero-Manigoto	
2.3	T-granite (no weathering).	0663402/4508297	South of Manigoto	x
2.4	++ granite.	0663597/4508102	South of Manigoto	
2.5 a	Schist with lots of quartz.	0662480/4502866	Lamegal	x
2.5 b	Metamorphic rock with lot of quartz, no clear schistosity.			

2.6	T-granite.	0661558/4500386	St. De Manina	x
2.7 a	T-granite with green minerals and a lot muscovite, light weighted.	0600949/4501075	St. De Manina (Uranium-mine)	
2.7 b	“			
2.7 c	“			
3.1	T-granite with very small grained granite dyke.	0655413/4496637	West of Montes	x
3.2	T-granite, weathered	0656794/4497860	North of Montes	
3.3 a	T-granite, weathered but with hard very fine grained (dyke).	0654031/4497665	Agromil	
3.3 b	“			x
3.3 c	“			
3.4	T-granite, weathered, but also with hard “core rocks”.	0651706/4497461	Pera de Moco	
3.5	“	0651310/4496591	Verdugal	
3.6 a	Brown rock from big brown vein, very fine grained, together with granite.	0650905/4494260	Menoita	x
3.6 b	Black soft material from vein.			
3.6 c	T-granite with pink crystals.			x
3.7	Schists, clear biotite layers.	0649926/4495320	North Menoita	x
3.8	T-granite, a little weathered, but clear layers present.	0651538/4492650	Quarry, U-mine	
3.9 a	Mafic vein (greenish)	0641930/4500429	Aldeia Rico - Acores	
3.9 b	++ granite ( almost no faults and joints in quarry).			
3.10	Pink fine grained T-granite.	0636753/4501479		
3.11	Quartz vein.	0639086/4508931	Quartz mine	
4.1	Medium grained T-granite (weathered).	0659327/4510915	NNE of Freixedas	
4.2 a	++ Granite (weathered).	0654901/4506577	West of Freixedas	
4.2 b	Xenoliths from granite.			
4.3	T-granite (from quarry).	0654366/4507421	Freixedas-Alverca de Beira (quarry)	x
4.4	++ granite, with xenoliths in it (weathered)	0651779/4507533	Quarry, W of Alverea de Beira	
4.5	Orange pink T-granite, weathered.	0655361/4502000	Gouveias	
4.6	T-granite, lots of biotite (little weathering).	0651850/4501969	Codeseiro	
4.7 a	++ Granite (no weathering).	0648730/4502344	Alvares de Beira-Acores	
4.7 b	Fine grained basic igneous clast.			
4.8 a	++ Granite.	0647114/4497813	Acores (N211 – A25)	
4.8 b	Green rock from fault gauge with K-feldspar + quartz, no biotite.			x

4.8 c	Quartz from vein.			
4.9	++ granite, more than 75% phenocrysts. no xenoliths present.	0643410/4496686	Cortez do Monteino	
4.10a	Dolerite dyke (4m wide) → full of black circular structures that are filled with black spheroids.	0641712/4493770	Quarry Cadafaz	x
4.10b	++ Granite (weathered).			
4.11	++ Granite (weathered).	0648610/4506166	Bouca Nova	
6.1 a	Grey fine grained T-granite with flow structures.	0665479/4514329	East of Pinhel	
6.1 b	++ granite and clast (lots of flows structures in both granites).			
6.1 c	Quartz from vein.			
6.1 d	mafic dyke (in granites).			
6.2	++ granite (lot of quartz veins and xenoliths in granite).	0669500/4511545	Quarry East of Pereiro	x
6.3	++ Granite (lots of xenoliths).	0670178/4507829	Carvalho	
6.4	++ Granite.	0665016/4501636	South of Almeida	
6.5	++ Granite (green mica's, lots of phenocrysts, quartz vein cuts clast).	0666400/4499352	Freixo	x
6.6	++ Granite (with xenoliths).	0669755/4501611	Freixo - Peva	
6.7	Very coarse ++ granite less than 15% phenocrysts.	0672755/4504086	Ansul	
6.8	++ Granite (very weathered).	0674846/4508129	Junca (Rio Coa)	
6.9	Schist (alligned biotite, crenulation cleavage).	0671669/4517115	Cinco Vilas	
6.10 a	Metamorphic rocks (less than schist) with clay.	0667164/4523238	NO Pinhel	
6.10 b	Metamorphic rocks with quartz (looks like sandstone).			
6.11	T-granite (lots of muscovite), fine grained.	0664361/4516044	South of Pinhel	
7.1	Medium grained T-granite / ++ granite (hard to see weathered).	0672450/4494043	Mesquitela	
7.2	++ Granite (weathered).	0670301/4492537	Ade	
7.3	T-granite (weathered).	0667851/4491492	North of Parada	
7.4	T-granite (weathered).	0668249/4485827	South of Parada	
7.5	Medium grained ++ granite < 10% phenocrysts (lots of joints/faults).	0670316/4487019	East of Miuzela	x
7.6	Dyke (same as 7.6b), very fine grained.	0659849/4487880	Quarry near Rochos	x
7.6 a	"			
7.6 b	Schist.			

7.7	Medium grained T-granite.	0652808/4493173	Arnifana	x
7.8	++ granite, very coarse.	0659847/4492200	Quarry Jarmelo Sao Pedro	
8.1	++ Granite (xenoliths).	0653598/4511775	Ervas Tenras	
8.2	++ Granite.	0651604/4510994	Cerejo	
8.3	Transition between ++ - T-granite (flow structures places with 0% - 90% phenocrysts).	0646270/4514009	Faital	
8.4	Fine ++ granite, but with 15% very large phenocrysts.	0645898/4520844	Quarry A-dos-Ferreiros	
8.5	T-granite.	0659006/4506481	Roque (small quarry)	x
8.6	Medium /coarse grained T-granite.	0660538/4496462	Granja	



15 km

Center Guarda Structure as suggested by Monteiro (1991)  
 40° 37' N 7° 6' W

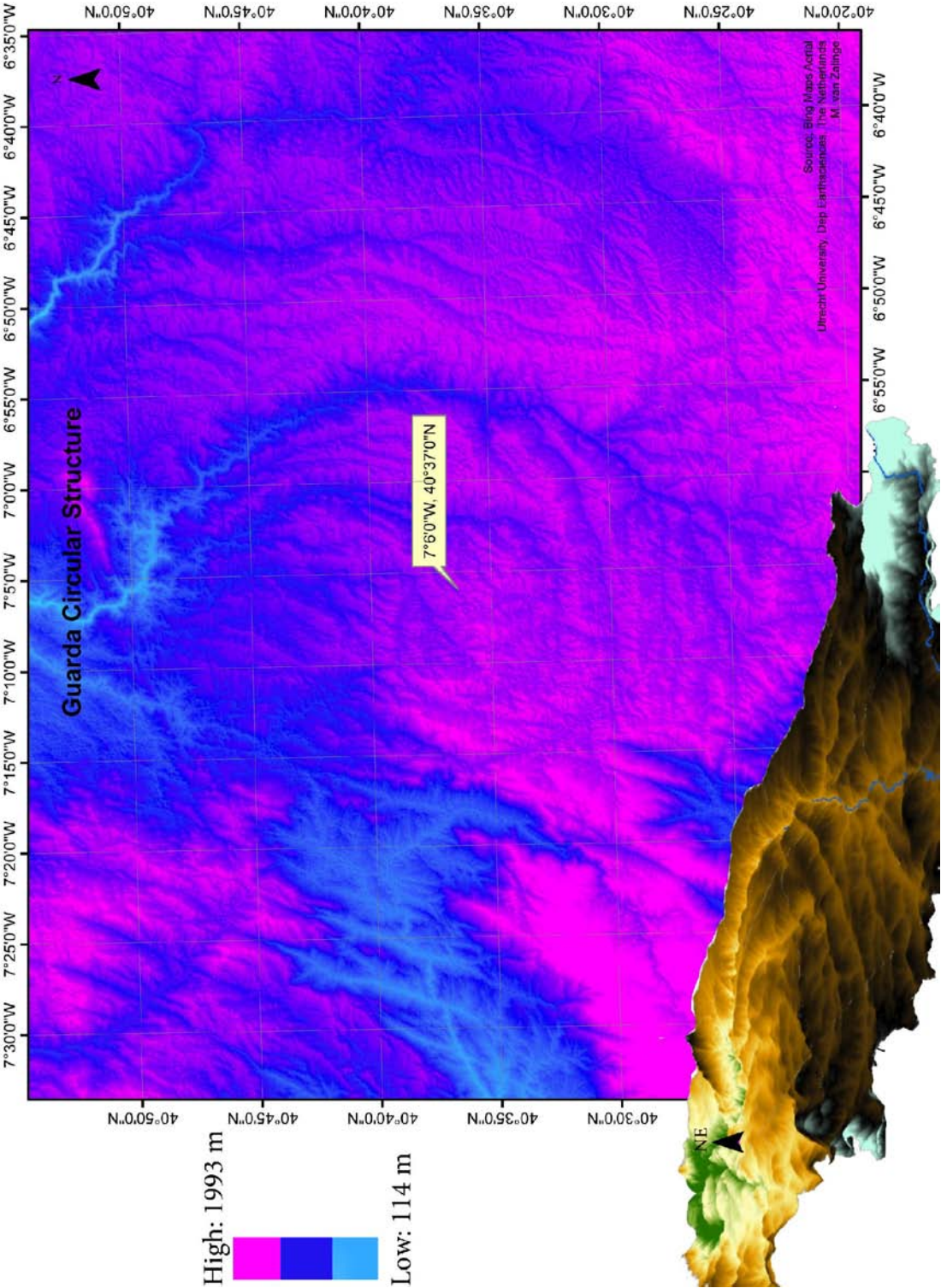
- Sample locations
- Thin sections
- Deformation lamellae
- Sample locations of analyzed zircons and monazites

Google earth

© 2012 Cnes/Spot Image  
 © 2012 Telet Atlas  
 © 2012 Microsoft/Tele Atlas

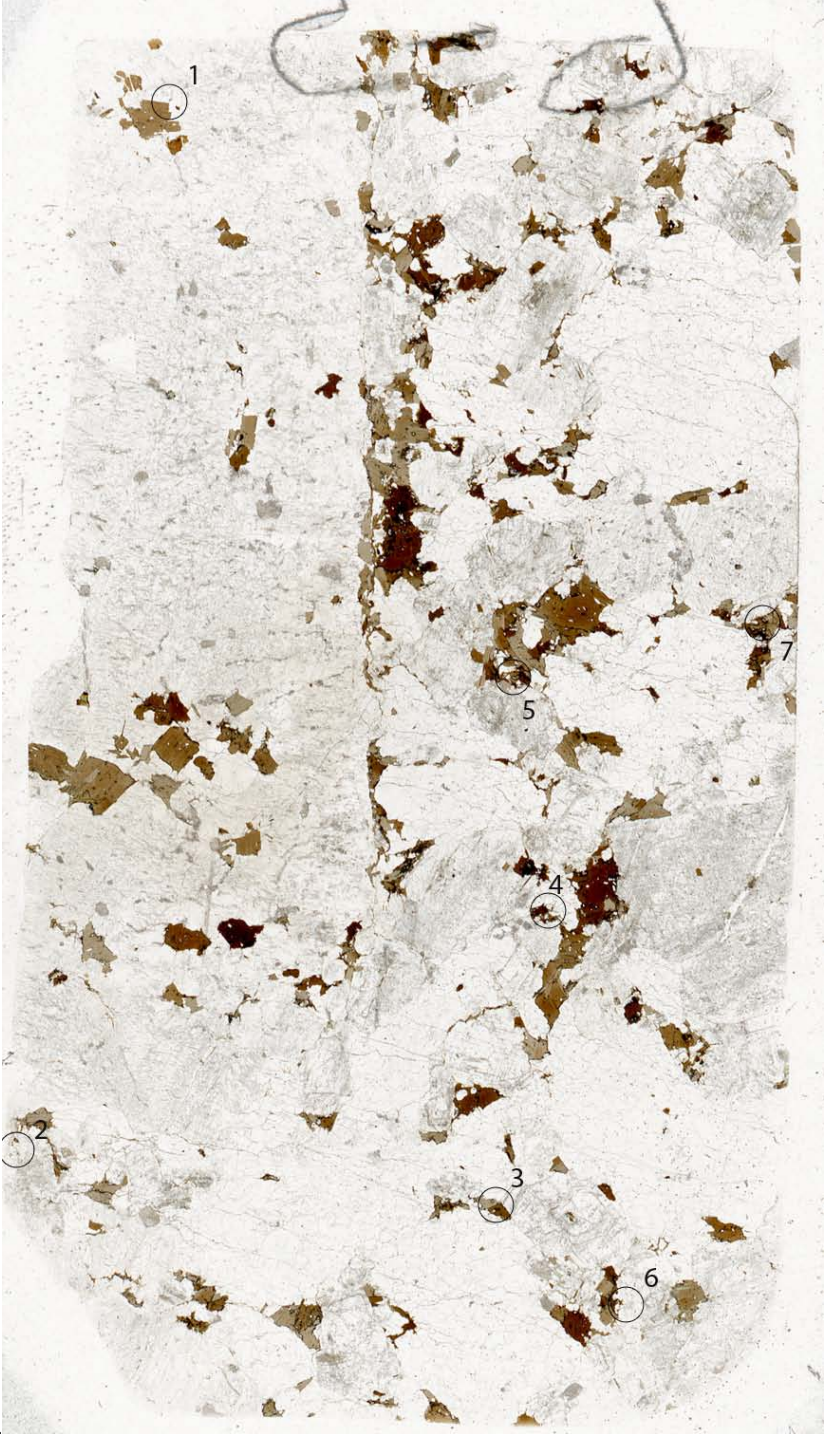
## Appendix 2: Elevation map and 3D-image of the Guarda Structure

Elevation map and 3D-image of the Guarda Structure. Monteiro (1991) suggested that the crater center was located at  $40^{\circ} 37'N$  and  $7^{\circ} 6'W$ . On the 3D-image (Modified from Jorge, 2009) the different rings is clearly visible. The inner part of the Guarda Structure has a high elevation. There are two rings with a low elevation and in between these rings there is a higher elevated ring. The circular structure is flattened in the east and missing in north.



**Appendix 3: Thin sections scans with the analyzed zircon and monazite grains**

**Sample 6.5:** ++ granite, 40°37'35"N 7°02'02"W, Guarda structure,



Portugal.

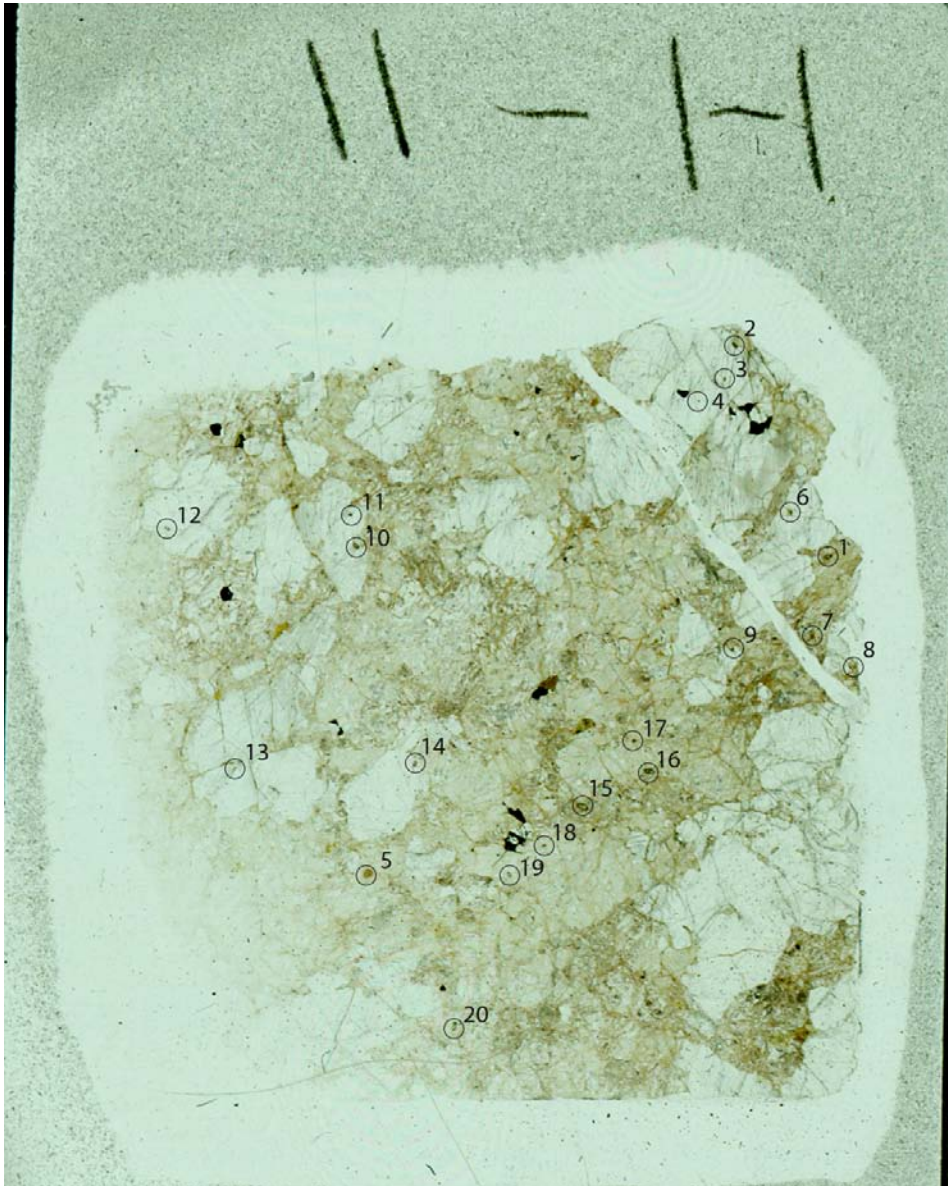
Grain / Mineral	Size	Structures	Grain/mineral	Size	Structures
1.zircon*	~90µm	NPFs	5. zircon	<90 µm	NPFs
2. zircon*	~90µm	NPFs	6. zircon	<90 µm	NPFs
3. monazite*	~60 µm	-	7. zircon	<90 µm	NPFs
4. monazite*	~60 µm	-			

Sample 2.6: T-granite, 40°38'12"N 7°05'27"W, Guarda structure, Portugal



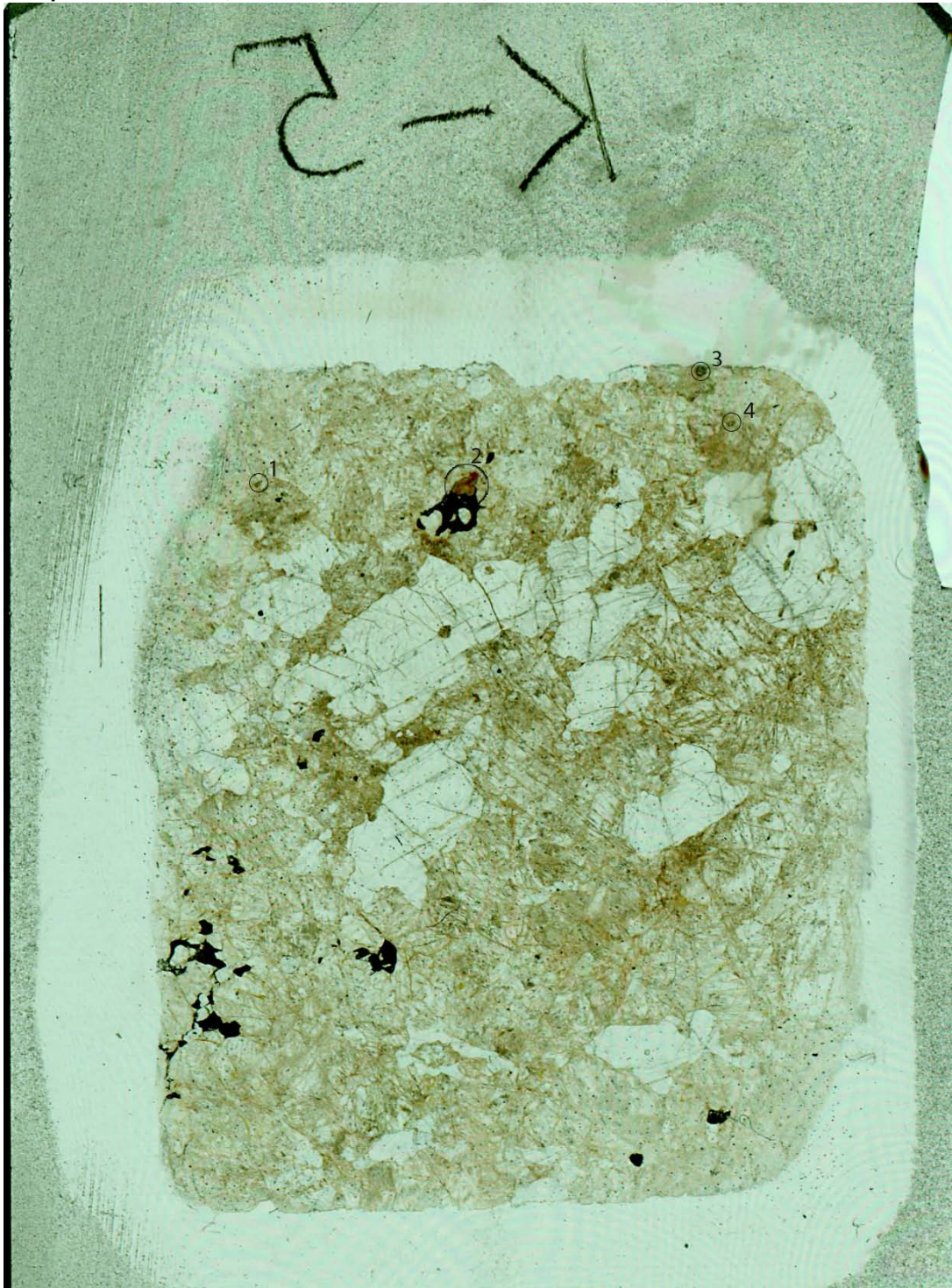
Grain / Mineral	Size	Structures
1. zircon*	~100 μm	NPFs
2. zircon	<100 μm	NPFs
3. zircon	<100 μm	NPFs
4. zircon	<100 μm	NPFs

**Sample H11:** Granulite, 26°58'15"S 27°23'19 E, Vredefort Dome, South Africa



Grain / Mineral	Size	Structures	Grain/mineral	Size	Structures
1. zircon*	~200 μm	2 sets PMs, NPFs	11. zircon	<100 μm	NPFs
2. zircon*	~200 μm	3 sets PMs, NPFs	12. zircon	>100 μm	NPFs
3. zircon*	~60 μm	NPFs	13. zircon	<100 μm	NPFs
4. zircon*	~60 μm	NPFs	14. zircon	>100 μm	2 sets PMs, NPFs
5. monazite*	~200 μm	3 sets PMs	15. zircon	>100 μm	1 set PMs, NPFs
6. zircon	<100 μm	NPFs	16. zircon	>100 μm	1 set PMs, NPFs
7. zircon	<100 μm	NPFs	17. zircon	<100 μm	NPFs
8. zircon	<100 μm	NPFs	18. zircon	<100 μm	NPFs
9. zircon	>100 μm	NPFs	19. zircon	>100 μm	2 sets PMs, NPFs
10. zircon	<100 μm	NPFs	20. zircon	>100 μm	NPFs

**Sample K5:** Granulite, 26°58'15"S 27°23'19"E, Vredefort Dome, South Africa.



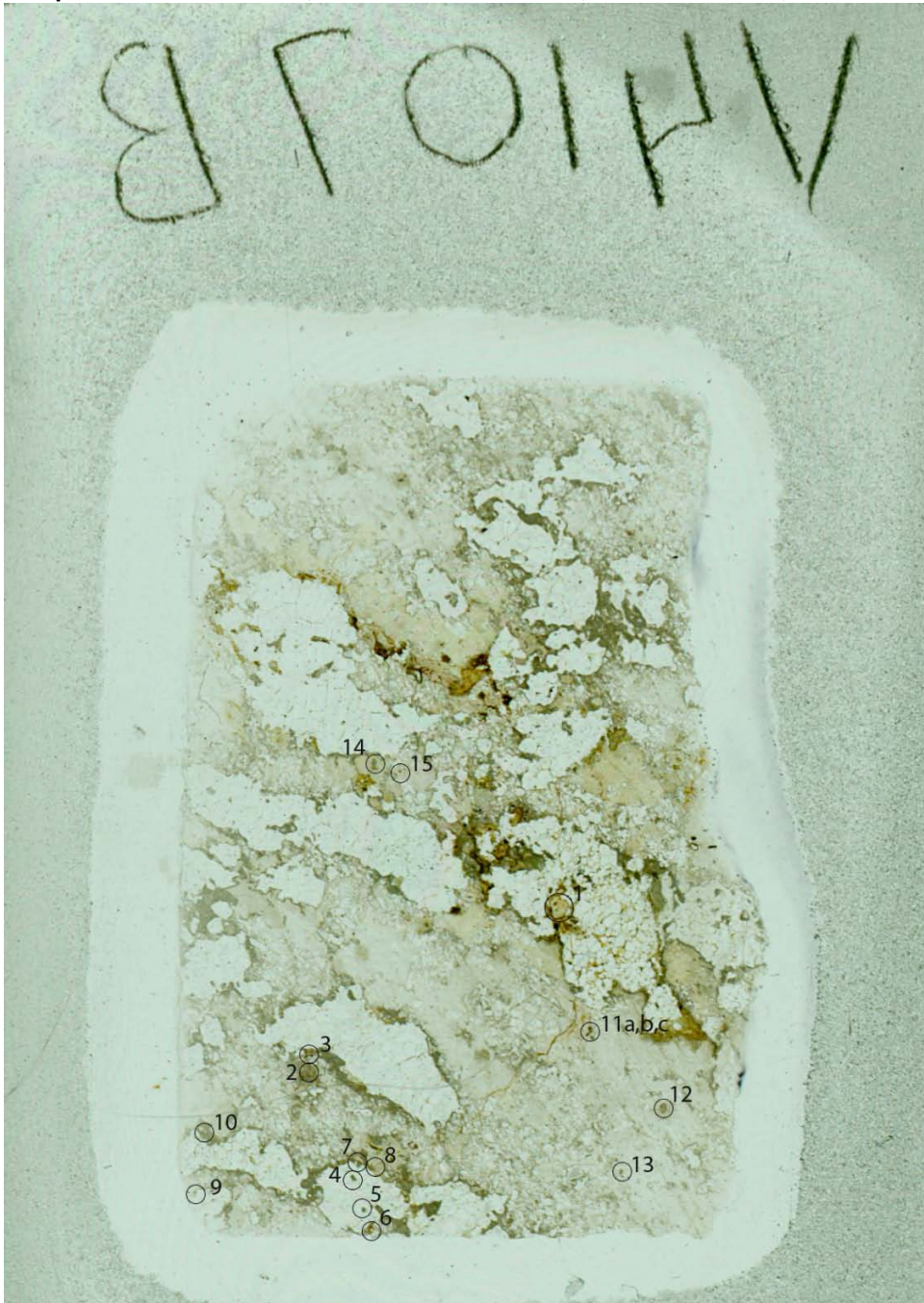
Grain / Mineral	Size	Structures
1. zircon*	~200 $\mu\text{m}$	2 sets PMs, NPFs
2. monazite*	~550 $\mu\text{m}$	3 sets PMs
3. zircon*	~260 $\mu\text{m}$	1 set PMs, NPFs
4. zircon*	~200 $\mu\text{m}$	1 set PMs, NPFs

**Sample J11:** Granulite, 26°58'15"S 27°23'19"E, Vredefort Dome, South Africa



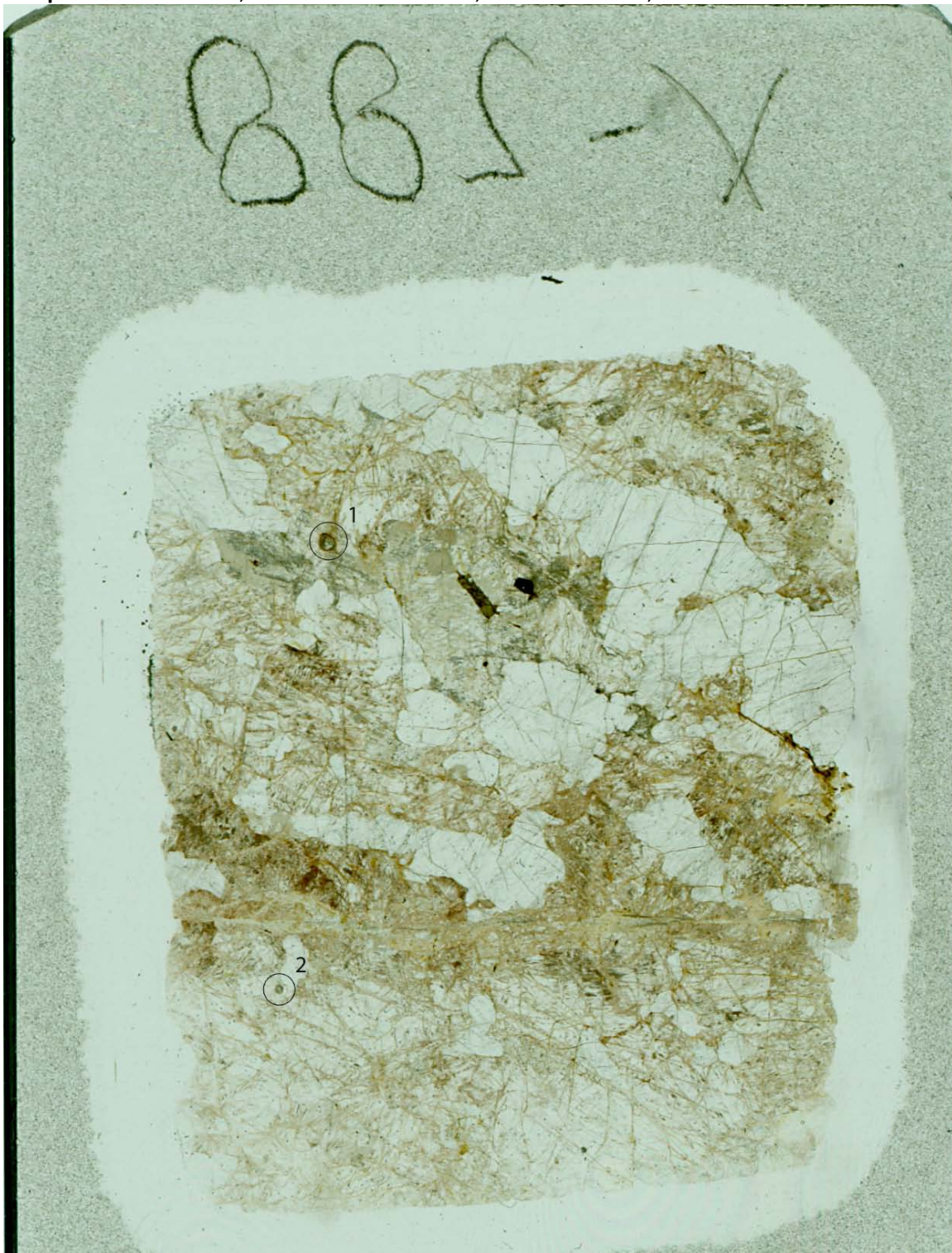
Grain / Mineral	Size	Structures	Grain/mineral	Size	Structures
1.monazite*	~150 μm	2 sets PMs	5. zircon	>100 μm	NPFs
2. zircon*	~150 μm	1 set PMs, NPFs	6. zircon	>100 μm	2 sets PMs NPFs
3. zircon*	~90 μm	NPFs	7. zircon	<100 μm	NPFs
4. zircon	<100 μm	NPFs	8. zircon	<100 μm	NPFs

**Sample V1407b:** Granulite, 27°02'52"S 27°29'36"E, Vredefort Dome, South Africa



Grain / Mineral	Size	Structures	Grain/Mineral	Size	Structures
1. monazite*	~500 μm	Granular texture	9. zircon	>100 μm	NPFs
2. zircon*	~400 μm	2 sets PMs, NPFs	10. zircon	>100 μm	NPFs
3. zircon*	~200 μm	1 set PMs, NPFs	11. 3x zircon	2x <100 μm 1x >100 μm	NPFs
4. zircon*	~200 μm	2 sets PMs, NPFs	12. zircon	>100 μm	1 set PMs, NPFs
5. zircon*	~100 μm	NPFs	13. zircon	<100 μm	NPFs
6. monazite	<100 μm	Granular texture	14. zircon	<100 μm	NPFs
7. zircon	>100 μm	NPFs	15. zircon	<100 μm	1 set PMs, NPFs
8. zircon	>100 μm	NPFs			

Sample V288: Granulite, 26°56'28"S 27°24'03"E, Vredefort Dome, South Africa



Grain / Mineral	Size	Structures
1. zircon	~500 $\mu\text{m}$	1 set PMs, NPFs
2. zircon	~200 $\mu\text{m}$	2 sets PMs, NPFs

Sample V284a: Granulite, 26°56'22"S 27°30'33"E, Vredefort Dome, South Africa



Grain / Mineral	Size	Structures
1. monazite	>100 $\mu\text{m}$	1 set PMs
2. monazite	$\sim$ 500 $\mu\text{m}$	3 sets PMs
3. zircon	<100 $\mu\text{m}$	NPFs
4. monazite	>100 $\mu\text{m}$	1 set PMs.
5. zircon	>100 $\mu\text{m}$	NPFs

**Sample V251b:** Granulite, 26°56'59"S 27°30'33"E, Vredefort Dome, South Africa



Grain / Mineral	Size	Structures	Grain/Mineral	Size	Structures
1. monazite	~250 $\mu\text{m}$	2 sets PMs	4. zircon	>100 $\mu\text{m}$	1 set PMs, NPFs
2. zircon x2	<100 $\mu\text{m}$	NPFs	5. zircon	>100 $\mu\text{m}$	1 set PMs, NPFs
3. zircon	~100 $\mu\text{m}$	NPFs	6. zircon	>100 $\mu\text{m}$	1 set PMs, NPFs